Bibliotheek Hoofdkantoor TNO
's-Gravenhage

797

protection against toxic compounds

CHEMICAL AND TECHNOLOGICAL ASPECTS

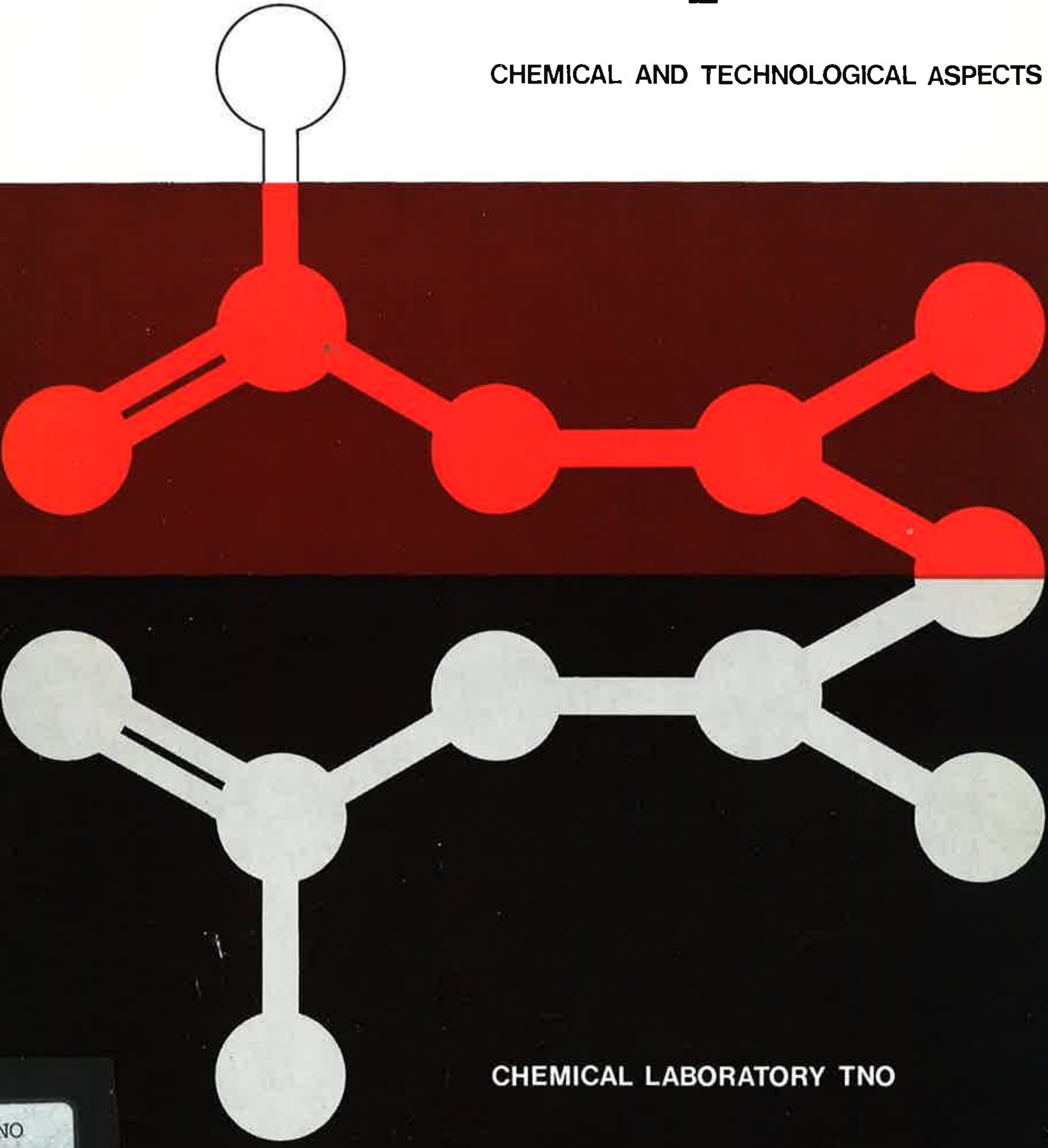

CHEMICAL LABORATORY TNO

protection against toxic compounds

CHEMICAL AND TECHNOLOGICAL ASPECTS

CHEMICAL LABORATORY TNO

Dedicated to Dr. A. J. J. Ooms, Director of the Chemical Laboratory TNO, to commemorate his twenty-five years of activity in research involving the protection against toxic compounds, in particular chemical warfare agents.

February 1, 1973
Rijswijk, The Netherlands

contents

	Preface	
H. L. Boter, C. van Hooidonk, L. P. A. de Jong and H. Kienhuis	Stereospecific interaction of cholinesterases and model compounds with chiral organophosphorus inhibitors	11
Joke Kaaijk	An atmospheric hydrogen fluoride monitor	23
H. L. Boter and A. Verweij	Sampling and identification of chemical warfare agents	33
M. van der Brink, D. van Leeuwen and J. Medema	The effect of gases on the conductive properties of organic semiconductors	43
C. J. P. van Buijtenen	Comparison of "light scattering" and aerodynamic diameters of aerosol particles	53
F. Oeseburg	Particle size analysis of dioctyl phthalate aerosols using the Stöber aerosol spectrometer	61
J. Medema and J. J. G. M. van Bokhoven	The determination of sarin adsorption isotherms on carbon black using a tracer technique	71
J. J. G. M. van Bokhoven and J. Medema	Microcalorimetric determination of sarin decomposition catalyzed by alumina	79
A. E. T. Kuiper and J. Medema	Infrared spectroscopy of sarin adsorbed on alumina	87
P. C. Stamperius and H. W. van der Klooster	Leaks in charcoal beds and the water content of charcoal determined using the ethane pulse technique	95
M. van Zelm and J. Medema	Analysis of breakthrough curves of benzene on active charcoal	103
M. van Zelm	Design of a simple gas-mask	121
A. van Vliet	Emergency water supply	131
	Acknowledgements	

preface

In this book thirteen scientific papers on experimental work of staff and employees of the "Chemisch Laboratorium TNO" have been bundled. The book is published on the occasion that the director of this laboratory, Dr. A. J. J. Ooms, twenty-five years ago was engaged as a young graduate by the laboratory. Primarily, the book is a gift to Dr. Ooms on his twenty-fifth anniversary with TNO.

For more reasons than one this seems to be a unique event. It is understood that homages of this kind have been paid before. However, on most of these occasions the person honoured was at the end of his career. This does not hold in the present case by a long way. Also the book itself is rather unique, in this sense that it has been written by staff and employees of one laboratory. Moreover, the contributions are of a good scientific quality and the spread in the kind of subjects is large.

Two coupled conclusions may be drawn from the above. Dr. Ooms possesses an unusual combination of qualities and the manner in which he executes his work meets with the approval of his personnel.

Undoubtedly, it will give Dr. Ooms a great deal of happiness to learn that his work is appreciated and that his intentions apparently have been so well understood. The elements to achieve this success, of course, have always been there. Intelligence, love for and skill in scientific chemical work – the promotion to the doctor's degree took place in Leiden on 7th of June 1961 on a biochemical subject, with Prof. Dr. J. A. Cohen as his promotor –, great interest in his fellow-man, to be deduced e.g. from the type of work chosen, a marked sense of humor and the faculty to stand for one's convictions. However, without the excellent response that is without the good standard of the qualities of those working in the laboratory, all this might not have been observed and appreciated. It is true that "outside" recognition of Dr. Ooms' qualities already occurred when he was called to succeed J. van Ormondt as director. However, the present gift and the coupled appreciation, coming from "inside", will give a deeper satisfaction. Most probably of all by the fact that he has been called to coach such a good team, which shares his belief in a practical translation of the idealistic goal to protect fellow-man.

Although perhaps not on purpose, the appearence of this book serves a second goal. To outsiders it gives a survey of the type of work done in the laboratory. This survey is not complete, but, it serves to show how many subjects of a different nature have to be studied in order to be able to obtain a proper basis for adequate measures against intentional and unintentional environmental pollution.

Those who took the initiative to publish this book are therefore to be thanked and to be complimented.

Professor P. M. Heertjes,

Chairman of the Advisory Committee

stereospecific interaction of cholinesterases and model compounds with chiral organophosphorus inhibitors

H. L. BOTER, C. VAN HOOIDONK,
L. P. A. DE JONG and H. KIENHUIS

A survey of kinetic studies on the stereospecific inhibition of acetylcholinesterase (AChE) and butyrylcholinesterase (BuChE) by asymmetric (chiral) organophosphorus compounds is given. The inhibition involves complex formation between the reactants followed by phosphorylation of the enzyme.

From a study of the relation between the overall rates of inhibition and the centre of chirality in the inhibitor molecule the following conclusions were drawn: 1) AChE is substantially more stereospecific than BuChE, 2) the stereospecificity of AChE increases with increasing reactivity of the inhibitor, 3) for AChE the stereospecificity is most distinct when the phosphorus atom is the centre of chirality, and 4) for BuChE the highest stereospecificity is observed when the chiral centre is located in the group which is split off during phosphorylation.

The separation of the overall inhibition reaction of AChE in complex formation and phosphorylation and a quantitative evaluation of the dissociation constant of the complex and the rate constant of phosphorylation revealed that the stereospecificity is reflected in the complex formation, but is maintained during the phosphorylation.

The reaction of organophosphorus compounds with cyclodextrins has been studied as a model system for enzyme inhibition. The reaction likewise involves complex formation and phosphorylation. Stereospecificity was established in both steps. However, for this system the stereospecificity must be ascribed to different rates of phosphorylation.

Introduction

During the past twenty-five years a large group of organophosphorus compounds has attracted much attention because of its remarkable pharmacological activity (1). This activity is based mainly on the irreversible inactivation of the enzyme acetylcholinesterase* (AChE) which acts as a catalyst for the hydrolytic fission of acetylcholine, a transmitter substance formed and released at the junctions between nerve cells, and between nerve cells and other cells (*e.g.* muscle cells) in the cholinergic part of the nervous system (2). Inactivation of the enzyme gives rise to accumulation of acetylcholine leading to a complex of typical symptoms of poisoning due to disturbance of the neural transmission.

Great structural variability may be derived from the general formula of this group of organophosphorus compounds

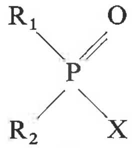

I

where R_1 and R_2 are alkyl, alkoxy or amino, X may be fluoride, cyanide, ω-(dialkylamino)alkylthio, aryloxy, *etc.*

This structural variability has stimulated several investigators to study organophosphorus compounds which has led to applications as insecticides and to possible use as chemical warfare agents (3). Facing the threat of the latter possibility, the laboratories of the National Defence Research Organization TNO considered the mechanism of cholinesterase inactivation and reactivation as an obvious research subject.

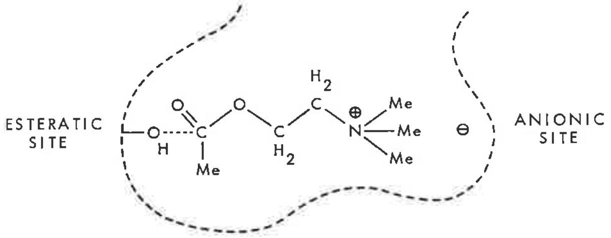

It is generally agreed that the interaction of cholinesterases with acetylcholine may be described by three steps: binding, acetylation of the enzyme and subsequent deacetylation. It is also generally accepted that two groups at the active site are essential in this reaction sequence: the esteratic site, where the enzyme is acetylated, and the anionic site containing one or more negatively charged groups giving an ionic interaction with the positively charged choline residue.

* acetylcholine acetyl-hydrolase, EC 3.1.1.7.

Stereospecificity of cholinesterases

Stereospecificity patterns

Any change of the chemical structure of a compound results in an alteration of its physical and chemical properties. On the contrary, enantiomers have identical chemical properties as far as interactions with symmetric reagents are concerned. It follows that a difference in activity of enantiomers towards an enzyme is directly related with the spatial structure of the active site.

In principle, asymmetric substrates (*e.g.* acetylcholine derivatives) as well as inhibitors (*e.g.* organophosphorus compounds) may be used for a systematic study of the stereochemical properties of the enzyme active site. The drawback in using acetylcholine derivatives is obvious; there exists only a very limited number of possibilities for insertion of the chiral centre into the molecule. For instance, it is impossible to introduce the chiral centre in the carbonyl group which is involved in the interaction with the esteratic site. Organophosphorus compounds allow more variations in the position of the chiral centre. From the general formula of organophosphorus compounds with cholinesterase inhibiting properties (see Introduction) it follows that the chiral centre may be placed in the groups R_1 and R_2, at the central phosphorus atom or in the group X, which is split off in the inhibition reaction. Particularly, the last-mentioned position provides the possibility to investigate the stereochemical properties of the environment of the esteratic site. A number of compounds belonging to various types of inhibitors and representing five different positions of the chiral centre (denoted by*) were selected. In almost all cases the stereoisomeric forms were isolated.

$$\mathrm{[n\text{-}Hex\overset{*}{C}H(Me)O]MeP(O)F}\qquad \mathrm{[n\text{-}Hex\overset{*}{C}H(Me)O]_2P(O)F}$$

II **III**

$$\mathrm{(i\text{-}PrO)Me\overset{*}{P}(O)SCH_2CH_2Y}\qquad \mathrm{(i\text{-}PrO)Me\overset{*}{P}(O)F}\qquad \mathrm{(i\text{-}PrO)Me\overset{*}{P}(O)OC_6H_4NO_2\text{-}p}$$

IV **V** **VI**

$$\mathrm{(EtO)_2P(O)S\overset{*}{C}H(Me)CH_2NMe_2}\qquad \mathrm{(EtO)_2P(O)SCH_2\overset{*}{C}H(Me)NMe_2}$$

VII **VIII**

$$\mathrm{[(i\text{-}PrO)MeP(O)SCH_2CH_2\overset{*}{S}Me(n\text{-}Hex)]^{\oplus}MeSO_4^{\ominus}}$$

IX

The majority of these compounds has its centre of chirality situated at the phosphorus atom. For the preparation of these compounds in optically active form the acid (i-PrO)MeP(O)SH was resolved by using both (+)- and (−)-α-phenylethylamine (14). Because of its rapidity this method is to be preferred to that in which quinine is applied as resolving base (15).

able that AChE and BuChE are preferably inhibited by the (−)- and (+)-enantiomers, respectively. However, this was not generally observed; *e.g.* in case of cyclopentyl S-2-dimethylaminoethyl methylphosphonothioate, which structure is closely related to *K*, both cholinesterases are preferentially inhibited by the (−)-enantiomer (19).

Table I. Rate constants (k_i) and ratios of activity (r_a) for the inhibition of AChE and BuChE by the enantiomers of isopropyl S-(2-substituted)ethyl methylphosphonothioates at pH 7.7 and 25°

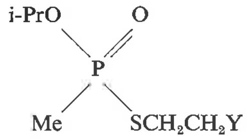

No.	Y	Enantiomer	AChE		BuChE	
			k_i(M^{-1}sec^{-1})	r_a	k_i(M^{-1}sec^{-1})	r_a
X	NMe_2	(−)	1.7×10^5	$\geqslant$ 330	4.5×10^3	4.9
		(+)	$\leqslant 5.2 \times 10^2$		2.2×10^4	
XI	$\overset{\oplus}{N}Me_3\overset{\ominus}{I}$	(−)	8.8×10^5	$\geqslant$ 1200	1.3×10^4	6.2
		(+)	$\leqslant 7.5 \times 10^2$		8.1×10^4	
XII	SMe	(−)	2.5×10^2	1.4	1.9×10^2	2.2
		(+)	1.8×10^2		4.1×10^2	
XIII	SEt	(−)	3.6×10^2	5.3	8.9×10^1	1.7
		(+)	6.8×10^1		1.5×10^2	
XIV	$\overset{\oplus}{S}Me_2\overset{\ominus}{I}$	(−)	6.3×10^5	$\geqslant$ 350	1.2×10^4	7.1
		(+)	$\leqslant 1.8 \times 10^3$		8.5×10^4	
XV	$CHMe_2$	(−)	9.7×10^0	1.2	2.6×10^0	3.8
		(+)	1.2×10^1		9.9×10^0	
XVI	F	(−)	1.2×10^2	3.2	1.3×10^1	9.2
		(+)	3.8×10^1		1.2×10^2	

In Fig. 1 the r_a values obtained for the isopropyl S-(2-substituted)ethyl methylphosphonothioates and for other compounds given in this paper are plotted on a logarithmic scale *versus* the coordinate of the active site represented in stretched form. Only r_a values obtained for more potent inhibitors were used to construct the figure. The chiral centres (denoted by *) involved are represented as parts of a hypothetic molecule.

In conclusion we may state that 1) AChE is substantially more stereospecific than BuChE, 2) the stereospecificity of AChE increases with increasing activity of the inhibitor, 3) for AChE the stereospecificity is more distinct when the phosphorus atom is the centre of chirality, indicating that the stereospecificity is centred on the isolated with a high degree of enantiomeric purity by using a recrystallization technique.

The enantiomeric purity of the preparation of the (+)-enantiomer* and the values of K_d and k_p for this enantiomer were derived from a combination of the results of aging** and inhibition experiments (12). The values of K_d and k_p for the (−)-enantiomer were determined directly from inhibition experiments. The results are given in Table II.

Table II. Dissociation constants (K_d) and rate constants of phosphorylation (k_p) for the inhibition of AChE by the enantiomers of (i-PrO)MeP(O)$SCH_2CH_2NMe_3$⊕I⊖ at pH 7.0 and 5°

Enantiomer	K_d (M)	k_p (sec^{-1})
(−)	3.5×10^{-7}	0.25
(+)	1.9×10^{-4}	0.04

The large difference between the K_d values suggests that in the binding step the conformation of the (−)-enantiomer is more complementary to the active site of the enzyme than the conformation of the (+)-enantiomer. Thus, the free energy of the enzyme-inhibitor complex of the (−)-enantiomer is lower than that of the (+)-enantiomer. The slight difference between the k_p values indicates that starting from the more stable enzyme-inhibitor complex the phosphorylation reaction proceeds at least as fast as starting from the less stable complex with the (+)-enantiomer. Consequently, the free energy of the transition state of the phosphorylation reaction with the (−)-enantiomer is lower than that connected with the (+)-enantiomer. Hence, the stereospecific behaviour of the enzyme with respect to this inhibitor is reflected in the binding step, but is maintained during the phosphorylation.

Stereospecificity of α-cyclodextrin

A useful contribution to a better understanding of the stereochemical factors involved in the inhibition process would be the study of model systems in which the enzyme is replaced by a simply organized organic molecule. This model system must display a number of characteristics of enzymatic reactions, including stereospecificity. α-Cyclodextrin (cyclohexa-amylose) seems to offer such a system.

α-Cyclodextrin (α-CD) formed by degradation of starch by *Bacillus macerans* amylase is a cyclic carbohydrate consisting of six 1,4 linked α-D(+)-glucose residues. This doughnut-shaped molecule has an internal cavity of about 6 Å and represents a exhibited by AChE for the enantiomers of **XI** has its basis in the binding of the inhibitor to the enzyme. In this respect, there seems to be a striking difference between α-CD and AChE in their reaction with enantiomeric organophosphorus compounds.

---

* The amount of the (−)-enantiomer in the preparation of the (+)-enantiomer turned out to be only 0.02%.

** Aging is the enzymatically catalyzed process in which the phosphorylated cholinesterase releases an alkyl group from the phosphorus moiety.

Table III. Rate constants of phosphorylation ($k = k_p/K_d$) of α-CD and rate constants of inhibition (k_i) of AChE by the enantiomers of **V**, **VI** and **X**

No.	Enantiomer	α—CD				AChE	
		K_d (M)	k_p (sec^{-1})	k (M^{-1}sec^{-1})	r_a	k_i (M^{-1}sec^{-1})	r_a
V	(−)	4.0×10^{-2}	2.0×10^{2}	5.0×10^{3}	5	2.3×10^{5}	$\geqslant 4600$
	(+)	6.0×10^{-3}	5.8×10^{0}	9.7×10^{2}		$\leqslant 5.0 \times 10^{1}$	
VI	(−)	3.2×10^{-2}	3.8×10^{-1}	1.2×10^{1}	$\geqslant 28$	1.8×10^{4}	$\geqslant 360$
	(+)	1.2×10^{-2}	$\leqslant 5.0 \times 10^{-3}$	$\leqslant 4.2 \times 10^{-1}$		$\leqslant 5.0 \times 10^{1}$	
X	(−)	9.8×10^{-2}	3.3×10^{-3}	3.4×10^{-2}	> 210	1.7×10^{5}	$\geqslant 330$
	(+)	1.9×10^{-1}	$< 3.0 \times 10^{-5}$	$< 1.6 \times 10^{-4}$		$\leqslant 5.2 \times 10^{2}$	

This conclusion must be regarded as tentative until K_d and k_p values for AChE inhibition by more organophosphorus compounds become available.

Another striking difference between α-CD and AChE is illustrated by a comparison of their r_a values. The r_a values obtained for AChE (11) are almost independent of the nature of the group which is split off during the inhibition. On the contrary, the r_a values observed for α-CD increase with decreasing reactivity of the organophosphorus compound.

Concluding remarks

The pronounced stereospecific behaviour of the esteratic site of AChE exhibited during inhibition by asymmetric organophosphorus compounds points to a rigid and sterically stringent structure of this part of the active site. This does not apply to BuChE which shows a relatively low stereospecificity.

It was found that the stereospecificity of AChE with respect to one selected inhibitor is reflected in the binding step, but is maintained during phosphorylation. This phenomenon was not observed in model studies carried out with α-CD, which may illustrate once more the unique character of enzyme reactions.

an atmospheric hydrogen fluoride monitor

JOKE KAAIJK

A monitor has been developed for the quantitative determination of atmospheric hydrogen fluoride in the range of 0.05 – 150 μg HF/m^3.

The atmospheric pollutant is collected by scrubbing an air flow with a buffer solution. The accumulation of the fluoride ion concentration is directly measured by using a fluoride ion-selective electrode. The collection efficiency exceeds 95%. The buffer solution in the apparatus is replaced every 24 hours. Values of hydrogen fluoride concentration measured with the fluoride monitor in the range of 0.2 – 150 μg HF/m^3 *agree well with concentration values calculated from the decrease in weight of permeation tubes.*

In order to obtain a complete separation of particulate and gaseous fluorides a pre-separation of particles with an aerodynamic diameter exceeding 1 μm from the gas-phase is necessary.

Introduction

Fluorine compounds can occur in the atmosphere in organic and inorganic form. Organic fluorides, *e.g.* carbon tetrafluoride (CF_4) and fluorinated hydrocarbons, are generally inert. Inorganic fluorides, *e.g.* sodium fluoride (NaF), cryolite (Na_3AlF_6), silicon tetrafluoride (SiF_4) and hydrogen fluoride (HF), are harmful to vegetation and animals. Damage to vegetation is mainly caused by gaseous fluorides; it has been shown that low concentrations of hydrogen fluoride ($0.2 \mu g/m^3$) cause damage to certain sensitive species of vegetation (1). Gaseous fluorides emitted by industries are hydrogen fluoride and silicon tetrafluoride; the latter reacts with moisture in the atmosphere to form hydrogen fluoride. In areas where cattle-breeding is practised, the precipitation of particulate fluorides may have harmful consequences. In general, ambient air quality standards are based on the susceptibility of plants towards gaseous fluorides, because they are the most susceptible receptors for this type of pollutant (2).

The atmospheric fluoride concentration generally ranges from 0.05–10 $\mu g/m^3$; in the neighbourhood of fluoride emitting factories concentrations up to 100 $\mu g/m^3$ may be reached (3).

This paper deals with the development of a fully automatic instrument for the determination of atmospheric hydrogen fluoride concentrations. The sampling principle of the instrument is derived from an apparatus, described by Adams *et al.* (4), for the determination of the concentration of fluorides in the atmosphere by using an automatic flow colorimeter embodying an air/reagent contacting cell. The method for collecting atmospheric hydrogen fluoride in a solution has been modified.

The accumulation of the fluoride concentration in the solution is measured potentiometrically using a fluoride ion-selective electrode, developed by Orion Research Inc., and a standard calomel reference electrode (5). The potentiometric method surpasses the colorimetric method in speed, accuracy and convenience (6).

Principle of operation

A cross-section through the sampling and measuring cell is shown in Fig. 1. The cell compartment A is filled with a buffer solution. This solution flows by gravity through the orifice B. The air coming in at C flows along this orifice, transports the solution to tube D and gives rise to a film of liquid against the inner surface of tube D. The atmospheric fluorides are collected in this film. After separation of the solution and the air in the cyclone head E, the solution runs down into the measuring cell A and the air leaves the apparatus at E. The fluoride electrode 1 and the reference electrode 2 are fixed in the measuring cell.

It turned out to be possible to collect atmospheric hydrogen fluoride from a large volume of air (flow rate 30 l/min) into a small volume of buffer solution (8 ml) with an efficiency exceeding 95%.

The potential (E) developed by the fluoride electrode against the reference electrode in this period of time the hydrogen fluoride present in the atmosphere is accumulated in the buffer solution. The potential of the fluoride electrode is amplified and can be read continuously on a recorder. It is possible to record the amplified output every half hour either on a magnetic tape or on a computer via a telecommunication data line. The reduction of the volume of the buffer solution in the apparatus by evaporation of water is compensated by adding water which is regulated by a photo-electric cell (F) serving as a liquid level control system.

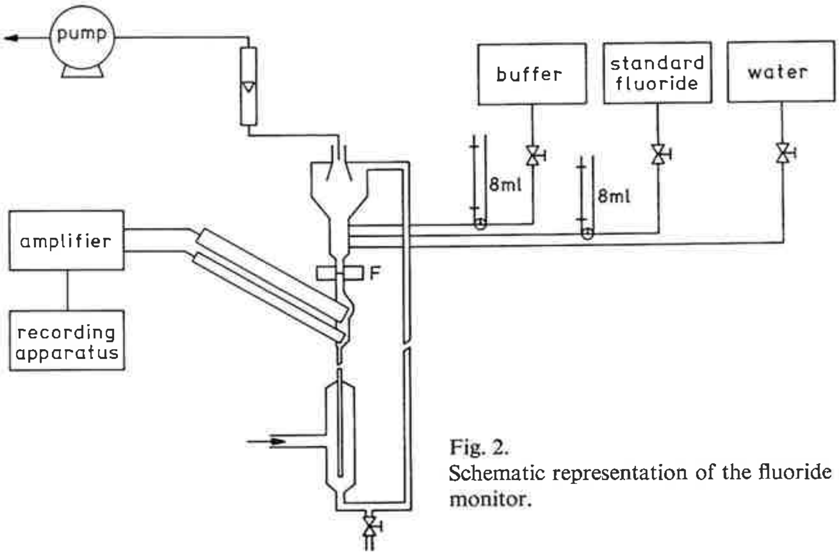

Fig. 2.
Schematic representation of the fluoride monitor.

3. The solution is removed from the apparatus and the apparatus is subsequently rinsed with distilled water.
4. A standard fluoride solution (8 ml) flows into the cell and after equilibration the potential is measured in order to check and eventually to correct the calibration curve of the fluoride electrode.
5. The solution is removed and the apparatus is rinsed with distilled water. The cycle starts again.

A photograph of the prototype of the fluoride monitor is given in Fig. 3. In case the potential of the fluoride electrode is recorded every half hour, the half-hour average of the atmospheric hydrogen fluoride concentration (C) is given by

$$C = \frac{V_s}{V_g} \Delta c_F$$

where V_s represents the volume of the circulating buffer solution, V_g the volume of the atmospheric air passed through the apparatus, and Δc_F the increase of the fluoride ion concentration in the solution.

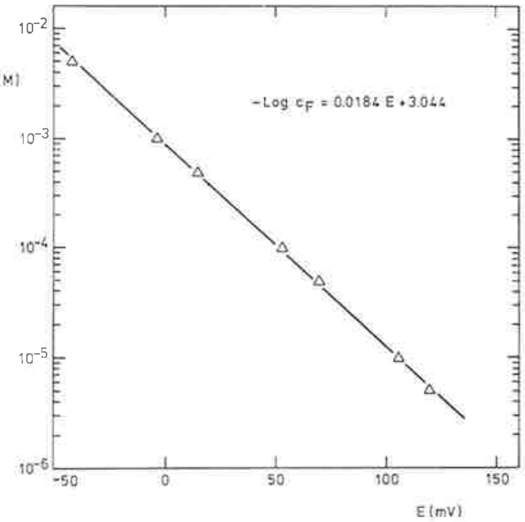

Fig. 4.
Relationship between the fluoride concentration in the apparatus (c_F) and the potential (E).

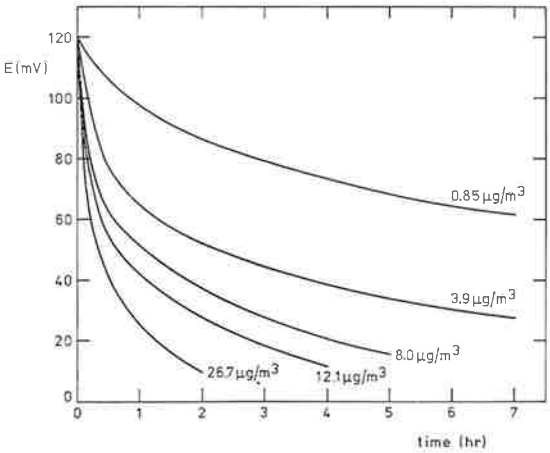

Fig. 5.
Fall of the potential by passing constant hydrogen fluoride concentrations through the sampling cell.

measured potential in the monitor caused by passing through various hydrogen fluoride concentrations is shown in Fig. 5. The concentration measurements carried out with the fluoride monitor have been compared with those calculated from the decrease in weight of the permeation tubes and the volume flow of the air stream. To obtain hydrogen fluoride concentrations below 2 µg/m³ the gas stream was diluted. In this case the hydrogen fluoride flow was passed through a sodium carbonate impregnated filter and the fluoride quantity on the filter was determined with a fluoride electrode. This value was compared with the measurement of the fluoride monitor. Fig. 6 shows that there is a satisfactory agreement in the measured concentration range.

Table I. Relation between the atmospheric hydrogen fluoride concentration (C) and the increase of the fluoride ion concentration in the solution (Δc_F) after sampling half an hour and 24 hours.

C (μg/m³)	$\Delta c_F \times 10^6$ (M) ½ hr	$c_F \times 10^4$ (M) 24 hr
0.05	0.3	0.13
0.1	0.6	0.27
1.0	5.6	2.7
10	56	27
15	85	41
100	560	270

In order to separate the particulate fluorides from the gaseous fluorides it is necessary to collect the larger particles before the air enters the sampling cell. Considering the high air sampling rate of the fluoride monitor and the desire to measure continuously during a long period of time a miniature cyclone seems to be useful for this purpose. The collection efficiency of a glass cyclone was tested with a Royco particle counter, model 225 (Table II).

Table II Collection efficiency of the cyclone as a function of the particle size

particle size (μm)	collection efficiency (%)
0.3–0.4	68
0.4–0.9	89
0.9–1.6	96
1.6–2.0	98
2.0	99

These results show that the cyclone is suitable to collect the particles which otherwise would be collected in the sampling cell in the fluoride monitor.

The inner surface of the glass cyclone is coated with a polyurethan lacquer in order to minimize the adsorption of the hydrogen fluoride gas to the cyclone.

Concluding remarks

The hydrogen fluoride monitor can measure the atmospheric concentrations (0.05 – 15 μg/m³) if the buffer solution in the apparatus is replaced every 24 hours. During this time it is possible to measure the half-hour averages of hydrogen fluoride. The calibration of the monitor can be checked and corrected every 24 hours. The measuring range of the monitor can be changed up to 150 μg/m³ by changing the cycle-time of the instrument to one hour.

sampling and identification of chemical warfare agents

H. L. BOTER and A. VERWEIJ

The need for the identification of agents used in chemical warfare and in connection with controlled abolition of chemical weapons is given. The different aspects of the identification including sampling, isolation and structure elucidation are briefly discussed. In order to develop a methodology for identification background studies concerning the fate of chemical warfare agents in the environment (soil, water and air) have been performed. The standardization of gas chromatographic data for insertion in a data storage and retrieval system is described.

Introduction

In the event of chemical warfare, it is important to establish the chemical identity of the agent as quickly as possible. This is necessary in order to take the required protective, medical and tactical measures within the shortest possible delay. Moreover, the results of the identification provide information concerning an enemy's chemical warfare capability being of interest for intelligence services.

The identification of chemical agents present in the biosphere is also of political importance, *e.g.* for the confirmation of a suspected breach of any chemical disarmament agreement. This aspect is of increasing interest in view of negotiations in this field conducted in Geneva since 1969.

In order to differentiate between chemical agents and pollutants, arising from other sources and from natural components in the environment, it is necessary that background information on these compounds is available.

Methodology

In the course of the elucidation of the chemical nature of an agent contaminating the environment three main aspects are of importance, *viz.* sampling, isolation and identification. The agent may be sampled in air, water or ground (soil or vegetation). Among these, the ground seems to be the most suitable sampling medium as the dilution of the agent is slow in comparison with that in air or water. The ideal sample consists of unexploded or malfunctioned munitions, however, reliance cannot be placed upon such samples being found. Consequently, it is unlikely that sampling will take place under optimum conditions and this will affect the nature and quantity of the sample obtained. Anyhow, sampling should be carried out as quickly as possible as the conditions to take a sample are becoming less favourable from the moment the agent is disseminated; the agent is diluted in the air by diffusion, evaporates from a surface or decomposes in the biosphere. As the sample must be transported to a laboratory for further investigation, the sampling equipment must be easy to handle and readily portable. This implies that methods based *e.g.* on the suction of a large volume of air through a minimum amount of an adsorbent are suitable. In the case of sampling soil or vegetation, knowledge of the movement of agents into these media is necessary to take optimum samples.

In order to isolate the chemical agent from a sample taken in the air, on soil or on vegetation a separation of the agent from other chemical pollutants and from natural components of the environment has to be performed. The potency of current chemical warfare agents is such, that they are likely to be encountered in low concentrations. As a result of this and considering that chemical warfare operations may well take place in an industrialized and highly cultivated environment air pollutants and agricultural chemicals may occur at concentrations comparable with those of the chemical agents. Generally, the isolation of the agent will require an extraction of the

Table I. Chemical and physical characteristics of some soil types

	organic matter content (g/100 g)	pH	CEC* meq./100 g	moisture content (%)
sand	3.9	5.3	10.7	10
marine clay	3.1	7.3	19.3	18
clayey peat	43.5	5.4	107.4	49
quartz sand**	0	–	–	4

* Cationic Exchange Capacity

** used as a reference

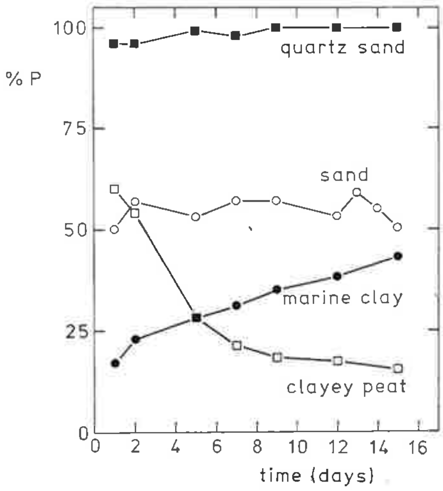

Fig. 1.
Plot of the phosphorus recovery *versus* the time elapsed after contamination of different soil types with VX.

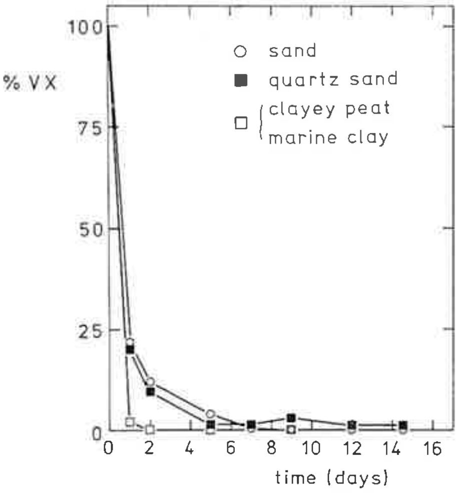

Fig. 2.
Plot of the percentage of water-extractable VX *versus* the time elapsed after contamination of different soil types.

The decrease of water-extractable VX given as a function of time and measured by gas chromatographic analysis using a thermionic detector is represented in Fig. 2. The rapid decrease of extractable agent may be ascribed to a breakdown mechanism and possibly to chemisorption onto soil components. In the case of sand and quartz sand it is most likely that the degradation plays a predominant role, because it was found that despite the decrease of extractable VX the phosphorus recovery remains at a rather high level (Fig. 1).

Ethyl methylphosphonic acid (I) and methylphosphonic acid (II) proved to be the only phosphorus containing breakdown products in the aqueous extracts. In quartz sand the degradation stops after the formation of I. For the other soil types it was centrated and identified as methyl esters by means of their gas chromatographic retention indices as shown in the scheme below.

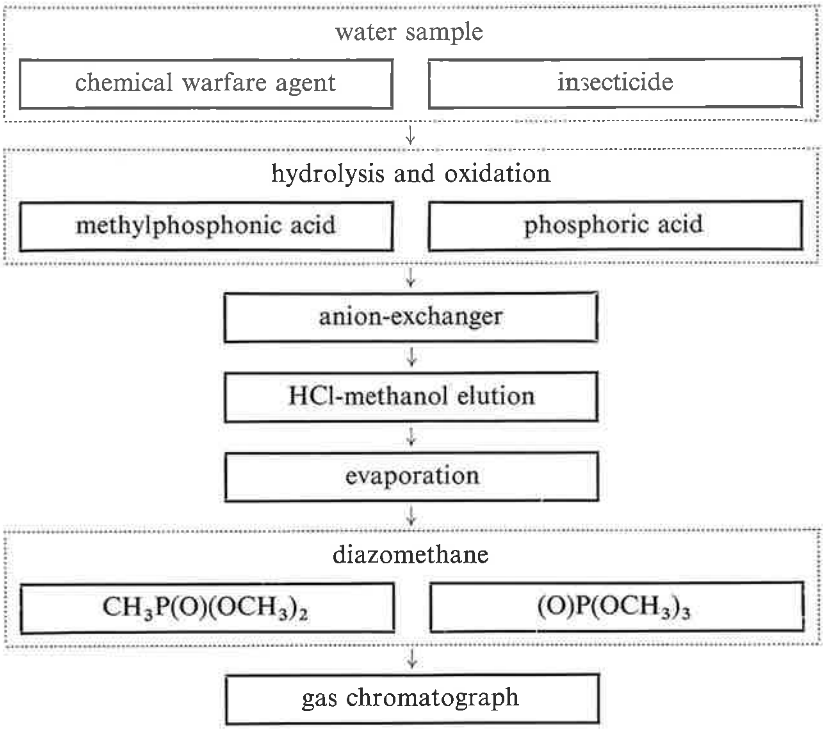
water sample
chemical warfare agent
insecticide
hydrolysis and oxidation
methylphosphonic acid
phosphoric acid
anion-exchanger
HCl-methanol elution
evaporation
diazomethane
$CH_3P(O)(OCH_3)_2$
$(O)P(OCH_3)_3$
gas chromatograph

It was found that up to 100 mg of methylphosphonic acid in 1 litre of water adsorbed nearly quantitatively onto an anion-exchanger column (Amberlite IRA-400 in formate form). The acid was eluted in a volume of 10 ml in 80–90% yield using a mixture of methanol and hydrochloric acid. The conversion into the corresponding methyl esters with diazomethane is complete within a few minutes. Gas chromatographic analysis on Triton X-305 as the stationary phase at 120°C gave a complete separation of the esters. The retention indices according to Kováts (see Standardization of gas chromatographic data) are 1415 ± 4 and 1481 ± 3 for dimethyl methylphosphonate and trimethyl phosphate, respectively.

According to a literature survey the hydrolysis is preferably carried out at pH 4 and 100°C over a 1–2 days period (4).

Air

It has been put forward that chemical warfare operations may well take place in an industrialized environment with the intent to gain control of industrial equipment in undamaged condition. In these cases it is necessary to have available back-

Standardization of gas chromatographic data

As has been stated (see Methodology) the identification of chemical warfare agents will be considerably facilitated by using a suitable data storage and retrieval system.

Gas chromatographic retention data as such are not suitable for insertion in such a system as the result of variations in gas flow, column dimensions and the amount of the stationary phase. These difficulties are overcome in the retention index system according to Kováts (5) which is now considered as the most reliable system to express retention data. The retention index of a particular compound is derived by comparison of the retention time on a given column with those of reference saturated normal hydrocarbons, preferably by interpolation. The index still depends on the type of the stationary phase and on the temperature.

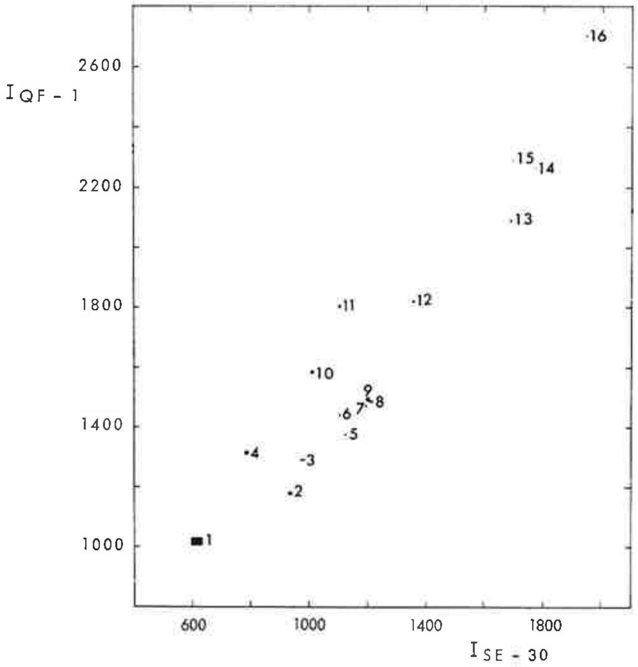

1 chloroacetone
2 ethyl bromoacetate
3 ethyl iodoacetate
4 sarin
5 benzylbromide
6 benzoylchloride
7 α-bromo-*m*-xylene
8 α-bromo-*o*-xylene
9 α-bromo-*p*-xylene
10 soman
11 tabun
12 ω-bromoacetophenone
13 VX
14 dibenzoxazepine
15 thiolo systox
16 parathion

Fig. 4.
Plot of the retention indices (I) of some irritants, nerve gases and organophosphorus insecticides obtained on the stationary phases SE-30 and QF-1 at 190 °C. The dimensions of the spots indicate the standard deviations.

Retention indices of some irritants, nerve gases and phosphorus containing insecticides have been determined in this laboratory (6). Measurements were carried out on four stationary phases of various polarities at three temperatures. These preliminary experiments gave strong indications that within the group of compounds investigated the respective retention indices are acceptable as a means for identification. However, additional experiments will be carried out to study the influence of the age of the column, different batches of the column material, *etc.* on the value of the retention index.

the effect of gases on the conductive properties of organic semiconductors

M. VAN DER BRINK, D. VAN LEEUWEN
and J. MEDEMA

Strong electron-donating and strong electron-accepting gases (dimethylamine, ammonia, nitrogen dioxide, and chlorine) have great effect on the conductivity of certain organic semiconductors such as phenothiazine, violanthrone, thionine, and phthalocyanine.

In some cases pressures as low as 10^{-3} Torr are sufficient to cause a deviation of 50% in conductivity. Other vapours, such as sulfur dioxide, oxygen, air, and water result in much less strong changes in conductivity.

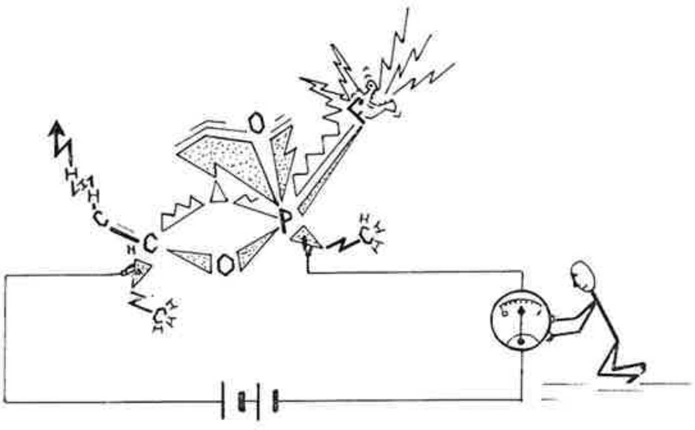

Introduction

The aim of this study is to investigate the applicability of organic semiconductors as gas sensors; the basis is formed by the well-known effect of gases on electrical conductivity.

In the past two decades the conductive properties of organic semiconductors have frequently been investigated. The effects of temperature, light, electric field, impurities, ambient gas, and structure defects on conductivity have been described. A general theory about the conducting mechanism in organic solids is unknown. Nevertheless, it is accepted (1–4) that conductivity can be described as transport of π-electrons, weak interactions of molecules give rise to energy bands, which can be occupied by excited π-electrons. The excitation energy is determined by both the degree of conjugation and the allied energy of delocalisation in the molecules. A second effect that can influence conductivity is the transfer velocity of the charge carriers from one molecule to another (5).

Upon adsorption of gases on semiconductor surfaces both effects may be influenced and as a result the conductivity is changed. It is possible that on the one hand charge carriers are immobilized by adsorbed molecules while on the other hand, the excitation energy might change by injection of charge carriers.

In a previous paper (6) the influence of gases on the light and dark conductivity of phthalocyanine and β-carotene was described. The effect of temperature on conductivity was also considered. Here, we will confine ourselves to the effect of some gases, on the dark conductivity of semiconducting films of phenothiazine, violanthrone, thionine, and phthalocyanine on quartz substrate and the role of gas pressure in these effects. The semiconducting solids were selected because of their chemical and thermal stability as well as differences in sign of the charge carriers and in resistance. Our investigations were mainly focussed on $(CH_3)_2NH$, NH_3, SO_2, O_2, Cl_2, NO, NO_2, CH_3SH, Air and H_2O. The results will be presented in terms of changes in resistance, *viz.* the reciprocal value of the conductivity.

Experimental

Except for some minor modifications, the apparatus and procedure used throughout this study were the same as described before (6). The essential part of the apparatus is the surface cell, a quartz substrate with gold electrodes on which a film of semiconductor has been sublimated. It has been selected over several other measuring techniques for the following reasons:

1. the large surface-volume ratio, which gives the system a short response time,
2. the absence of anisotropy at amorphous or polycrystalline films,
3. the good physical contact between electrodes and semiconductor, and
4. the large gas-semiconductor contact area.

Results

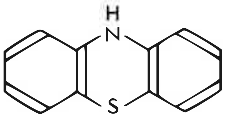

Phenothiazine

Phenothiazine sublimates very easily (b.p. 371 °C at 1 atm). The gold-coloured, polycrystalline film has a good ohmic character in the range of 0–200 V. The resistance of the fresh film, 5 μm in thickness, was 3.10^{12} Ω as calculated from the i—V characteristics. From the i—V characteristics, it can be derived that the space charge limited currents do not appear in vacuum.

When a strong electron-donating gas was adsorbed, it appeared that the resistance after adsorption and subsequent evacuation was higher than the resistance of the fresh film. The resistance decreased, however, when an electron-accepting gas was dosed and evacuated. The first effect is probably caused by the irreversible introduction of donor levels resulting in a decreased mobility and a relatively increased recombination velocity. The second effect results from the introduction of acceptor levels which increases the number of positive charge carriers and therefore the conductivity. After the first exposure to NH_3 these memory effects caused a change in the resistance from 3.10^{12} Ω to 9.10^{12} Ω.

During the next series of experiments the resistance varied between 8.10^{12} Ω and 12.10^{12} Ω.

Phenothiazine was subsequently exposed to NH_3, $(CH_3)_2NH$, CH_3SH, Air 35% RH, O_2, SO_2, C_2H_4, and CO at various pressures. A typical experiment with $(CH_3)_2NH$ is shown in Fig. 1.

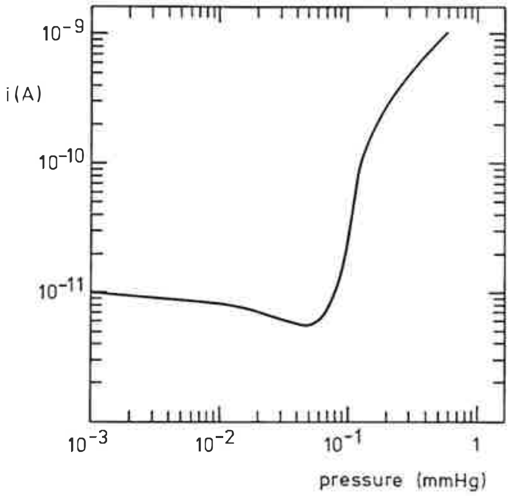

Fig. 1.
Current *versus* pressure of $(CH_3)_2NH$ in contact with a phenothiazine film.

Conductivities measured as a function of the gas pressure does not always decrease or increase continuously. There are minima present in the curves for NH_3, $(CH_3)_2NH$, CH_3SH, O_2, and SO_2. In Fig. 2 gas pressures are given for which there is a 10%

Fig. 2.
Pressures for which the deviation in resistance of a phenothiazine film is 10% from the initial value. Negative (dotted) and positive (full) changes are indicated on the same scale.

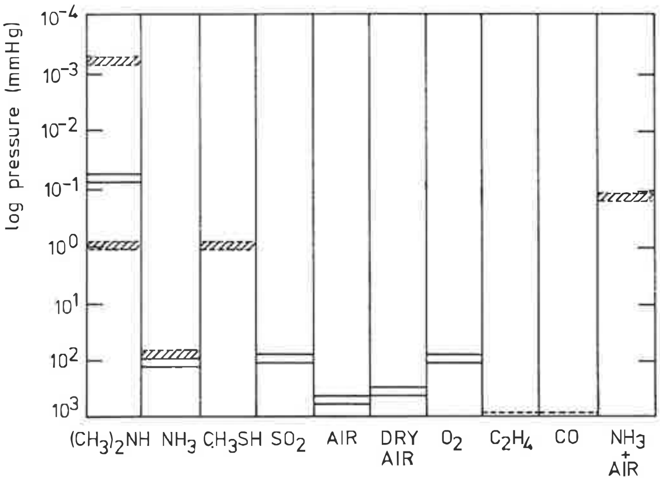

deviation in resistance of the film from the initial value. For $(CH_3)_2NH$ and NH_3 different pressures may cause the same change in resistance. This is due to the pronounced minima in the i—p curves, as can be deduced from Fig. 1. Experiments with ammonia in dry and moistened air shows that air does influence the effects of NH_3, but does not mask them.

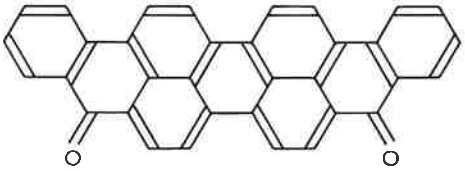

Violanthrone

Evaporation of this violet-blue compound is difficult (decomposition occurs at 490 °C and 1 atm). Under the microscope the film showed a polycrystalline nature with a thickness of about 1 μm. From the i—V characteristics for the fresh film the resistance was calculated to be 1.10^{15} Ω in the range of 0–900 V. Memory effects were observed after experiments with NH_3 and CO. In general, the variation in resistance amounted to 50% relative to the resistance of the fresh film except for the case of Cl_2 adsorption experiments in which the resistance decreases by a factor of 10^5 as a result of irreversible adsorption.

$(CH_3)_2NH$, NH_3, CH_3SH, SO_2, O_2, CO, C_3H_6, C_6H_6, Air 30% RH, Cl_2, and NO were subsequently admitted to violanthrone. In Fig. 3 values of pressures are given for which the deviation in resistance is 10%.

Violanthrone, in common with phenothiazine showed minima in the i—p characteristics for electron-donating gases, such as $(CH_3)_2NH$, NH_3 and SO_2. The strongest electron-donor, $(CH_3)_2NH$, had the most pronounced minimum, while SO_2 exhibited the least. As a result several pressures may correspond to a single value of the deviation in resistance for these gases.

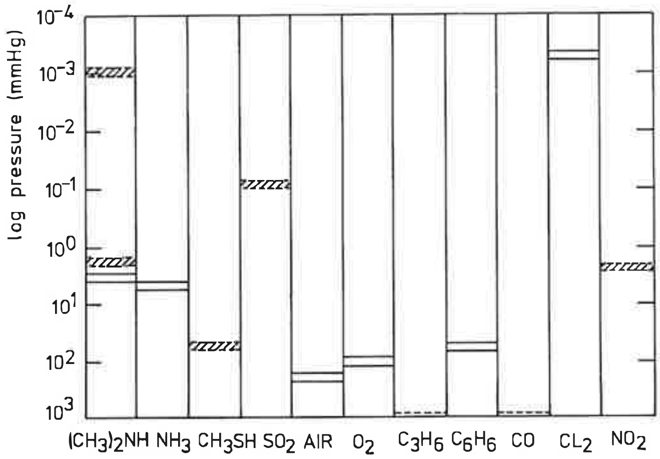

Fig. 3.
Pressures for which the deviation in resistance of a violanthrone film is 10% from the initial value. Negative (dotted) and positive (full) changes are indicated on the same scale.

The sensitivity of violanthrone towards $(CH_3)_2NH$ is about the same as that of phenothiazine, but towards NH_3, SO_2 and especially, O_2 and moistened air the sensitivity is greater.

Thionine

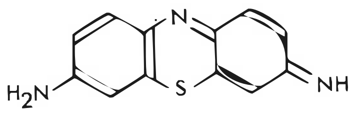

The evaporated film of thione (a cationic *n*-type semiconductor, ref. 7) had a thickness of 5–10 µm and showed a homogeneous structure under a microscope. The resistance calculated from the i—V characteristic for the fresh film was 2×10^{11} Ω in the range of 0–900 V. During adsorption of NH_3 (10 Torr) the resistance decreased to 2×10^{10} Ω in contrast with the increase found for phenothiazine and violanthrone. During the course of the experiments the resistance of the film in vacuum increased continuously until a value of 2×10^{12} Ω was found.

During the experiments it appeared that mercury vapour caused a strong temporary increase in current yield; after evacuation for 15 minutes the original value was reproduced again. This phenomenon may be ascribed to the formation of a mercury-thionine complex (7).

$(CH_3)_2NH$, O_2, C_3H_6, C_6H_6, Air 30% RH, SO_2, NO, Cl_2, NH_3, and NO_2 were subsequently admitted to thionine. In plots of current versus pressure, minima were obtained for O_2, C_3H_6, C_6H_6, SO_2, and NO_2. All these gases have, to some extent, electron-accepting properties. On phenothiazine and violanthrone (both non-ionic *p*-type semiconductors, ref. 6) the electron-donor gases were responsible for the minima. After passing the minimum in the i—p characteristics for thionine the current increased to values higher than the original ones. The pressure at which this increase started, determined the detectability of the thionine film. In Fig. 4 the pressures at deviations in resistance of 10% are given.

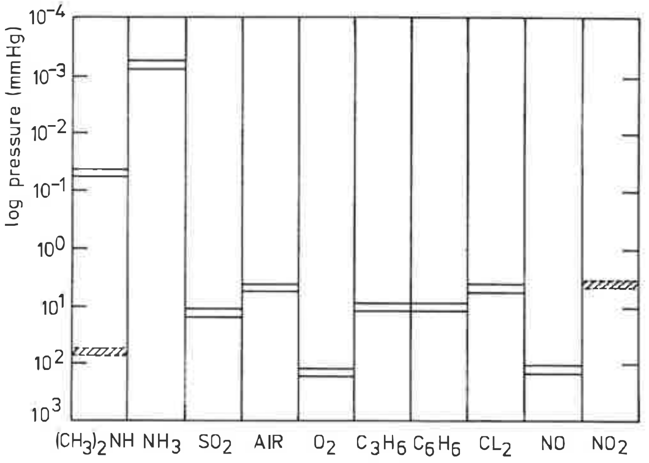

Fig. 4.
Pressures for which the deviation in resistance of a thionine film is 10% from the initial value.
Negative (dotted) and positive (full) changes are indicated on the same scale.

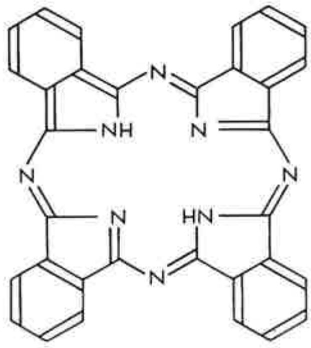

Phthalocyanine (metal-free)

The phthalocyanine (metal-free) compound was sublimated onto the quartz substrate with a Bunsen burner (~ 450 °C). This resulted in a blue-violet polycrystalline film (thickness 15 µm). In the range of 0–500 V the fresh film had a resistance of 2.10^{13} Ω. In this case memory effects were observed. After experiments with moistened air the resistance has decreased by a factor of 10.

Experiments with phthalocyanine have been described elsewhere (6). In general the results obtained during this study are comparable to the earlier one.

The number of measuring points were too small to give reliable i—p characteristics such that the minima in the i—p curves were not measured accurately. Therefore in Fig. 5 only approximate values for 10% deviation in resistance are given. However, these results show that phthalocyanine is very sensitive towards NH_3, NO_2, $(CH_3)_2NH$, and Cl_2. In this case also sarin, a potential chemical warfare agent, was admitted to the surface cell. An effect comparable to the more effective gases is observed. He, SO_2 and CH_3SH did not affect the resistance of the phthalocyanine film. With respect to the minima in the i—p curves, phthalocyanine behaved like a non-ionic *p*-type semiconductor just like phenothiazine and violanthrone.

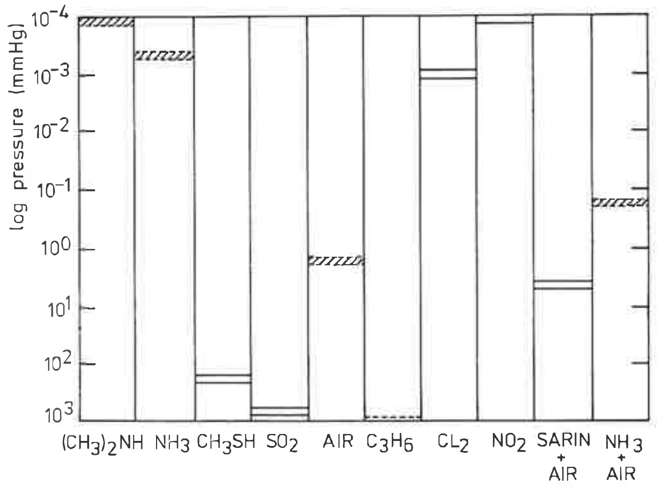

Fig. 5.
Pressures for which the deviation in resistance of a phthalocyanine film is 10% from the initial value. Negative (dotted) and positive (full) changes are indicated on the same scale.

Discussion and conclusions

Without going into detail about the effects of particular gases and the theoretical models concerning the influence of gases upon the mobility and number of charge carriers, it can be stated that electron-donating and electron-accepting gases change the resistance of organic semiconductor films. The magnitude of the change in resistance depends on the electron-donating or -accepting strength of the gas and on the type of semiconductor. Strong electron-donating gases ($(CH_3)_2NH$, NH_3) are already "visible" at pressures as low as 10^{-4} Torr. The same value can be given for strong electron-accepting gases (Cl_2, NO_2); however, the sign of the change of resistance is now the opposite. If we transfer these values to ppm gas in air we obtain values as low as 0.1 ppm for strong electron transferring gases. However, one must remember that the organic semiconductors exhibit, at most, only marginal selectivy. To date these semiconductors can only registrate a change in the electron-accepting or -donating properties of the total gas whether this is caused by 1 ppm NH_3 or 500.000 ppm air. In the present study little attention has been given to the influence of mixtures of gases upon conductivity. It is quite possible that the sensitivity decreases when mixtures are used. Perhaps, it may be possible to increase the sensitivity and selectivity by using for instance p—n junctions of organic semiconductors or by measuring the photo conductivity.

In summary, regarding the feasibility of employing certain semiconductors as gas sensors, the following conclusions can be drawn:

1. the resistance of organic semiconductor films is dependent on the type of ambient gas,
2. the resistance is dependent on the gas pressure,
3. memory effects did not seriously influence the sensitivity,
4. the sensitivity for some gases is satisfactory,
5. the selectivity, if present, must be improved.

References

1. D. D. Eley, G. D. Parfitt, N. D. Perry and D. H. Taysum, Trans. Faraday Soc. **49,** 79 (1953).
2. D. D. Eley and G. D. Parfitt, *ibid.* **51,** 1529 (1955).
3. D. D. Eley, J. Polym. Sci. (C) **17,** 73 (1967).
4. P. K. Datta, J. Sci. Ind. Res. **30,** 222 (1971).
5. F. Guttman and L. F. Lyons, *Organic Semiconductors*, John Wiley & Sons, Inc., New York, (1967).
6. Th. G. J. van Oirschot, D. van Leeuwen and J. Medema, J. Electroanal. Chem. **37,** 426 (1972).
7. A. Ternin, Proc. Chem. Soc., 321 (1961).

comparison of "light scattering" and aerodynamic diameters of aerosol particles

C. J. P. VAN BUIJTENEN

A Royco particle counter, model 225, was used for the determination of the "light scattering diameter" of heterodisperse aerosol particles.

As aerosols were used particles of NaF, $CuSO_4.5H_2O$, $NiSO_4.6H_2O$, *malachite green, particulate carbon, and atmospheric aerosol. The Stöber aerosol spectrometer which measures the aerodynamic diameter was used as reference. The median of the aerodynamic diameter was approximately 0.5µm.*

It turned out that the "light scattering diameter" is usually larger than the aerodynamic diameter by a factor ranging from 1.05 to 2.4.

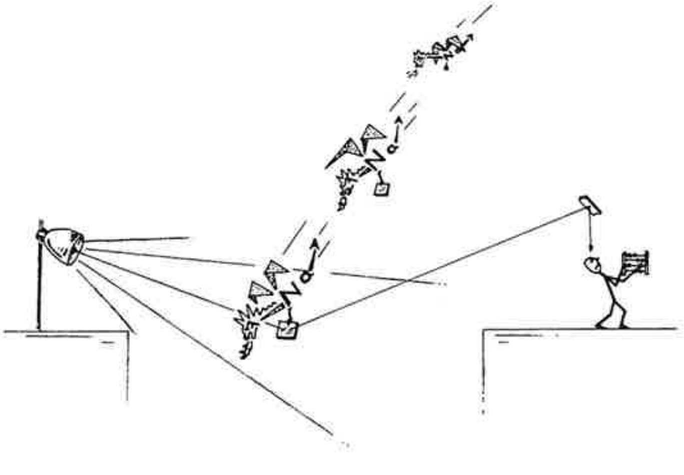

Introduction

In the course of testing the Royco particle counter, model 225, (further called Royco) which is based on light scattering, the response of the device to a variety of aerosols was determined. This was considered of importance as it is known from the Mie theory (1) that the light scattering by small particles is strongly dependent on their refractive index and their absorption coefficient. In addition, this dependence is a function of the way in which the scattered light is collected. According to the theory (1) the influence of the optical properties of the particles can be minimized by collecting the light scattered in the forward direction only. This was the reason for choosing the Royco which has as angles of the light collecting cone 9° and 41°.

The Stöber aerosol spectrometer (STAS) was used as reference device. This instrument seemed very suitable for this purpose, because it is based on a different principle, namely sedimentation under centrifugal forces, and because it has a high resolution. For a short description and literature references for this device see the paper by F. Oeseburg in this issue.

Principle of operation

The principle of operation of the Royco is schematically shown in Fig. 1. With the aid of an incandescent lamp, several lenses and a diaphragm a bright focus is formed. The aerosol particles pass through this focus. The main light beam is intercepted by a light trap. The light scattered by an aerosol particle in a forward direction is led around this light trap with the aid of two lenses (the light trap fits in holes cut in these lenses) and reaches a photomultiplier.

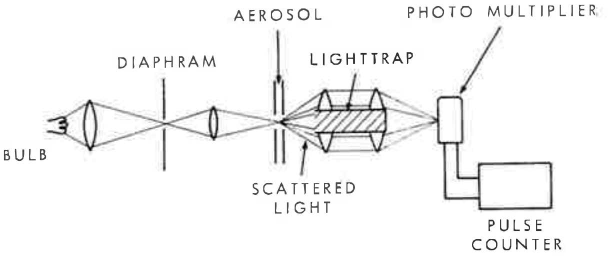

Fig. 1.
Principle of the Royco particle counter, model 225.

The amount of light scattered by a particle is a function of its diameter. Thus, the height of the electrical pulses given by the photomultiplier is a measure for the diameter of the particles. This makes it possible to count the particles by means of suitable electronics in different size classes.

Calibration

The calibration curve for polystyrene spheres (PSL), giving the height of the electrical pulses as a function of the particle diameter, is shown in Fig. 2. The polystyrene latex

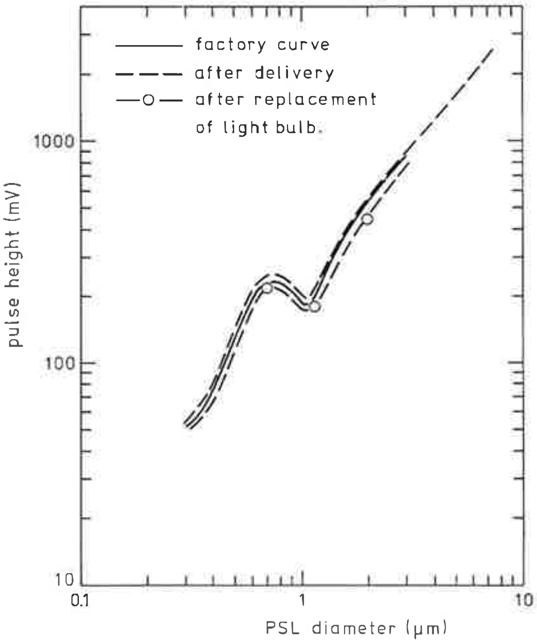

Fig. 2.
Calibration curves of the Royco particle counter, model 225.

was the same material as used for the calibration of the STAS. The refractive index is approximately 1.58; the absorption in the visible region is small and therefore usually neglected.

Fig. 2 also shows the calibration curve as given by the manufacturer. This curve was checked shortly after delivery (2). It was found that the calibration curves agree reasonably well, our pulse heights being somewhat higher. Almost one year later the light bulb had to be replaced and therefore the calibration was checked again. The results were now about 20% lower (in pulse height) and somewhat below the curve of the manufacturer.

Experimental

As test aerosols were used polystyrene latex, NaF, $CuSO_4.5H_2O$, $NiSO_4.6H_2O$, malachite green, particulate carbon, and atmospheric aerosol. All aerosols, except the last one, were generated by nebulizing a solution or suspension of the material in water. After drying an aerosol of solid particles remained.

The measurements with the STAS were evaluated by making microscopic photographs of the deposits and then counting the particles on the photographs (3).

Results and discussion

Fig. 3 and Fig. 4 show the results of the comparison for the different aerosols. The graphs are all presented in the form of a cumulative distribution using such axis as to

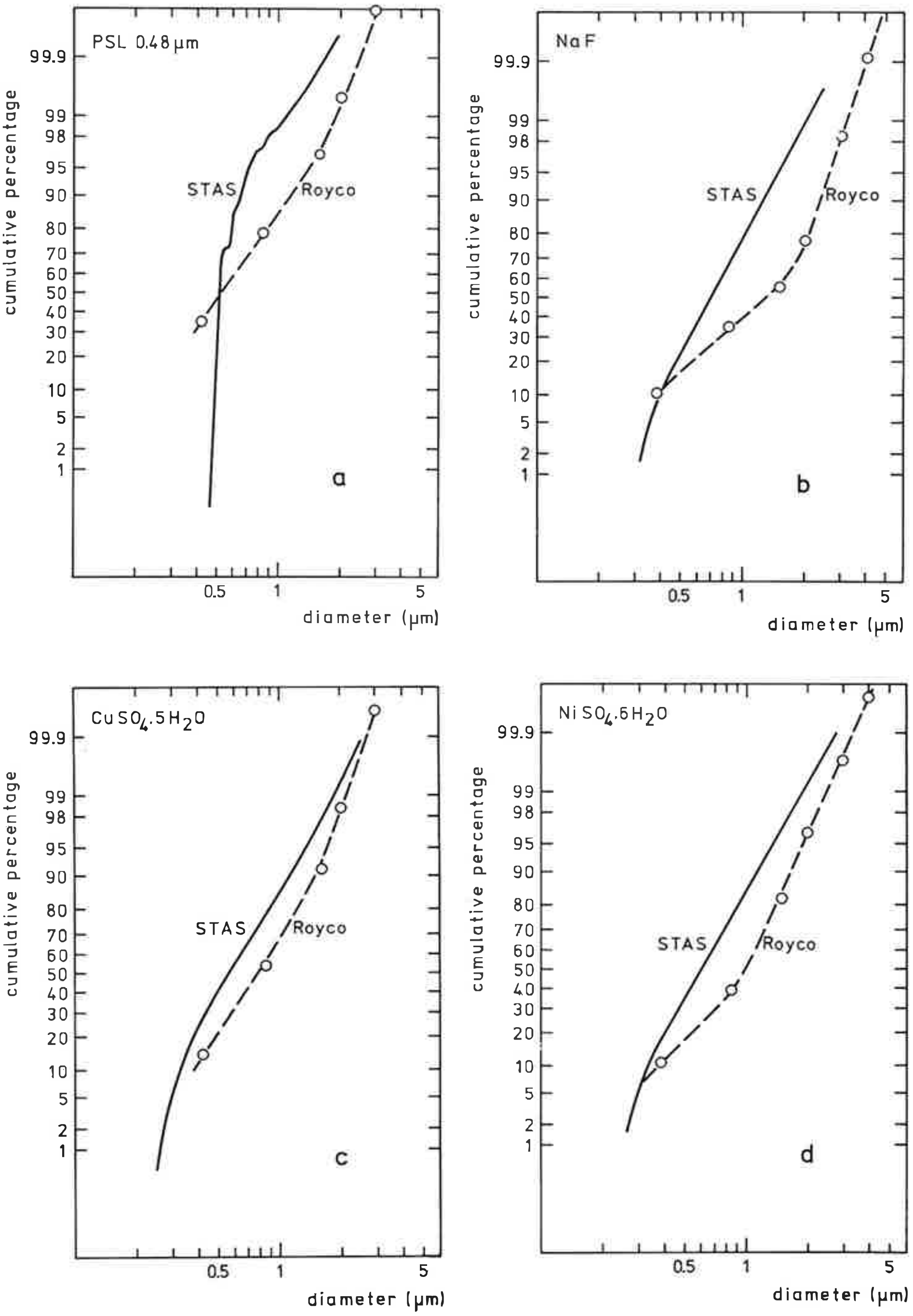

Fig. 3. Comparison of aerosol diameters determined with the Royco particle counter, model 225, and with the Stöber aerosol spectrometer. a. PSL; b. NaF; c. $CuSO_4.5H_2O$; d. $NiSO_4.6H_2O$.

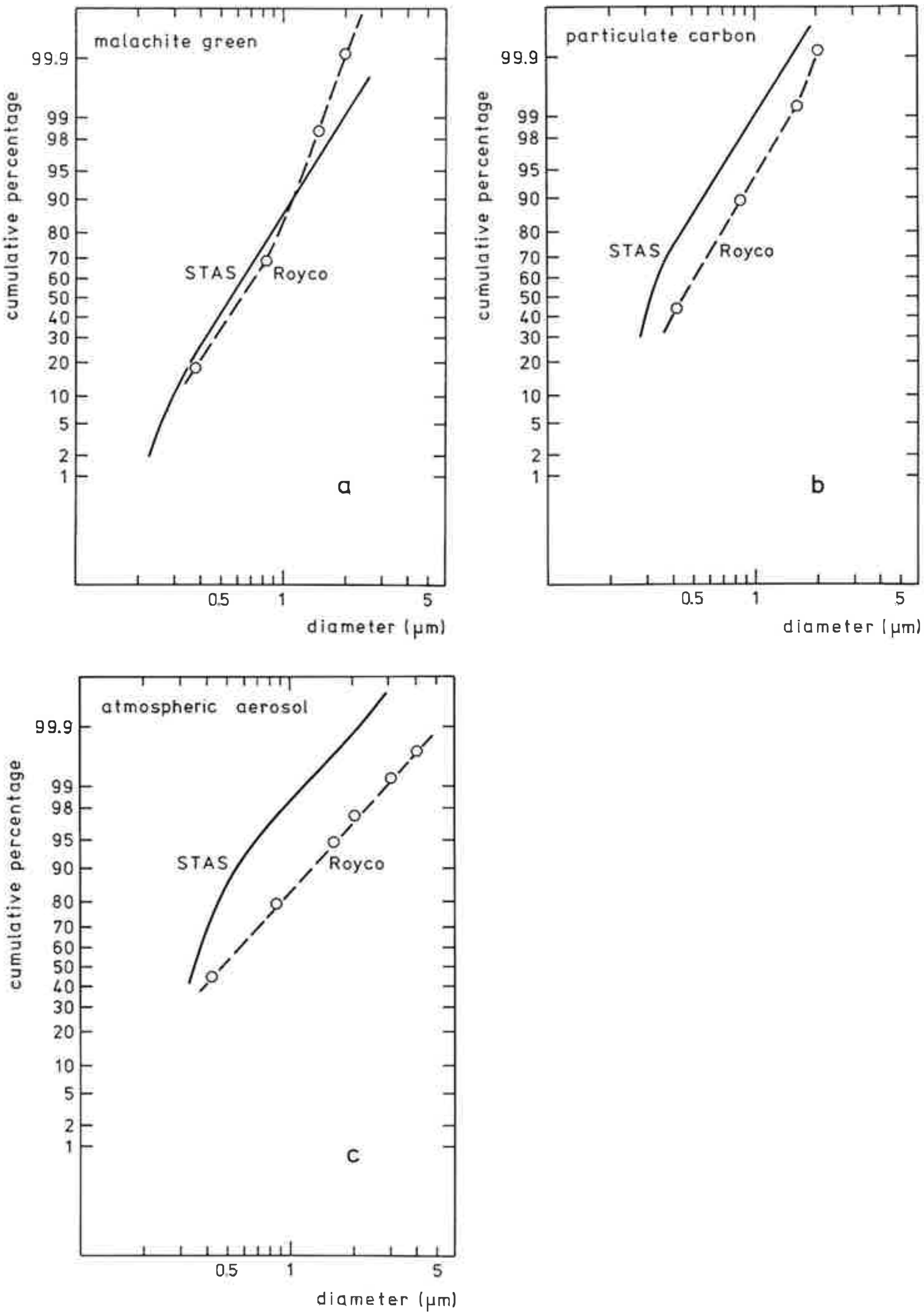

Fig. 4. Comparison of aerosol diameters determined with the Royco particle counter, model 225, and with the Stöber aerosol spectrometer. a. malachite green; b. particulate carbon; c. atmospheric aerosol.

give a straight line for a logarithmic normal distribution. This was done because the limited number of classes used on the Royco does not permit to draw frequency distributions with reasonable accuracy. The diameters for the STAS are given as aerodynamic diameter; those measured with the Royco are given according to the PSL calibration curve. Considering the graphs one must bear in mind that the Royco does not detect particles smaller than 0.3 µm, unless several particles would pass the light spot at the same time. With the STAS it becomes increasingly difficult to count the number of particles as the diameter decreases. This causes uncertainty and thus inaccuracy in the counts of particles smaller than 0.4 µm. Therefore, in generating the aerosols care was taken that not many particles smaller than 0.4 µm were produced. In the case of the atmospheric aerosol the particles in the STAS smaller than 0.3 µm were not counted. Both instruments were calibrated with PSL. In spite of this, Fig. 3a shows that the measured distributions do not coincide. Only the medians of the distribution are the same, as they should be.

The various fractions present in the quasi monodisperse PSL aerosol can be distinguished in the distribution measured with the STAS, whereas this is impossible for the Royco. This is partly due to the limited number of classes used with the Royco, partly to the fact that many particles are counted in the wrong class, because of inhomogeneities of the light spot.

In addition there is another important effect when aggregates are present, as was the case for our PSL aerosol. It is known from theory and demonstrated by Gebhart *et al.* (4) that aggregates of particles such as doublets can scatter four times as much light as single particles, if $d < \lambda$. Depending on the characteristics of the calibration curve such as the derivative and the non-linearity, this can have a large effect on the apparent diameter. Because of the singular form of the calibration curve of the Royco it is to be expected that some doublets can have an apparent diameter up to four times the diameter of a single particle. The effect of doublets on the aerodynamic diameter is much less, because as was observed by Stöber (3), the ratio between the aerodynamic diameter of a doublet and a monoplet is 1.18.

The effect of aggregates can therefore explain that even for PSL the Royco gives a larger apparent diameter than the STAS for a part of the distribution. Figs. 3b, c and d give the results for aerosols without aggregates and with a fairly wide particle size distribution. Despite the fact that these distributions are based on the PSL calibration curve, there exist additional differences in the distributions. The observed differences are therefore mainly attributable to the differences in refractive index and absorption coefficient.

Figs. 4a, b and c give the results for strongly absorbing aerosols. Particulate carbon and atmospheric aerosol do not follow the behaviour of malachite green. As shown by Kattawar (5) the influence of the refractive index for these cases is much smaller. Therefore, these differences have to be attributed to the presence of aggregates in the two aerosols.

Table I gives the measured ratio between the Royco apparent diameter ("Royco diameter") and the aerodynamic diameter, as well as the ratio for the Royco apparent diameter and the equivalent diameter measured for the medians of the distribution.

Table I. Ratio between "Royco diameter" and aerodynamic diameter as well as "Royco diameter" and equivalent diameter at the 50% points of the distributions

type of aerosol	density	$\frac{\text{"Royco diameter"}}{\text{aerodynamic diameter}}$ at 50%	$\frac{\text{"Royco diameter"}}{\text{equivalent diameter*}}$ at 50%
NaF	2.79	1.9	3.2
$CuSO_4 \cdot 5H_2O$	2.28	1.4	2.1
$NiSO_4 \cdot 6H_2O$	1.9	1.7	2.3
malachite green	1.31	1.05	1.2
particulate carbon	1.65	1.5	1.9
atmospheric aerosol	–	2.4**	

* the equivalent diameter calculated as the aerodynamic diameter divided by the square root of the density.

** measured at the right end of the distribution.

Conclusions

The comparison between the Royco particle counter, model 225, and the Stöber aerosol spectrometer, used as a reference, reveals considerable variations in the response of the Royco particle counter to particles of different nature.

Qualitatively the differences may be explained by the differences in the optical properties of the particles and the influence of aggregates. For applications where a high accuracy is desired, the Royco particle counter should be especially calibrated for the aerosol under consideration.

References

1. J. R. Hodkinson, in *Aerosol Science*, (C. N. Davies, ed.), Academic Press, Inc., New York (1964), p. 287.
2. C. J. P. van Buijtenen, Chemical Laboratory TNO, Report 1972-8.
3. W. Stöber and H. Flachsbart, Environ. Sci. Technol. **3**, 1280 (1969).
4. J. Gebhart, J. Bol, W. Heinze and W. Letschert, Staub **30**, 238 (1970).
5. G. W. Kattawar and G. N. Plass, Appl. Opt. **8**, 1377 (1967).

particle size analysis of dioctyl phthalate aerosols using the stöber aerosol spectrometer

F. OESEBURG

Particle size distributions (diameters between 0.5 and 1.7μm) of nearly monodisperse dioctyl phthalate aerosols have been determined with the Stöber aerosol spectrometer. Generally, the distributions observed are not lognormal. This is probably due to an erroneous estimation of the number of small particles as a result of their diminished microscopic visibility and their relatively high rate of evaporation. The standard deviation of the particle size distributions amounts to about 15%.

The particle diameter determined with the higher order Tyndall spectrometer agrees well with the mean of the particle size distribution determined with the Stöber spectrometer.

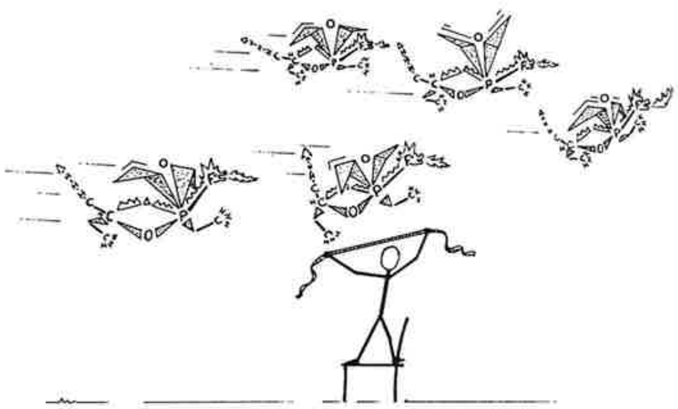

Introduction

Aerosol studies in this laboratory are mainly focussed on problems connected with the protection against toxic aerosols of chemical warfare agents (*e.g.* nerve gases, mustard gas) by means of filtration through fibrous filters (1–4). Because these toxic aerosols are difficult to manipulate they were replaced by an aerosol of dioctyl phthalate (DOP) which is internationally accepted as a standard aerosol for filter testing.

Filter efficiencies are derived from a comparison between the concentration of aerosol before and after passage through the filter. Concentrations are determined using a photometer developed by Clarenburg and Princen (5), which is based on light scattering. The particle size of the aerosol is determined with a higher order Tyndall spectrometer (6). An accurate determination of the particle size is important as both the photometer signal and the filter efficiency are strongly dependent on the particle size. Moreover, Bos (4) showed that generally the accuracy in the filter efficiency determination decreases when the width of the particle size distribution increases.

Prerequisites for an accurate determination of the filter efficiency are both a correct particle size determination and a narrow particle size distribution of the aerosols. Therefore, particle size distributions were determined for a number of DOP aerosols using an aerosol spectrometer recently developed by Stöber (7). Mean particle sizes derived from these distributions were compared with the particle sizes obtained from the higher order Tyndall spectrometer measurements.

Stöber aerosol spectrometer

General description

The settling velocity of aerosol particles under laminar flow conditions depends on their aerodynamic diameter and the centrifugal force field acting on the particles, (this diameter is defined as the diameter of a sphere of unit density attaining at low Reynolds numbers in still air the same settling velocity). This is the physical basis for particle size analysis with the Stöber aerosol spectrometer. Particles are submitted to an increasing force field by transporting them through a spinning spiral duct (Fig. 1). Separation according to the different aerodynamic diameters is achieved by sedimentation on a removable foil, which covers the outside wall of the duct. The place where a particle is deposited (called deposition distance) on the foil is a measure for its aerodynamic diameter. The aerosol is introduced by the aerosol inlet (a) as a thin layer into the clean air flow running from the air inlet (b) through the laminator (c) to the end of the duct (d). Besides by the aerodynamic diameter the deposition distance is also determined by operating conditions such as rotor speed and air flow.

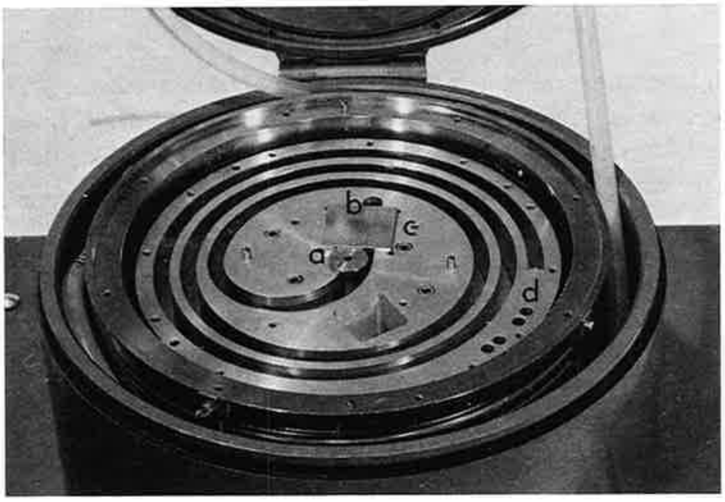

a. aerosol inlet section;
b. clean air inlet;
c. laminator;
d. duct exhaust.

Fig. 1. Uncovered rotor of the Stöber aerosol spectrometer.

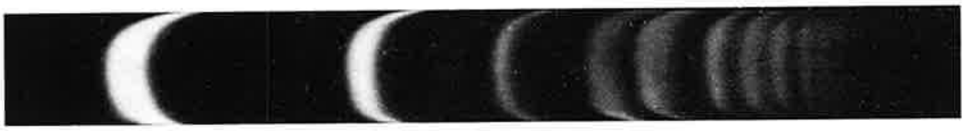

Fig. 2. Deposit of a quasi monodisperse latex aerosol (0.50 μm). Operating conditions: aerosol flow rate 0.1 l/min; total flow rate 7.4 l/min; rotor speed 3360 r.p.m.; slit width 0.3 mm.

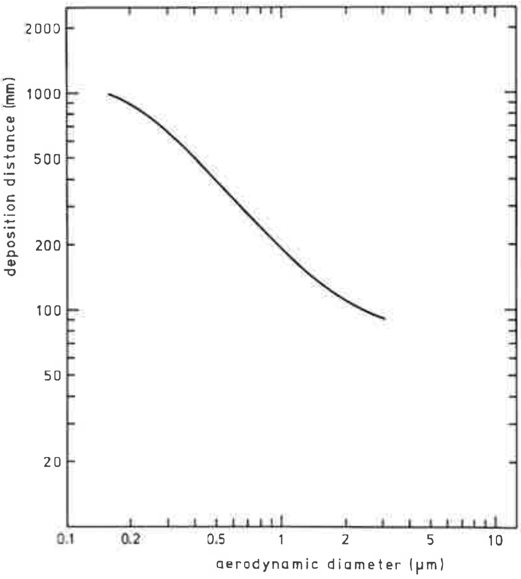

Fig. 3.
Calibration curve of the
Stöber aerosol spectrometer.

Calibration

The relation between the aerodynamic diameter and the deposition distance along the foil is established by calibrating the instrument with quasi monodisperse polystyrene latex aerosols with known diameters. These aerosols consist of a mixture of single latex spheres (monoplets) and of aggregates containing two or more particles (multiplets). They are obtained by nebulizing aqueous suspensions of uniform latex spheres. A photograph of a deposit of such an aerosol (diameter latex spheres 0.50 μm) is shown in Fig. 2. The monoplet and multiplet particles are deposited separately. A practically complete separation is still obtained between particles with diameters of 1.026 and 1.050 μm indicating a high resolution. The corresponding calibration curve is given in Fig. 3.

Analysis

The analysis of the deposits is carried out with a microscope. The particle number distribution along the foil axis is determined as a function of the deposition distance by counting the number of particles present on the photomicrographs. The photographs were taken by means of a Polaroid camera attached to a Leitz Ortholux microscope (incident illumination; magnification 500 ×). Subsequently, the particle size distribution is calculated according to a procedure described by Stöber (8).

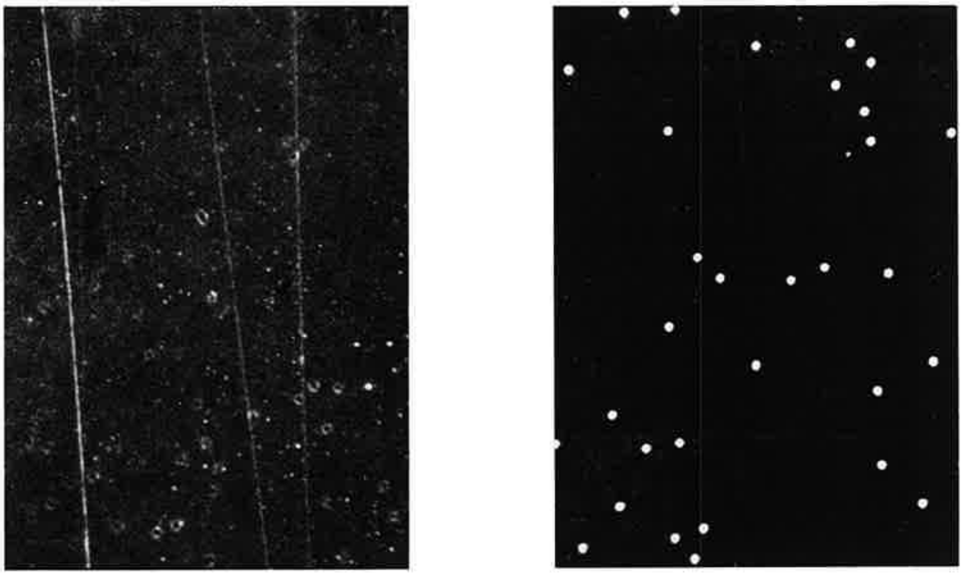

non-coated foil coated foil

Fig. 4. Photomicrographs of deposits of 1.0 μm DOP aerosols (magnification 500 ×).

Experimental difficulties

Particle size analysis of liquid aerosols using sedimentation techniques are affected by spreading of the collected liquid particles resulting in a decrease in microscopic visibility, and evaporation of the collected particles giving too low numbers for the smaller diameter particles.

Spreading of the liquid particles may be prevented effectively by coating the foil with a fluorocarbon compound (FC 134 from the 3M Company, Minnesota). Photomicrographs of a deposit of a DOP aerosol on a non-coated and on a coated foil are given in Fig. 4. The rate of evaporation of the collected particles was calculated by considering them as free droplets in still air. This assumption seems reasonable as the evaporation is roughly proportional to the droplet surface, and it turned out from a comparison of the radii of polystyrene spheres with the radii of DOP spheres with identical aerodynamic diameters that the surface of the particles in contact with air does not alter very much on sedimentation. Using a formula derived by Klein Nagelvoort (9) the half-life time of particles was calculated for a number of initial particle diameters. The graph showing the relation between half-life time and the initial particle diameter is given in Fig. 5. When the photomicrographs are taken in approximately one hour evaporation only plays a part in the analysis of aerosols with particles smaller than about 0.35 µm.

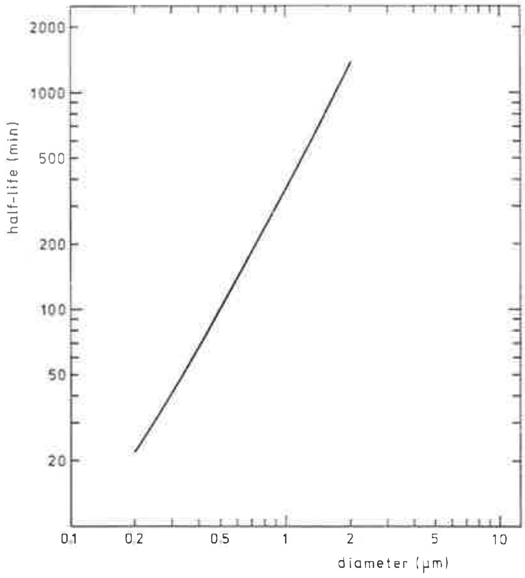

Fig. 5.
The half-life time of an evaporating aerosol particle as a function of the initial diameter.

Experimental

Aerosols of DOP with mean diameters ranging from 0.5 up to 1.7 µm were generated with a modified type La Mer generator, developed by Lassen (10). Aerosols were introduced into the higher order Tyndall spectrometer (6) and the diameter was derived from the observation angles of the first, second and third order spectral red bands with the aid of a calibration curve reported by Berner (11). The aerosols were likewise introduced into the Stöber aerosol spectrometer. The operating conditions were: aerosol flow rate 0.1 l/min, total flow rate 7.4 l/min, rotor speed 3360 r.p.m., and slit width 0.3 mm. After collection about 20 photomicrographs were taken at different deposition distances. These were assessed according to the procedure described earlier in this paper. In order to avoid statistical errors, care was taken to ensure that the number of particles, present on the photomicrographs, was not too low. Because coalescence leads to counting errors, high particle numbers were also avoided. Generally, the sampling time was chosen such that the maximum particle number per photomicrograph varied between 200 and 800. Photomicrographs at large deposition distances were taken first in order to diminish the influence of evaporation.

Results and discussion

The mean ($\bar{d}$) of the particle size distribution, the standard deviation (σ), which is a measure for the width of the particle size distribution, and the relative standard deviation ($\sigma/\bar{d}$) were calculated (Table I). The cumulative particle size distributions were calculated using standard methods, and were plotted on logarithmic normal probability paper. It was found that the graphs obtained in four experiments only can be represented by straight lines, indicating that in these cases the particle size distributions are probably logarithmic normal. A typical example is given in Fig. 6 (graph a).

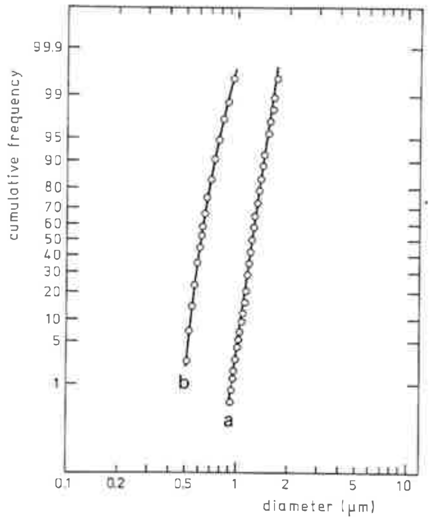

Fig. 6.
Cumulative particle size distributions of DOP aerosols.

In these cases the observations are in agreement with results reported in the literature (12). The graphs obtained in the other experiments are generally convex to the diameter axis (Fig. 6; graph b) indicating a shortage in the number of small particles.

Possible causes of this deficiency are evaporation and the limited microscopic visibility of small particles, which is due to the limited resolving power of the microscope and, probably to a larger extent, to the contamination of the foil as a result of the coating. As was shown before in this paper evaporation plays only a part in case of particles smaller than about 0.35 μm. However, these particles were not present in the aerosols used in this study. Obviously the former calculations are questionable. Therefore, the evaporation of collected DOP particles was studied experimentally. A preliminary analysis showed that the calculated evaporation rate is significantly lower than the rate found in experiments.

Table I illustrates that the aerosols investigated in this study are slightly hetero-

Table I. Results of the particle size analysis of DOP aerosols obtained with the Stöber aerosol spectrometer

experiment number	$\bar{d}$ (μm)	σ (μm)	$\sigma/\bar{d}$
A18	0.615	0.10	0.16
A22	0.63	0.09	0.13
A19	0.66	0.10	0.16
A21	0.70	0.09	0.13
A10	0.75	0.09	0.12
A13	0.775	0.11	0.15
A4	0.855	0.14	0.16
A12	0.925	0.14	0.15
A8	0.97	0.14	0.14
A9	1.035	0.14	0.14
A11	1.235	0.16	0.13
A3	1.235	0.14	0.12
A17	1.63	0.49	0.30
A16	1.69	0.49	0.29

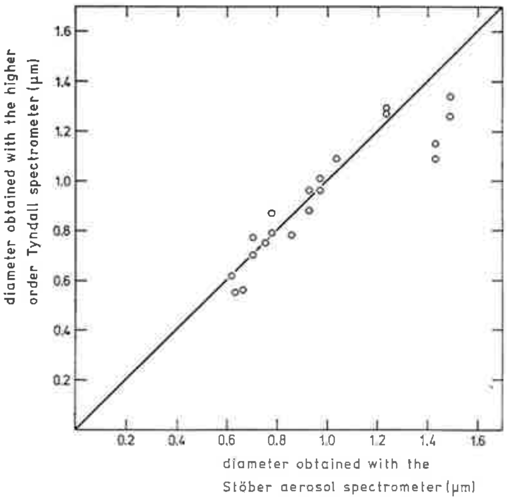

Fig. 7.
Comparison of the higher order Tyndall spectrometer with the Stöber aerosol spectrometer.

disperse. Relative standard deviations amounting up to 0.16 μm are obtained. Large standard deviations are obtained in the experiments A16 and A17. However, the aerosols used in these experiments showed distinct spectra in the higher order Tyndall spectrometer. There is evidence from the literature (11–14) that aerosols show spectra only if the standard deviation of the particle size distribution is smaller than 0.10–0.20 μm. The standard deviations obtained in the experiments A16 and A17 are much higher. Obviously, some experimental errors are made.

The particle size measured with the higher order Tyndall spectrometer is compared with the particle size obtained with the Stöber spectrometer. Fig. 7 illustrates that a good agreement is obtained between the measurements with the two spectrometers. Only large deviations were encountered at particle sizes of about 1.6 μm, which are probably due to the errors made in the experiments A16 and A17.

Concluding remarks

The DOP aerosols used in the filtration studies were slightly heterodisperse. The relative standard deviation of the particle size distribution amounted to 15%.

A satisfactory agreement was found between diameters obtained using the higher order Tyndall spectrometer and the Stöber aerosol spectrometer.

References

1. L. A. Clarenburg and J. F. van der Wal, Ind. Eng. Chem. Process Des. Develop. **5,** 110 (1966).
2. J. F. van der Wal and L. A. Clarenburg, Chemical Laboratory TNO, Report 1967-4.
3. J. F. van der Wal, Chemical Laboratory TNO, Report 1968-18.
4. A. Bos, Chemical Laboratory TNO, Report 1969-18.
5. L. A. Clarenburg and L. H. Princen, Staub **23,** 234 (1963).
6. D. Sinclair, in *Handbook on Aerosols*, Atomic Energy Commission, Washington D.C. (1950), p. 97.
7. W. Stöber and H. Flachsbart, Environ. Sci. Technol. **3,** 1280 (1969).
8. W. Stöber, H. Flachsbart and C. Boose, J. Colloid Interface Sci. **39,** 109 (1972).
9. R. Klein Nagelvoort, Report Reactor Institute Delft, (1968).
10. L. Lassen, Z. angew. Phys. **12,** 157 (1960).
11. A. Berner, Thesis, Wien (1964).
12. N. A. Fuchs and A. G. Sutugin, in *Aerosol Science* (C. N. Davies, ed.), Academic Press, London (1966), p. 1.
13. G. G. Goyer and F. D. Pidgeon, J. Colloid Sci. **11,** 697 (1956).
14. S. Kitani, J. Chem. Soc. Jap., Pure Chem. Sect. **77,** 1181, 1621 (1956).

the determination of sarin adsorption isotherms on carbon black using a tracer technique

J. MEDEMA and J. J. G. M. VAN BOKHOVEN

A method for the determination of adsorption isotherms of organophosphorus compounds was developed. The method is based on the determination of the quantity adsorbed using radioactive labeled compounds. Isotherms of a typical organophosphorus compound, isopropyl methylphosphonofluoridate (sarin), on Spheron 6 (carbon black) and on Spheron 6 impregnated with chromium oxide were determined.

Isotherms on impregnated carbon blacks appeared to be not well-defined because of sarin decomposition. The heat of adsorption on pure Spheron 6 was calculated from isotherms determined at different temperatures.

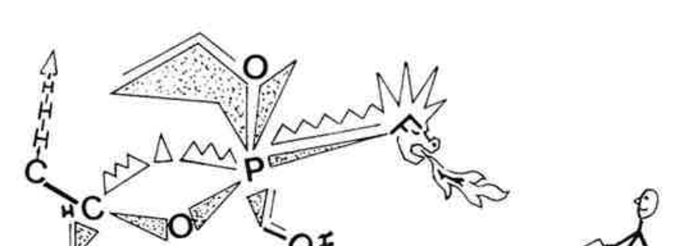
O
C
C
O
P
F
C

Introduction

In the context of a study on the possibilities of catalytic decomposition of organophosphorus compounds (nerve agents) adsorbed on active carbon it is useful to have a reliable method for the determination of the adsorption isotherms of these compounds. Active carbons, like charcoal, normally have a high specific surface area and a microporous structure. The latter causes difficulties in kinetic measurements due to slow diffusion. In order to avoid these problems a macroporous carbon black, Spheron 6, was chosen as a model for active carbons. As adsorbate a typical organophosphorus compound, isopropyl methylphosphonofluoridate (sarin), was chosen.

Adsorption isotherms are generally determined by means of volumetric or weighing techniques. In the case of sarin the volumetric technique fails because of long equilibration times and inaccurate pressure measurements. The corrosive properties of sarin make the application of an adsorption balance impossible. Therefore, a new method for the determination of the quantity adsorbed was developed. This method is based on the measurement of the radioactivity emitted by adsorbed ^{32}P labeled sarin, and on the conversion of radioactivity in terms of quantity adsorbed by means of a calibration procedure. Isotherm measurements were performed by keeping the pressure at definite values until equilibrium was reached.

From isotherms measured at different temperatures the heat of adsorption may be calculated. The influence of impregnation of carbons with chromium oxide upon the adsorption isotherms can be deduced from isotherms determined on Spheron 6 samples impregnated with various quantities of chromium oxide.

Experimental

Apparatus

The apparatus (shown schematically in Fig. 1) consists of a rotary pump (A) and a mercury diffusion pump (B) connected to a vacuum tube via a liquid nitrogen trap (C). The pressure is measured by means of a Penning tube (D) or a thermistor pressure gage (E) connected to the vacuum tube at two different points. In addition there is a connecting point for the sarin dosing vessel (F) and a connecting point for the adsorption cell (G). All connecting points consist of ground glass joints and are fitted with

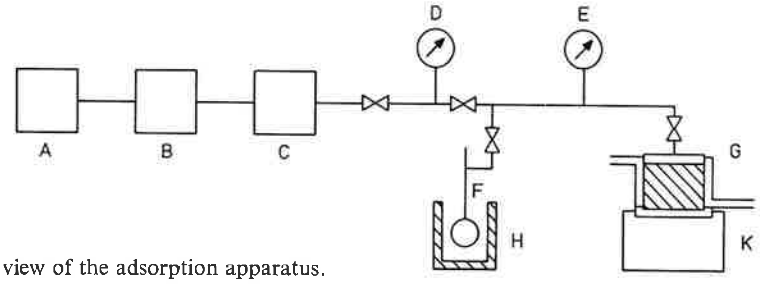

Fig. 1. Schematical view of the adsorption apparatus.

valves. Moreover, a valve is situated between the pumping part and the adsorption part of the apparatus.

The sarin dosing vessel (F) consists of a tube with two ports, one for refilling the tube with sarin and the other for connection to the apparatus. The sarin in the tube is kept at a constant temperature, lower than that of the adsorbent, by means of a Peltier cooling unit (H) with adjustable power supply. Temperature instalments between −25 °C and +25 °C are possible corresponding to sarin vapour pressures of 0.06 and 3 Torr, respectively.

The adsorption cell (G) together with the Geiger-Muller (G.M.) counter (K) is shown schematically in Fig. 2. During an experiment the adsorption cell is kept at a constant temperature between 20 and 40 °C by means of thermostated water flowing through the jacket. The G.M. counter is placed with its window in contact with the bottom of the cell as closely as possible. To reduce absorption of the radiation the bottom of the cell has been made very thin. During the experiments the positions of the cell and the counter are fixed in order to maintain the geometry. The background of the G.M. counter is lowered by shielding the tube with lead.

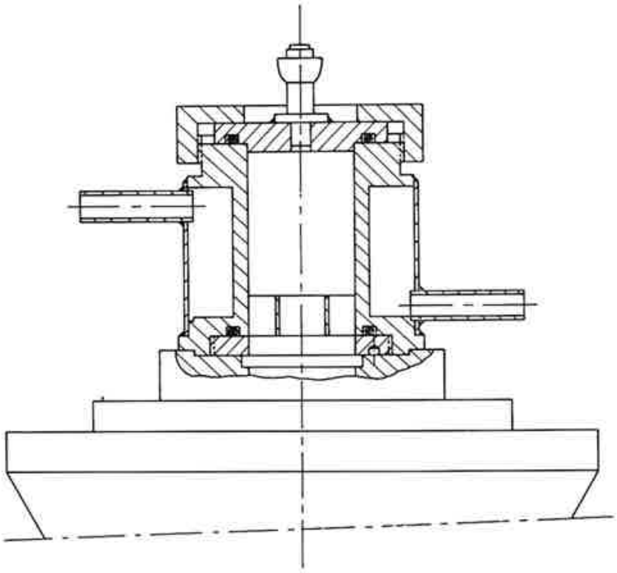

Fig. 2.
Adsorption cell with counter.

Calibration

By keeping the liquid sarin at a chosen temperature a definite sarin pressure is obtained. The relation between vapour pressure and temperature is taken from an earlier report (1).

After equilibration the measured radioactivity is directly proportional to the quantity adsorbed. The proportionality factor is obtained by comparison of the total number of counts for the last measuring point with the quantity of sarin analyzed after extraction of the adsorbent. The extracted quantity sarin was determined according to a procedure described before (2). By means of the proportionality factor it is possible to calculate the quantity adsorbed. As a matter of fact the measured radioactivity was corrected for background, dead time of the counter and decrease in specific activity as a result of the decay of ^{32}P.

Radioactive labeled sarin

^{32}P labeled sarin was prepared by the Organic Section according to a procedure described by De Borst (3). The specific activity was approximately 25 µCi/g. The half-life time of ^{32}P is 14.5 days.

Adsorbant

Commercial Spheron 6 (obtained from Cabot, France) was washed with acid to remove iron and other contaminants. Before use the samples were dried at 120°C; specific surface area was 115 m^2/g. Samples were impregnated with chromium trioxide from aqueous solutions according to a procedure described before (4).

Procedure

Before starting an adsorption experiment the adsorbent is evacuated until the pressure is lower than 10^{-4} Torr. Then, all valves are closed and the increase in pressure in the different parts of the apparatus due to leakages or desorption is measured during several hours. If the increase in pressure does not exceed 0.005 Torr/h, the adsorbent is exposed to sarin at the lowest temperature, followed by measurement of the radioactivity introduced into the adsorption cell. When the corrected counting rate does not increase during one day, it is assumed that equilibrium has been established. Then, the temperature of the dosing vessel is increased and the radioactivity is measured again until equilibrium is reached. This procedure is repeated until the highest desired vapour pressure is reached. Sometimes it was necessary to remove air that had leaked in during the measurements. This was done simply by evacuating the adsorption part of the apparatus, however, this procedure disturbs the equilibrium between adsorbed and gasphase sarin. Therefore, after evacuation it was checked if equilibrium had been re-established. At the end of the measurements the adsorption cell is evacuated in order to remove gaseous sarin. After evacuation the radioactivity is measured again. In most cases the desorption is negligible. Then, the adsorption cell is disconnected from the vacuum system and the adsorbent is removed to an extraction apparatus in which sarin is extracted with methylisobutylcarbinol (MIC).

Results and discussion

In Fig. 3 three isotherms of sarin on Spheron 6 determined at different temperatures are shown. The isotherm determined at 20.5°C is constructed from the results of two independent measurements. As a result of inaccuracies in the calibration procedure (mainly the chemical analysis) there exists a systematic difference (approximately 5%) between the two measurements. We were not able to avoid these inaccuracies in the calibration procedure. Therefore, in all isotherms a systematic error is present.

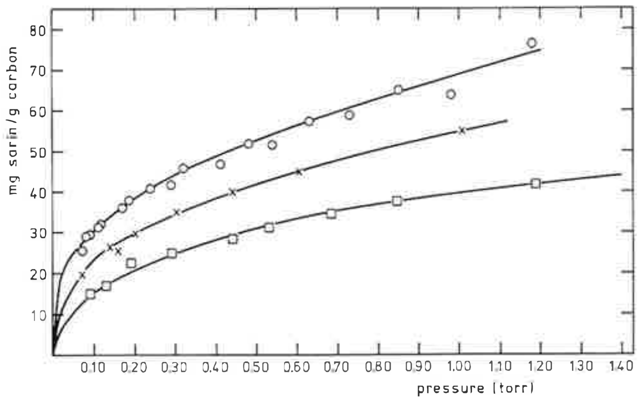

Fig. 3.
Adsorption isotherms of sarin on Spheron 6 at different temperatures.

○ = 20.5 °C;
× = 28 °C;
□ = 39 °C.

From the isotherms given in Fig. 3 it is possible to calculate the heat of adsorption with the aid of the relation:

$$\left(\frac{\partial \ln p}{\partial T}\right)_{\theta} = \frac{q_{st}}{RT^2}$$

where p represents the equilibrium pressure, T the absolute temperature, θ the degree of surface coverage, and q_{st} the isosteric heat of adsorption. At surface coverages between 25 and 45 mg sarin/gram Spheron 6 the heat of adsorption appeared to be 15 kcal/mol. The results are not accurate enough to see an influence of surface coverage on the heat of adsorption, anyhow, this influence must be small. This is not surprising because the surface coverage varied between 40 and 75% of a monolayer, a region in which the heat of adsorption usually does not change very much. The value of 15 kcal/mol agrees well with the heat of adsorption found in calorimetric experiments carried out in this laboratory.

Isotherms determined on Spheron 6 impregnated with chromium oxide are given in Fig. 4; the higher the chromium content the lower the position of the isotherm. This phenomenon cannot be ascribed to:

1. a reduced surface area because the specific surface of Spheron 6 hardly changes on impregnation,
2. systematic inaccuracies in the calibration, or
3. decreased adsorption capacity as a result of impregnation.

However, a possible explanation may be that not all adsorbed sarin is extracted from impregnated carbon as was found in some experiments. It might well be possible that decomposition occurs and that the remaining decomposition products are adsorbed very strongly. Moreover, one may expect that the reaction products influence the shape of the isotherm.

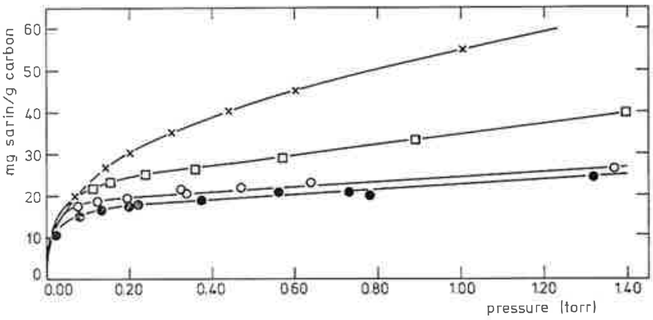

Fig. 4.
Adsorption isotherms of sarin on impregnated Spheron 6 at 28 °C.

× = 0% Cr;
□ = 1.0% Cr;
○ = 5.2% Cr;
● = 9.7% Cr.

As can be seen in Fig. 4 the shape of the adsorption isotherm indeed changes upon impregnation. This change, however, might be due also to a change in heat of adsorption. In fact, the steep rise of the adsorption isotherms at low values of the relative pressure (the decomposition in this region is probably small) points to the conclusion that the increase in heat of adsorption causes the change in the shape of the isotherms.

The extremely slow adsorption of sarin on Spheron 6 (equilibration for each point takes at least three days) induced us to study the mobility of the sarin molecules through the carbon bed. An example of the measurements is given in Fig. 5. In this experiment sarin was dosed during a short time (15 min) into the adsorption cell. The molecules appeared to adsorb first in the upper Spheron 6 layer. The counting efficiency of this part of the Spheron bed is low due to absorption of beta-radiation in the underlying carbon layers and less favourable geometry towards the counter.

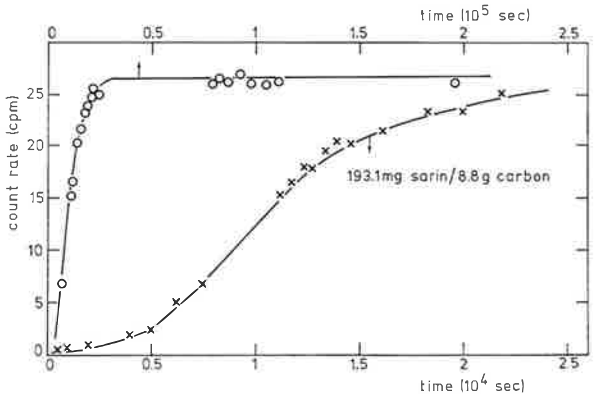

Fig. 5.
Count rate as a function of time for a small dosage of sarin.
The two curves represent the same experiment on two differently scaled time axes.

Without further dosage of sarin the radioactivity increased continuously indicating that sarin molecules move downwards through the bed. Then, after approximately 10 hours, the count rate became constant. The Spheron bed was now divided into several fractions and the quantity of sarin extracted from each fraction was determined. These determinations revealed that sarin was homogeneously distributed throughout the carbon bed. Similar experiments with impregnated carbons showed that sarin molecules are much less mobile on these impregnated surfaces. A more or less immobile type of adsorption on impregnated surfaces is in agreement with the increase in heat of adsorption as deduced from the isotherms.

Because the actual adsorption isotherm is not known and because the mobility experiments showed an immobile type of adsorption the conclusions concerning impregnated samples are only tentative. In the near future an attempt will be made to measure adsorption isotherms under circumstances where decomposition is prevented (rapid equilibration, low temperature).

References

1. E. Neale, Porton Technical Paper No. 341, C.D.E.E., Porton, England (1953).
2. B. Gekauf *et al.*, Anal. Chem. **29**, 278 (1957).
3. C. de Borst, Chemical Laboratory TNO, Report 1973-5.
4. H. Cuppers and J. J. G. M. van Bokhoven, Chemical Laboratory TNO, Report 1970-10.

microcalorimetric determination of sarin decomposition catalyzed by alumina

J. J. G. M. VAN BOKHOVEN and J. MEDEMA

A microcalorimetric technique is employed to determine the kinetics of sarin decomposition on alumina. This technique offers the possibility to measure the reaction rate continuously.

The experimental rate curves are explained with the aid of a model in which a distribution in the activation energy for the decomposition is assumed. Indications for the nature of the catalytic active sites are obtained.

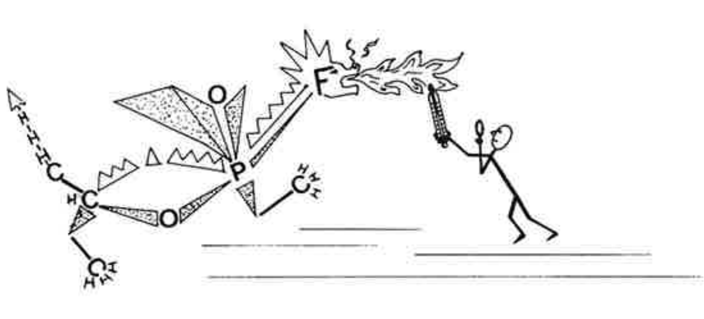
O
F
P
C
O
H

Introduction

Heterogeneous catalytic decomposition of sarin (isopropyl methylphosphonofluoridate) over alumina takes place mainly via two different reactions, so-called dealkylation and defluoridation. Defluoridation is the replacement of the fluorine atom by a hydroxyl group in a hydrolysis process. Dealkylation results in the formation of propene from the ester group. Investigations have shown that the dealkylation is strongly hampered by water vapour; on the other hand, defluoridation is favoured by water. Therefore, it seems most suitable to base a catalytic process for the removal of sarin from contaminated air, which always contains water, on the defluoridation reaction. In order to optimize the catalytic system it is necessary to obtain information concerning the kinetics and mechanism of the defluoridation process. The decomposition products are hydroxysarin (isopropyl methylphosphonic acid) and hydrogen fluoride. Both species strongly adsorb onto the surface of the catalyst. Therefore, in this case a quantitative determination of the reaction products by extraction is not reliable for kinetic measurements.

Microcalorimetry has proved to be an adequate technique for kinetic measurements of the defluoridation reaction in the system sarin/catalyst. Microcalorimetry is applicable to all types of reactions providing the accompanying heat production is large enough to be determined accurately.

Reaction rate and heat production are related by the equation:

$$\dot{Q} = \frac{\mathrm{d}c}{\mathrm{d}t} \cdot \Delta H_r$$

where $\dot{Q}$ represents heat flow or heat production, $-\mathrm{d}c/\mathrm{d}t$ reaction rate, and ΔH_r reaction enthalpy.

A disadvantage of this technique may be that every phenomenon causing a heat effect is detected. When two or more heat effects occur simultaneously, it is necessary to make additional assumptions with respect to the shape and the intensity of the separate signals in order to distinguish between the kinetics of different processes.

In the sarin/adsorbent system there is an overlap of adsorption and reaction processes; this lasts only during the first few minutes, however, and is therefore not important.

Another more important complication originates from the limited response velocity of the microcalorimeter, which is a result of thermal inertia. Sharp peaks tend to become blurred. In the sarin decomposition experiment sharp peaks are only caused by the adsorption process. The slope of the reaction rate curve is too flat to be deformed.

In this paper attention will be paid to the rate of decomposition of sarin on the pattern catalyst alumina derived from heat flow curves which are exclusively due to heat of reaction and which are not deformed. In order to establish the complete kinetics of the decomposition it is necessary to obtain information from the blurred part of the curves.

A procedure to correct for the deformation by thermal inertia is under development now.

Experimental

The calorimeter, which has been described before (1), is schematically shown in Fig. 1. Some changes in the original design have been made. One of them is the replacement of the stainless steel reaction vessels by thin walled copper ones, responding much faster. Another improvement is the registration of the heat flow on paper punch tape, which enables us to plot graphs on the scope output of a computer. Moreover, the possibility to pretreat the samples outside the calorimeter (evacuation and heating) without having to expose it to open air again was introduced.

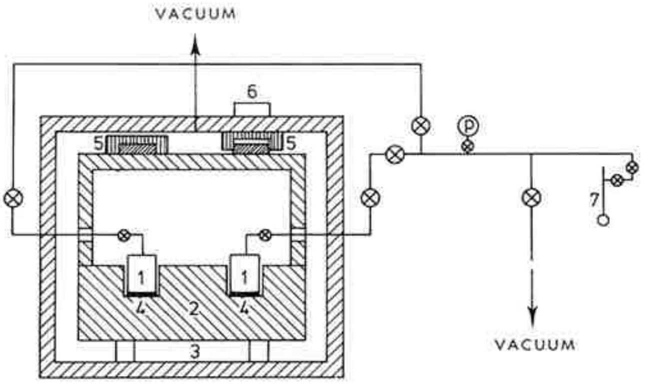

Fig. 1.
A schematic representation of the microcalorimeter. During an experiment it is immersed in a thermostat.

1. reaction and reference vessel
2. aluminium block
3. vacuum isolation
4. heat flow detector
5. heat conductance disc
6. magnet to handle 5
7. dosing vessel

Experiments were carried out according to the following procedure:

1. reaction and reference vessel were filled with an equal quantity of adsorbent,
2. after a pre-treatment the vessels were positioned onto the heat flow detectors and the system was evacuated to 10^{-4} Torr,
3. after temperature equilibration sarin was dosed to the adsorbent at a pressure of 2.5 Torr; the quantity adsorbed was determined from the loss of weight of the dosing vessel; correction for the quantity of sarin that remained in the gasphase was made, and
4. the heat flow signal was registrated for a period of one day or longer; in none of the cases the heat flow had fallen below the detection limit when the experiment was stopped.

Experiments were carried out with different quantities adsorbed on samples that had been evacuated at 80 °C or at room temperature. Most experiments were performed with alumina as adsorbent. Preliminary experiments with samples of carbon black impregnated with chromium oxide were done.

Results and discussion

The experimental heat flow curve of a sarin adsorption experiment onto alumina is shown in Fig. 2. A relatively high signal immediately after adsorption drops in about 500 minutes to a 10^4 times lower level. The main part of the high starting signal must be ascribed to heat of adsorption. Comparison with the heat flow curves obtained from similar adsorption experiments with vapours that do not react after being adsorbed (*e.g.* cyclohexane) showed that 200 minutes after the start the heat flow signal caused by adsorption alone, has become lower than the detection limit.

Fig. 2.
A linear plot of the heat evolution of sarin adsorption and decomposition on alumina, a. large scale; b. small scale (pre-treatment: vacuum at 25 °C; 253 mg sarin on 5.0 g alumina).

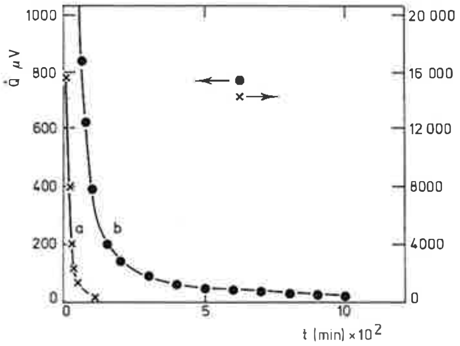

Thus, the curves obtained in sarin adsorption experiments show after 200 minutes exclusively the heat of reaction. Because the slope of this curve is small, the thermal inertia of the microcalorimeter does not influence this slope.

In order to deduce the reaction order from the experimental curve several relations were tried. It appeared that the time functions belonging to zero, first, second or third order kinetics did not fit the experimental rate curves. It was also impossible to fit the curves with formulas in which poisoning effects were introduced. Moreover, description of the rate curves with consecutive reactions fitted the experimental curves reasonably well but in this case it appeared that the rate constant derived in this way depends on the time at which the experiments were stopped. Thus, none of the time functions that could be expected on the basis of normal chemical kinetics could fit the experimental curves satisfactorily.

It was found that a plot of rate *versus* $1/t$ yields a perfect straight line for $t \geqslant 200$ min (Fig. 3).

This kind of kinetics is also found in adsorption processes (2), and is usually presented in the integrated form: the quantity adsorbed *versus* logarithm of time.

Several models have been constructed to explain these so-called Elovich kinetics in adsorption (2). All these models assume a variation in the basic parameters of adsorption, the number of sites or the activation energy for adsorption. One of these models, described in detail by Peers (3), assumes a distribution in activation energy for adsorption. When this feature is employed for the reaction of adsorbed sarin this essentially means that the reaction rate constant is no longer considered to be constant. The model described below, containing this feature is able to explain the linear relationship between the reaction rate and $1/t$. Some additional assumptions have to be made in order to complete the reaction model from which the linear relation between rate and reciprocal time may be derived mathematically.

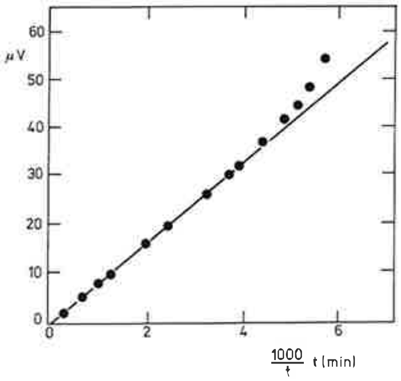

Fig. 3.
Reaction heat production as a function of reciprocal time.

1. Sarin molecules are adsorbed in an immobilized state; this seems to be very probable because a long time after adsorption the molecules are still inhomogeneously distributed over the exposed surface.
2. Decomposition is first order in sarin and zero order in other reactants (*e.g.* water).
3. There is a distribution in activation energy for the decomposition reaction.
4. The enthalpy of reaction is equal for all molecules.
5. Additional heat effects arising from accompanying phenomena which are fast in comparison with the defluoridation (consecutive reactions, desorption of reaction products, *etc.*) need not be precluded because they do not change the shape of the experimental curve.

The total rate of reaction is composed of the reaction rates on the different parts of the surface (patches) with different activation energies. The contribution to the total rate of reaction from a patch of the surface with activation energy E is given by:

$$-\frac{\mathrm{d}C_E}{\mathrm{d}t} = K_0 e^{-E/RT} \cdot C_E$$

where C_E = concentration of sarin adsorbed on this patch
t = reaction time
K_0 = frequency constant
E = activation energy

The total rate is found by integrating over all actual activation energies:

$$\text{rate} = \int_{E_1}^{E_2} -\frac{\mathrm{d}C_E}{\mathrm{d}t}\mathrm{d}E$$

E_1 and E_2 are the extreme values of the activation energy. If it is assumed that all activation energies in between E_1 and E_2 occur equally frequently, it appears that:

$$\text{rate} = \frac{RTC_0}{E_2-E_1}\frac{1}{t}(e^{-K_2t}-e^{-K_1t})$$

where K_1 and K_2 are the reaction rate constants corresponding to E_1 and E_2. If K_1 is sufficiently large and K_2 sufficiently small, there is a time interval in which one exponentional (e^{-K_1t}) becomes practically zero whilst the other (e^{-K_2t}) still hardly deviates from one. In this interval the rate becomes proportional to $1/t$. This is in accordance with the experimental rate curve. A remarkable feature of the rate expression is the slight temperature dependence. In the interval where the sum of the exponentials is one, the rate is proportional to the absolute temperature. In normal kinetic models it is always found that the rate depends on the temperature in an exponentional form. Preliminary experiments at different temperatures have shown that the time interval in which the linear relationship is obtained changed with temperature but that the rate in these intervals is indeed only slightly dependent on temperature.

Values for K_1 and K_2 can be derived from the deviations the experimental curve shows from the $1/t$ plot at small respectively large t, *i.e.* in the regions where the exponentionals start to differ markedly from zero respectively one. However, in our experiments the deviations at both sides are not visible; for large t the total rate is small and consequently the heat flow is measured less accurately and for small t the heat of adsorption overlaps the heat production of the reaction.

Nevertheless, it is possible to calculate a lower limit value for K_1 in terms of a half-life of molecules on the most active sites. This half-life appeared to be half an hour, to all intents and purposes it may be less.

So far it can only be guessed which type of surface sites is responsible for the decomposition reaction. Experiments have shown that the decomposition proceeds through a defluoridation reaction. This is in fact a hydrolysis reaction which is enhanced by acid or basic sites. If this reaction pattern is correct then the assumption about the existence of a distribution in activation energy becomes very plausible, because it is a well known fact that the acidity and basicity on the alumina surface show a distribution in strength (4).

Some preliminary experiments were carried out with carbon black, which showed no decomposition at all. When carbon was impregnated with chromium oxide a heat flow curve was observed which decreased proportionally with reciprocal time. This indicates that supported chromium oxide contains an ensemble of active sites that is similar to that of alumina. Because chromium oxide possesses, like alumina, acid as well as basic sites, comparison of these oxides does not allow of distinction between the two types of sites. Therefore, a study with catalysts possessing a definite acid or basic character is required.

Conclusions

The kinetics of sarin decomposition on an alumina surface are described by a proportional relation between rate and reciprocal time. These kinetics resemble the Elovich-kinetics of adsorption processes. If it is assumed that there is a distribution in the activation energy for defluoridation, it is possible to form the correct time equation for the rate of decomposition.

It is still uncertain which type of sites are active; the existence of a distribution in activity on the one hand and in basicity and acidity on the other hand suggests the hypothesis that either acid or basic or both types of surface sites are the active ones.

References

1. J. J. G. M. van Bokhoven and J. Medema, Chemical Laboratory TNO, Report 1970-28.
2. C. Aharoni and F. C. Tompkins, Advan. Catal. **21,** 1 (1971).
3. A. M. Peers, J. Catal. **4,** 499 (1965).
4. J. Medema, J. J. G. M. van Bokhoven and A. E. T. Kuiper, *ibid.* **25,** 238 (1972).

infrared spectroscopy of sarin adsorbed on alumina

A. E. T. KUIPER and J. MEDEMA

The adsorption of sarin on alumina has been investigated by means of infrared spectroscopy. By comparison with the spectroscopic features of organophosphorus compounds related to sarin the contribution of each group in the sarin molecule to the adsorption has been elucidated and an adsorption model is proposed.

Sarin adsorbs in two different ways on the alumina surface. Either, the oxygen atom of the phosphoryl group is linked to the surface, or interaction between surface and sarin takes place mainly through the fluorine atom.

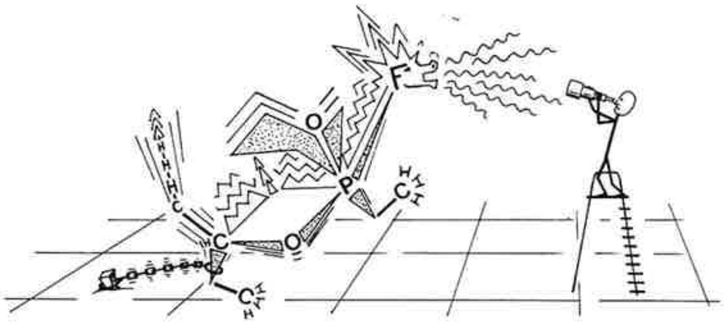
O
F
P
O
C
HC
CH

Introduction

Until now active carbon has generally been used as an adsorbent for chemical warfare agents partly because of its extremely large surface area of about 1000 m^2/g. Organophosphorus compounds, belonging to the class of warfare agents, adsorb very well on active carbon, but they either do not decompose in the adsorbed state or only very slowly. Because desorption is possible, it is necessary to impregnate the carbon with salts or metal oxides that act as catalysts in the decomposition of organophosphorus compounds.

There are two possible methods to obtain a catalyst; one can either screen as many impregnated carbons as possible until an active product is found; or one can investigate how the adsorbed compound might be decomposed and then select an agent that promotes this reaction. The second route was chosen because of the advantage that basic knowledge about adsorption mechanism might be obtained.

However, the surface structure of impregnated carbon is very complicated and therefore a pattern catalyst has been studied.

There are several reasons to choose alumina for this purpose:

1. the surface properties are well-known;
2. the transmission to infrared radiation is sufficiently large to apply infrared spectroscopy succesfully;
3. organophosphorus compounds decompose when they are adsorbed on alumina, which enables the study of both adsorption and decomposition with the same system.

Sarin (isopropyl methylphosphonofluoridate) was selected as a typical organophosphorus compound of interest to this study (Fig. 1).

Fig. 1. Structure of sarin.

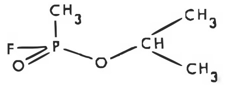

The investigations of the interactions of organophosphorus compounds with the alumina surface by means of infrared spectroscopy have not been finished yet. Therefore, this paper contains only preliminary results and the conclusions are tentative.

Infrared spectra of sarin and other compounds were recorded according to an experimental procedure described before (1).

Results and discussion

Fig. 2 shows the infrared spectrum of sarin; the assignments are indicated in the figure. Comparison with Fig. 3, the spectrum of sarin adsorbed on alumina, reveals some interesting features. In the first place changes in the adsorbent itself are visible.

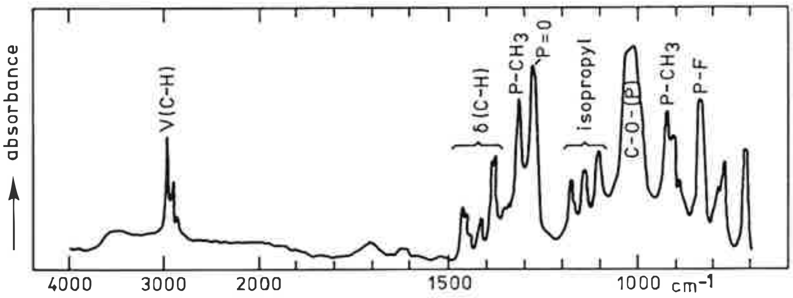

Fig. 2. Infrared spectrum of sarin.

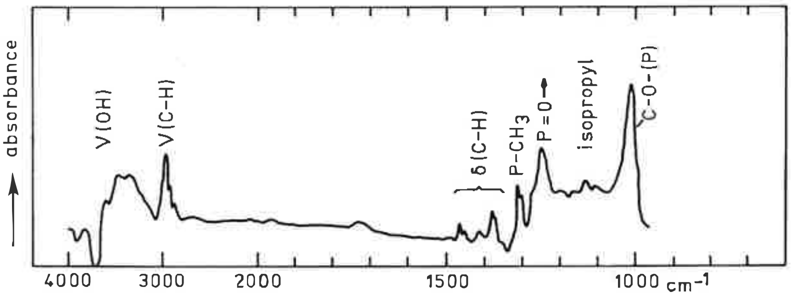

Fig. 3. Infrared spectrum of sarin adsorbed on alumina.

Alumina contains hydroxyl groups on its surface absorbing in the region of 3800–3300 cm^{-1}. The spectral changes indicate that hydroxyl groups absorbing between 3700 and 3800 cm^{-1} (strongly acidic groups) are replaced by hydroxyl groups absorbing between 3600 and 3300 cm^{-1} (the nature of these groups is unknown, they are, however, non-acidic). Without additional indications there are several possible interpretations of this shift. Therefore this phenomenon will not be discussed any further.

At frequencies lower than 1000 cm^{-1} the alumina used is not transparent to infrared radiation because of the absorption by lattice vibrations. This implies that the P—F vibration (840 cm^{-1}) cannot be observed. Therefore, direct observation of the behaviour of this group is not possible. The very intense C—O—(P) absorption (1010 cm^{-1}) is not affected upon adsorption; but the P═O band is shifted from 1277 cm^{-1} to 1245 cm^{-1}.

In the region between these two bands the absorbance has been increased, but there is no well defined maximum. The three absorptions of the isopropyl group (1100–1200 cm^{-1}) are still distinguishable and appear at frequencies just a little different from the values found for liquid sarin. All carbon-hydrogen stretching (2870–3000 cm^{-1}) and deformation (1350–1470 cm^{-1}) vibrations absorb in the adsorbed state at the same frequencies and with comparable intensities as in the liquid phase. Only the P—CH_3 band appears as a doublet, possibly caused by some distortion of the methyl group. The frequency, however, is not changed significantly.

As the frequencies of the P—CH_3, the C—O—(P) and all other carbon-hydrogen vibrations do not change upon adsorption of sarin on alumina, these groups obviously do not interact with the alumina surface.

A shift of approximately 35 cm^{-1} of the P═O stretching vibration can be explained in two ways: 1) The P═O interacts with the surface or 2) another substituent group interacts with the surface in such a way that the electronegativity of this group is reduced. As it is well-known (2) that the electronegativity of the substituents in organophosphorus compounds strongly influences the frequency of the P═O stretching vibration, the second possibility cannot be ruled out. However, above we deduced that the only substituent able to cause this effect is the fluorine atom. If the fluorine atom in sarin is replaced by a chlorine atom or even by an isopropoxy, or methyl group, the spectra still show a shift of ~ 35 cm^{-1} in the frequency of the phosphoryl vibration. Therefore, we feel justified in concluding that this shift is due to a direct interaction between the P═O and the alumina surface. The P═O surface linkage lowers the bond order of the phosphoryl group, causing a decrease in absorption frequency. As alumina contains acid sites (3) it seems most likely that these centres are responsible for this type of adsorption (compare with the shift in acid hydroxyl groups).

In order to ascribe the increase in absorbance in the region between 1100 and 1200 cm^{-1} upon adsorption of sarin onto alumina a number of organophosphorus compounds related to sarin have been investigated. These experiments show that for compounds without fluorine the absorbance between 1200 and 1100 cm^{-1} is low, whereas compounds with fluorine invariably show absorption of at least medium intensity in this region.

An interesting result has been obtained when using dimethylphosphinic fluoride, $(CH_3)_2P(O)F$ (Fig. 4), where the frequency of the phosphoryl vibration is shifted approximately 100 cm^{-1}. As shown before, adsorption by means of the phosphoryl group causes a shift of only 35 cm^{-1}. Therefore, another adsorption structure is required to explain this large shift. As none of the frequencies of the methyl vibrations changed upon adsorption, a linkage between the fluorine and the surface is proposed. This is confirmed by the observation that addition of water to the adsorbed species does not change the spectrum.

In all spectra with a phosphoryl shift of 35 cm^{-1} (where the fluorine atom is supposed to be "free") a new band at 1120 cm^{-1} arises due to hydrolysis of the adsorbed compound and a further shift of the phosphoryl frequency due to a change in electronegativity. The band at 1120 cm^{-1} is found also in the spectrum of adsorbed hydrogen fluoride (Fig. 5). The high shift of the phosphoryl frequency and the absence of any evidence for hydrolysis in the spectrum of this adsorbed compound points to the conclusion that the P—F is linked to the surface.

With this conclusion we overlooked the possibility that dimethylphosphinic fluoride

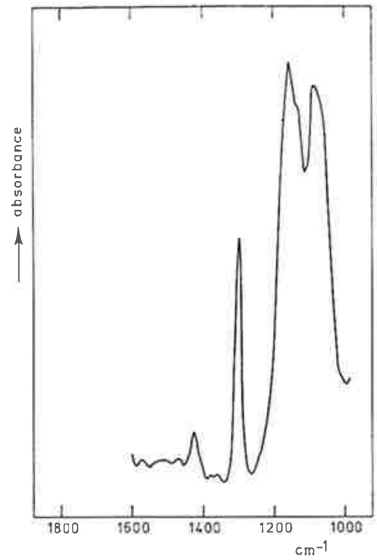

Fig. 4.
Infrared spectrum of
dimethylphosphinic fluoride
adsorbed on alumina.

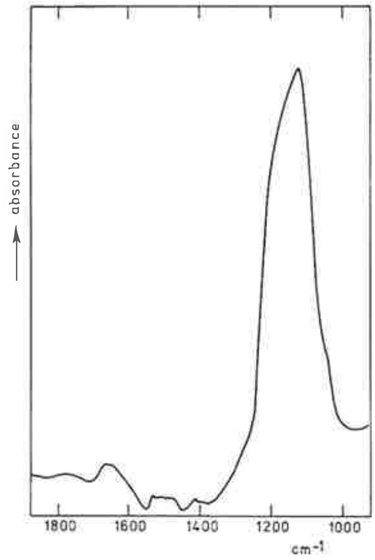

Fig. 5.
Infrared spectrum of
hydrogen fluoride adsorbed
on alumina.

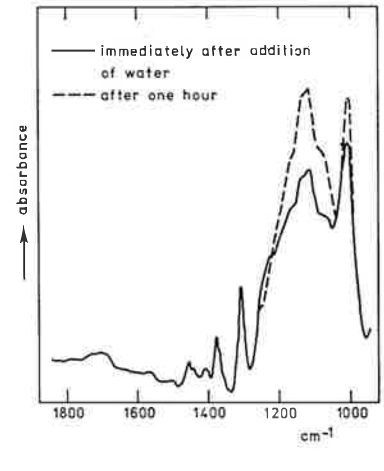

Fig. 6.
Infrared spectrum of
sarin adsorbed on alumina,
after addition of water.

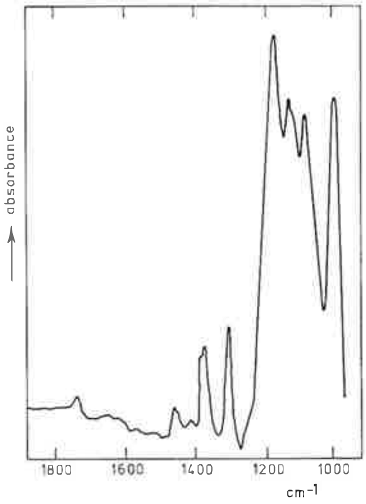

Fig. 7.
Infrared spectrum of
isopropyl methylphosphonic
acid adsorbed on alumina.

is hydrolyzed immediately upon adsorption into HF and dimethyl phosphinic acid. However, in that case a band at 1120 cm^{-1}, originating from adsorbed HF, should have been observed.

The above-mentioned effects do not completely explain the spectrum of adsorbed dimethylphosphinic fluoride. Together with a band at 1160 cm^{-1} (a shifted phosphoryl frequency) a band at 1080 cm^{-1} has been observed. The appearance of these two bands is probably due to the formation of a P—F/surface as well as P=O/surface bond. However, this assignment is rather speculative.

For sarin the absorbance between 1200 and 1100 cm^{-1} might equally well be ascribed to the formation of a P—F/surface linkage. The phosphoryl frequency would then be shifted approximately 100 cm^{-1} and appear at 1180 cm^{-1}; moreover, a second absorption at 1100 cm^{-1} appears. As in the case of the spectrum of dimethylphosphinic fluoride it could not be ascertained whether this absorbance is due solely to a P—F/surface bond or to a simultaneous interaction of the P—F and P=O with the surface.

Addition of water changes the spectrum of adsorbed sarin (Fig. 3) into that given in Fig. 6. The spectral changes can be interpreted in terms of hydrolysis of the no-bonded fluorine atom. The intensity of the phosphoryl frequency at 1245 cm^{-1} is decreased and the absorbance in the region around 1120 cm^{-1} is increased, indicative of HF formation. Consequently, spectrum 6 can be considered as being the sum of the spectrum of adsorbed phosphonic acid and adsorbed HF (Fig. 7 and 5).

The infrared spectra do not give information about the P—F stretching vibration. Therefore, the hypothesis about a P—F surface linkage and a hydrolysis reaction cannot be confirmed by means of infrared spectroscopy. The application of laser-Raman spectroscopy is expected to provide this information.

Concluding remarks

Based on infrared spectra the existence of two different adsorption structures I and II (Fig. 8) of sarin on alumina can be established:

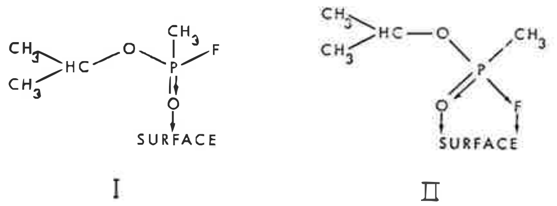

Fig. 8.
Adsorption structures of sarin.

The surface sites acting in structure I are acid sites probably of a Lewis acid nature. Part of the sarin molecules adsorb via the fluorine atom according to structure II. Simultaneous adsorption via the phosphoryl oxygen may occur but has not been ascertained as yet.

Addition of water to the adsorbed species causes hydrolysis of the "free" fluorine and confirms the existence of the adsorption structures as drafted.

An indication of the occurrence of two adsorption structures is also found in extraction experiments. One form can be removed from the alumina surface by extraction with methyl isobutyl carbinol, whilst the other form cannot. The ratio between these two structures depends on catalyst pre-treatment and temperature. Investigations are now focused on the study of catalyst pre-treatment, especially the influence of the surface coverage with hydroxyl groups, and on the existence of an adsorption structure with both P—F and P═O linked to the surface. Moreover, the application of laser-Raman spectroscopy is being studied as it provides the direct perceptibility of the P—F frequency in the adsorbed state.

References

1. A. E. T. Kuiper, J. Medema and J. J. G. M. van Bokhoven, J. Catal. in the press.
2. L. C. Thomas and R. A. Chittenden, Spectrochim. Acta **20,** 467 (1964).
3. J. Medema, A. E. T. Kuiper and J. J. G. M. van Bokhoven, J. Catal., **25,** 238 (1972).

leaks in charcoal beds and the water content of charcoal determined using the ethane pulse technique

P. C. STAMPERIUS and
H. W. VAN DER KLOOSTER

When a pulse of ethane is applied to a charcoal bed, channels in the bed will show their presence by a double elution peak.

The shape of the eluted peak will also depend on the water content of humidified charcoal. A quantitative relationship between the height of the eluted peak and the water content has been established.

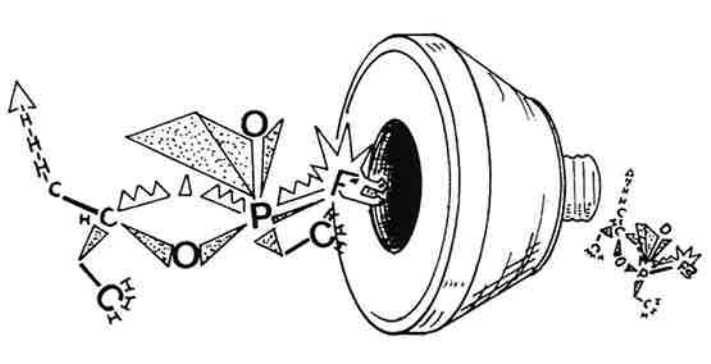
O
P
F
O
C

Introduction

Active charcoal has a high adsorption capacity for most organic vapours and is widely used for the removal of undesired gases from the air. The adsorption capacity is usually expressed in terms of breakthrough-time, *viz.* the time in which the maximum permissible exit concentration (breakthrough criterion) will not be exceeded. The breakthrough-time is considerably reduced when the charcoal has taken up water vapour.

Table I illustrates the effect of the water content of a charcoal on the breakthrough-time for chloropicrin (CCl_3NO_2) adsorbed on the charcoal in equilibrium with air of various relative humidities.

Table I. Effect of water on the breakthrough-time for chloropicrin adsorbed on charcoal.

Charcoal in equilibrium with the relative humidities (%)	Breakthrough-time (min)
20	290
50	275
75	75
90	35

The most striking feature of Table I is that the breakthrough-time shows a sharp fall at relative humidities above 50%, which is related to the phenomenon that the water vapour isotherm of charcoal rises very sharply above 50% relative humidity. Because relative humidities exceeding 50% very often occur in Western Europe this forms a serious problem in connection with the protection against toxic organic vapours in a moist atmosphere.

In most cases charcoal filters are manufactured using "dry" charcoal, *viz.* charcoal containing less than 2% by weight of water. This condition is preserved by keeping the filter closed when not in use. However, each time when ambient air is drawn through the filter, *e.g.* in trial runs of the filter installation, water vapour is taken up rapidly with consequent loss of adsorption capacity for organic vapours. It is therefore useful to know at any time the water content of the charcoal filter.

The water content of the charcoal can be determined by the loss of weight upon drying of a sample of the charcoal from the filter. However, this is not possible without destruction of the filter. Therefore, there is a need for a rapid non-destructive method for the determination of the water content of a charcoal filter. Then, in combination with data as given in Table I, it will be possible to determine the remaining adsorption capacity.

The adsorption efficiency, *viz.* the ability of a charcoal filter to reduce the influent concentration of a vapour to the desired low effluent concentration, is adversely affected by leaks in the charcoal filter (channeling) resulting from improper packing of the charcoal particles.

A part of the air/gas mixture passes rapidly through the channels in the charcoal bed without sufficient contact and this leakage gives rise to an appreciable penetration already at the beginning of the period of use. In case of the removal of a toxic substance from air, that is to be inhaled, this may be very dangerous. A rapid test that would indicate the presence of leaks in a charcoal filter, without destruction of the filter, would be useful.

In this paper we will describe how the changes in the shape of a pulse of ethane upon passage through a charcoal filter offer the possibility to determine the water content of charcoal and indicate the presence of leaks without destruction of the filter.

Principle

In an adsorbent bed a pulse of a gas is mainly dispersed by diffusion into the fluid phase, viscous flow variations and hold-up due to adsorption and desorption processes at the charcoal surface.

For a properly packed charcoal bed and fixed flow conditions the shape of the eluted pulse depends only on the repeated process of adsorption and desorption which is related to the degree of surface coverage of the charcoal. It is to be expected that a short pulse of a gas will undergo little dispersion if all adsorption sites are occupied.

When the surface of the charcoal is practically clean, the pulse will be broadened considerably (Fig. 1). The test gas must not interfere with the water occupying the adsorption sites and must be adsorbed weakly and reversibly. Furthermore, it should be easy available, non-toxic, and easy to determine with great sensitivity. Carbon dioxide may be used when the adsorbed substance is an organic vapour (1). However, with humid charcoal extra peak broadening occurs because of dissolution of carbon dioxide into adsorbed water. Ethane, which has a low solubility in water, proved to be useful as a test gas (2,3).

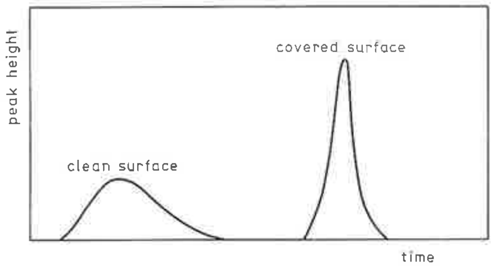

Fig. 1.
Effect of the degree of surface coverage of the charcoal on the shape of the elution peak (schematically).

Stamulis and Thompson (1) demonstrated earlier that with carbon dioxide as a test gas the pulse technique is quite useful to detect leaks or channels in charcoal filters. A leak permits a small volume of gas to move relatively undisturbed through the bed. Consequently, a double elution peak is obtained; the first peak represents the volume of gas passing through the channel and the second peak represents the volume of gas submitted to adsorption and desorption in the charcoal layer (Fig. 2). We demonstrated that a pulse of ethane is equally well suited for the detection of leaks (2,3).

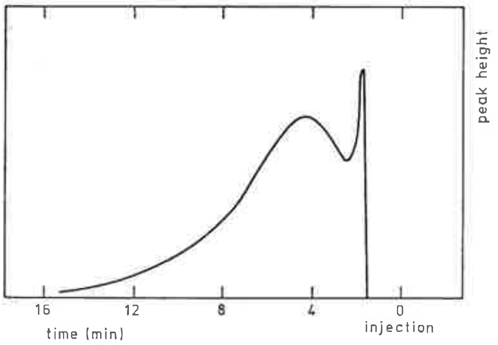

Fig. 2.
Elution peaks for a charcoal layer with a leak (schematically).

Experimental

The apparatus used to carry out the pulse experiments is given schematically in Fig. 3.

An air stream is divided into two adjustable parts: one part passes a humidifier, the other is dried with molecular sieves. By recombination of both air streams it is possible to obtain air with a relative humidity varying between 5 and 90%.

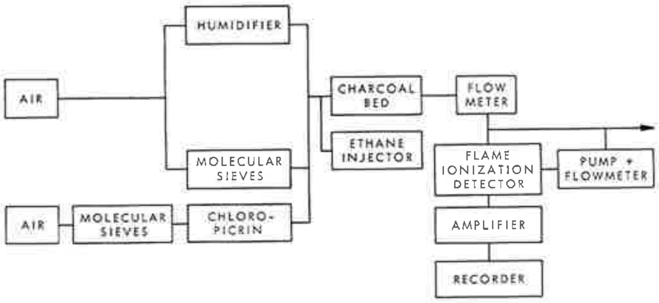
HUMIDIFIER
AIR
CHARCOAL BED
FLOW METER
ETHANE INJECTOR
MOLECULAR SIEVES
FLAME IONIZATION DETECTOR
PUMP + FLOWMETER
AIR
MOLECULAR SIEVES
CHLORO-PICRIN
AMPLIFIER
RECORDER

Fig. 3.
A schematic representation of the apparatus for the ethane pulse experiments.

A second air stream may be loaded with a gas that is to be adsorbed on the charcoal bed, *e.g.* chloropicrin, in order to correlate the water content with the remaining adsorption capacity.

The pulse of ethane is injected at the entrance of the charcoal bed by means of an adjustable plunger. From the effluent air a sample is passed continuously through a flame ionisation detector. The electrical signal is amplified and recorded as a function of time.

Laboratory-made charcoal beds and canisters of the Netherlands military K-respirator were used in the experiments. In both cases the charcoal was Norit RG1 (Norit Verkoop Maatschappij, Amsterdam).

The charcoal filters were loaded with water vapour at various relative humidities at 23±1°C to varying moisture contents. In some experiments, in order to simulate practical situations, the humidification was carried out in steps with interruptions of several hours. After humidification the charcoal filters were subjected to the ethane pulse test. Because the injected amount of ethane is kept constant, the height of the eluted peak is a direct measure for the degree of coverage of the charcoal surface.

Experiments on the detection of leaks with the ethane pulse technique have been carried out using so-called Norithene charcoal tiles or briquets consisting of a rigid mass of charcoal and powdered polyethylene moulded in a prototype gas-mask canister.

Results and discussion

The results of the tests with laboratory-made charcoal beds are given in Fig. 4. The water content is expressed as grams of water per test-tube, containing 11 grams of charcoal. There exists a relation between peak height and water content. The peak height does not depend on the way the final water content is attained, (stepwise at various relative humidities or at once at the highest relative humidity). Similar results have been obtained with canisters of the Netherlands military K-respirator (Table II and Fig. 5).

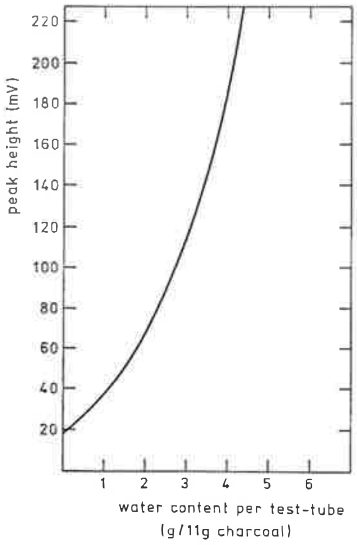

Fig. 4.
Height of the ethane peak *vs.* the water content of the charcoal.

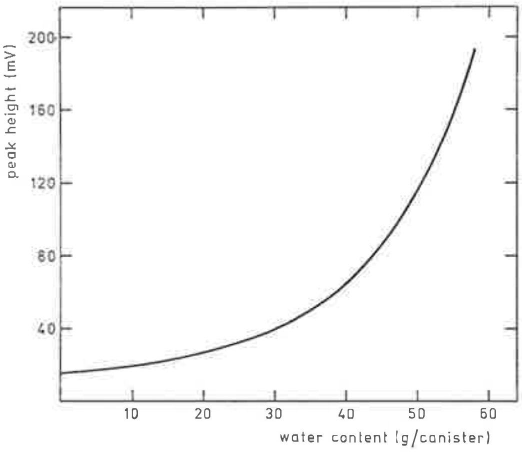

Fig. 5.
Height of the ethane peak *vs.* the water content of the charcoal in canisters of the Netherlands military K-respirator.

Similar curves will be obtained if the adsorbed substance is not water but an organic vapour like chloropicrin which is strongly adsorbed. From the relation

Table II. Water uptake by canisters of the Netherlands military K-respirator.

Experiment number	Relative humidity (%)	Humidification time (min)	Water uptake (g)	Total water content (g)
1	50	0–490	15.1	15.1
	75	490–1410	34.4	49.5
	90	1410–1920	9.6	59.1
2	50	0–290	7.2	7.2
	75	290–1350	40.6	47.8
	90	1350–1800	10.1	57.9
3	90	0–740	55.7	55.7
4	90	0–750	58.7	58.7

between water content and breakthrough-time for a certain organic vapour, that can be determined independently in small-scale laboratory experiments, the remaining capacity of the charcoal filter can be estimated.

It has been found that the ethane pulse technique can be used for the detection of leaks (3). This conclusion is based on laboratory experiments in which an intentionally placed leak in a charcoal bed was detected.

Recently, we had a few prototype gas-mask canisters at our disposal for which the breakthrough-time regarding the protection against chloropicrin and sarin (isopropyl methylphosphonofluoridate) had to be determined.

In these breakthrough tests a number of these filters showed an immediate breakthrough, whereas in similar experiments with laboratory-made filters such an immediate breakthrough was not found. Apparently, the charcoal beds used in these canisters had been damaged during manufacture and leaks were present. To detect these leaks, pulses of ethane were injected into an air stream passing through the filter. The double elution peaks associated with the presence of leaks were clearly found, particularly at low linear air velocities.

It appeared also that the height of the first peak is a semi-quantitative measure for the size of the leak. Table III gives the relation between the concentration of sarin that penetrates the filter at zero time and the height of the first peak.

Table III. Relation between effluent sarin concentration at immediate breakthrough and the height of the first peak of the eluted ethane pulse.

Effluent sarin concentration (mg/m^3)	Height of the first peak (mV)
0.001	0*
0.5	46
6	46
35	118

* no double elution peak present

From these values we estimated that leaks in the order of 0.01% can be detected with the ethane pulse technique, provided low linear air velocities (in the order of 2 cm/sec) are used.

Conclusions

If water is the only adsorbed substance on a charcoal filter the water content of this filter can be determined rapidly by injecting pulses of ethane in the air flow through the charcoal bed. The shape of the eluted peak depends on the final water content only, irrespective of the way this water content has been reached. In combination with data on the adsorption capacity for organic vapours and the water content of the charcoal concerned a non-destructive method for the determination of residual capacity is obtained.

At low linear air velocities small leaks or channels leading to concentrations of 0.01% in the effluent air can easily be detected. The height of the first of the two peaks observed is an indication for the size of the leak.

References

1. A. Stamulis and J. K. Thompson, Naval Research Laboratory, Washington D.C., Report 6793 (1968).
2. L. J. M. Bollen and H. W. van der Klooster, Chemical Laboratory TNO, Report 1972-9.
3. H. W. van der Klooster, Chemical Laboratory TNO, Report 1972-24.

analysis of breakthrough curves of benzene on active charcoal

M. VAN ZELM and J. MEDEMA

The concentration-time profiles (breakthrough curves) resulting from the dynamic adsorption of benzene on active charcoal are analyzed on the bases of models described by Giddings and Rosen. Although the adsorption isotherm is not linear, the breakthrough curves may be described as if there were a linear adsorption isotherm for each concentration. It appeared that the breakthrough curves are controlled by internal and external diffusion simultaneously. The effective internal diffusion is found to be higher than the calculated pore diffusion by a factor equal to the equilibrium adsorption constant for each concentration. This result as well as the apparently linear adsorption isotherm indicate that during adsorption the pore-mouth is saturated first and that molecules progress further into the pores with successive saturation of the surface, either by surface diffusion or gasphase diffusion.

The effective external diffusion is found to be dependent on the square root of velocity and particle diameter, a relation which has often been found before.

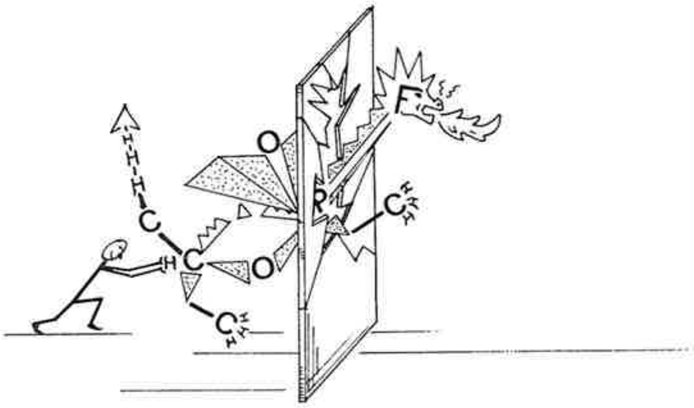
C
C
O
O
P
F
C

Introduction

For the removal of undesired constituents from air a process is frequently used in which the contaminants are continuously adsorbed from a flow of air onto fixed beds of active charcoal. The mass transfer from air to charcoal proceeds until the quantity adsorbed reaches a value corresponding to the concentration of contaminants in the feed stream. During the earlier stages of the process the quantity adsorbed is low and the adsorption capacity is still high. As a result the effluent of the adsorbent bed remains practically free of the contaminants over a certain period. After this period, in which the adsorption capacity is consumed, the concentration of solute in the effluent rises until the influent concentration is reached and the adsorbent is saturated with the contaminants. The change of effluent concentration with time is known as the breakthrough curve. In practical use the adsorbent bed is used until the effluent concentration reaches a given predetermined value (breakthrough concentration). The time elapsed from the start to this breakthrough point is called the breakthrough-time.

Breakthrough-time and breakthrough curve depend on a large number of parameters such as rate of air flow, nature and concentration of solute, dimensions of the fixed bed and adsorption characteristics of the adsorbent. The relation between these parameters and the breakthrough time is not known accurately. Therefore, in practice, breakthrough times and curves have to be determined for each set of conditions in order to evaluate the lifetime of the adsorbent bed. This involves a large amount of experimental work. To reduce the labour it would be advantageous to have a correlation between the breakthrough curves and the fore-mentioned parameters. In the ideal case this would allow prediction of the breakthrough curves under any set of conditions for every adsorbate-adsorbent combination from independently measured parameters. However, in practice, the mass transfer in a fixed bed of charcoal appears to be very complicated and it appears to be impossible to solve the differential equations describing the mass transfer. In the past this problem has been solved by making simplifying assumptions by means of which the differential equations became managable. Rosen (1) followed this last procedure and found a general solution for the breakthrough curve. However, in this solution the influence of the simplifying assumptions cannot be established. A second means of approach is the rigorous solution of the differential equation in Laplace transforms, but the inversion to the original parameters is in general not possible. It is, however, possible to derive the so-called statistical moments from the solution in Laplace coordinates. A series of these moments present the solution of the original system. This statistical approach was first presented by Giddings (2) and extended by McQuarrie (3) and Kucera and Grubner (4).

In this paper we will apply both solutions to the adsorption of benzene from air onto charcoal and compare the results with experiments.

Theoretical

A model for the dynamic adsorption

As a basis for theoretical considerations we have to select a model for the dynamic adsorption containing all transport phenomena involved.

Before a molecule can adsorb it has to diffuse from the gasphase to the surface of the solid (step 1). The charcoal particles are surrounded by flowing air. The linear velocity used in the experiments corresponds with laminar flow. The flow velocity at the outer surface of the particles will be zero and the charcoal particles can be described as surrounded by a stagnant film of air. Adsorbing molecules have to diffuse through this film in order to reach the outer surface (step 2). From this point the molecules will diffuse radially into the pores (step 3). The pore walls are considered to be covered with a stagnant film of air, introducing another diffusional resistance (step 4). Finally, the molecules can adsorb on the inner surface of the charcoal particles (step 5).

The fluid phase diffusional effects (step 1) to which also longitudinal and eddy diffusion contribute, may be described by an effective diffusion coefficient D, which is a function of linear velocity and particle size.

The rate of transfer through the film around the particles may be described as a first order rate process (step 2): a linear dependence of the rate on the difference between actual and equilibrium concentrations. If there should be a difference between the concentration in the pores and in the intraparticle volume, this is indicated by the ratio of these concentrations K_c.

The adsorbent particles (internal porosity ε_i) are considered as spheres through which straight pores are running and in this case the distance over which radial diffusion (step 3) takes place is $\frac{1}{2}d_p$, d_p being the diameter of the adsorbent particle. The diffusion coefficient in the pores is D_r, the value of which also allows for the irregularities of the pores.

The diffusion through the stagnant film on the pore walls (step 4) can again be described as a first order rate process. The ratio of the concentration in the pore volume and the concentration on the surface is now characterized by the equilibrium constant K_n.

In some cases the adsorption (step 5) is hampered by an activation energy for adsorption, introducing another resistance in the transfer process. The adsorption of benzene on charcoal is assumed to be purely physical and no activation energy for adsorption exists.

If in addition to this it is assumed that:

- the adsorption process is isothermal
- pressure drop over the column is negligible
- diffusion coefficients and rate constants are independent of concentration

it is possible to set up a mathematical description of the model.

Mathematical description

The mass balance equation including longitudinal and eddy diffusion is:

$$\frac{\partial C_e}{\partial t} + U\frac{\partial C_e}{\partial Z} - D\frac{\partial^2 C_e}{\partial Z^2} = Q_c \tag{1}$$

C_e = interparticle concentration
t = time
Q_c = amount of solute transferred to the surface per unit time
D = effective gasphase diffusion coefficient
U = linear velocity given by $U = W/\varepsilon_e F$ with W = volume flow, ε_e external porosity and F cross section of adsorbent bed
Z = length coordinate

The rate equation for the mass transfer through the stagnant film of air around the particles is given by:

$$Q_c = -H_c(K_c C_e - C_i) \tag{2}$$

H_c = rate constant
K_c = equilibrium constant relating the concentration in the pores and in the free volume between the particles
C_e = concentration in the external volume
C_i = concentration in the pore opening

The mass balance for radial diffusion is, according to the known diffusion laws:

$$\frac{\partial C_i}{\partial t} - D_r\left(\frac{\partial^2 C_i}{\partial r^2} + \frac{v-1}{r}\frac{\partial C_i}{\partial r}\right) = Q_n \tag{3}$$

r = length coordinate in direction of diffusion
v = shape factor given by the ratio volume and surface area of the particles
C_i, t, D_r, see previous descriptions
Q_n = rate of adsorption

The rate equation at the pore walls is again described as a first order rate process:

$$Q_n = -H_n(K_n C_i - q) \tag{4}$$

H_n = rate constant of adsorption
K_n = equilibrium constant relating the concentration in the pore and the concentration adsorbed
q = quantity adsorbed
Q_n, C_i, see previous descriptions

A numerical solution of the partial differential equations has been given by Rosen (1) for the case when longitudinal and eddy diffusion are negligible, $K_n \gg 1$ and $K_c = 1$. An analytical solution has been given by Rosen for columns of sufficient length:

$$\frac{C}{C_0} = \tfrac{1}{2}\left[1 + \operatorname{erf} \frac{t - \dfrac{LK_n(1-\varepsilon_e)}{U\varepsilon_e}}{K_n(1-\varepsilon_e)2\sqrt{\dfrac{L}{KU\varepsilon_e}}}\right] \tag{5}$$

In fact this equation shows that the breakthrough curve is symmetrical around $C/C_0 = \frac{1}{2}$ and that the shape of a breakthrough curve is Gaussian.

K in equation (5) represents the mass transfer coefficient given by

$$\frac{1}{K} = \frac{1}{K_{\text{internal}}} + \frac{1}{K_{\text{external}}} \quad \text{and} \quad \frac{1}{K_{\text{internal}}} = \frac{d_p^2}{60\varphi D_r} \tag{6}$$

φ = porosity function, $\varepsilon_i/\varepsilon_e$

The statistical moments derived from the solution in Laplace transforms are according to Grubner (5).

$$\mu_1 = \left(\frac{L}{U} + \frac{2D}{U^2}\right)\left[1 + \frac{\varepsilon_i}{\varepsilon_e}K_c(1+K_n)\right] \tag{7}$$

$$\mu_2 = \left(\frac{2DL}{U^3} + \frac{8D^2}{U^4}\right)\left[1 + \frac{\varepsilon_i}{\varepsilon_e}K_c(1+K_n)\right]^2 + \left(\frac{2L}{U} + \frac{4D}{U^2}\right)\frac{\varepsilon_i}{\varepsilon_e}K_c\left[\frac{d_p^2(1+K_n)^2}{60D_r} + \frac{\varepsilon_i}{\varepsilon_e}\frac{(1+K_n)^2}{H_c} + \frac{K_n}{H_n}\right] \tag{8}$$

The first statistical moment is in fact the geometrical mean of the breakthrough curve and coincides with $t_{\frac{1}{2}}$ in case of a symmetrical breakthrough curve. The second statistical moment is a measure for the width of the curve, characterized by the variance. The third statistical moment is a measure for the asymmetry of the distribution. The expression for the third and consecutive moments are much more complicated and will not be discussed here. Moreover, a numerical and detailed description of the breakthrough curve is needed for the application of these moments to the experiments.

The equations (7) and (8) may be simplified yet, when the following is taken into account:

- K_c equals unity, because the final amount adsorbed in a dynamic experiment is practically equal to that of a static experiment. The concentrations in internal and external volumes are thus equal

- K_n is supposed to be constant (linear isotherm)
- the order of magnitude of K_n for the system benzene on charcoal is 10^4 and $\varepsilon_i/\varepsilon_e$ is about 1, so that terms like

$$\left[1+\frac{\varepsilon_i}{\varepsilon_e}(1+K_n)\right]^n \quad \text{may be replaced by} \quad \left(\frac{\varepsilon_i}{\varepsilon_e}K_n\right)^n$$

- the gasphase diffusion coefficient is small and linear velocities are relatively large so that terms like

$$\frac{aD^{n-1}L}{U^p}+\frac{bD^n}{U^{p+1}} \quad \text{may be replaced by} \quad \frac{aD^{n-1}L}{U^p}$$

- the higher orders of the diffusion coefficients may be neglected.

In view of these approximations the expression for the first statistical moment becomes:

$$\mu_1=\frac{L}{U}\frac{\varepsilon_i}{\varepsilon_e}K_n \tag{9}$$

and for the second:

$$\mu_2=\frac{2DL}{U^3}\left(\frac{\varepsilon_i}{\varepsilon_e}K_n\right)^2+\frac{2L}{U}\frac{\varepsilon_i}{\varepsilon_e}\left[\frac{d_p^2K_n^2}{60D_r}+\frac{\varepsilon_i}{\varepsilon_e}\frac{K_n^2}{H_c}+\frac{K_n}{H_n}\right] \tag{10}$$

We can further distinguish two possibilities; the model operates in the diffusion region or in the kinetic region. In the first case diffusion in internal and external volume is rate controlling and the first order passage through the films is rapid. Then H_c and H_n are large in comparison with $d_p^2/60D_r$, and consequently the two kinetic terms may be neglected. In the kinetic region the diffusional terms $2DL/U^3$ and $d_p^2/60D_r$ may be neglected towards φ/H_c and $1/H_n$.

In the system benzene-charcoal the adsorption equilibrium is rapidly established. Therefore the diffusional region $H_{c,n}\rightarrow\infty$, $D_r=D_r$, $D=D$, probably controls the mass transfer.

The second statistical moment can be related to the Height of a Transfer Unit (HTU) according to:

$$\text{HTU}=\frac{\mu_2}{\mu_1^2}\cdot L \tag{11}$$

Substitution of equation (9) and the simplified equation (10) in (11) for H_c and H_n both infinite results in the following expression for the HTU:

$$\text{HTU}=\frac{2D}{U}+\frac{2d_p^2U}{60\varphi D_r} \tag{12}$$

Comparison of the simplified first statistical moment (eq. 9) with the expression of Rosen (eq. 5) shows that in both cases

$$t_{\frac{1}{2}} = \frac{L}{U} \cdot \varphi K_n \tag{9a}$$

In fact there is a small deviation between the two equations caused by the porosity term. Rosen ignored the volume of the solid phase and therefore found a slightly different porosity function.

The equation of Rosen, in fact a Gaussian, leads to the following expression of the HTU, derived from the denominator in the erf function:

$$\mathrm{HTU} = \frac{\sigma^2}{(t_{\frac{1}{2}})^2} = \frac{2U\varepsilon_e}{K} \tag{13}$$

Following Rosen's distinction in external and internal diffusional resistance:

$$\mathrm{HTU} = \frac{2U\varepsilon_e}{K_{\mathrm{int}}} + \frac{2U\varepsilon_e}{K_{\mathrm{ext}}}, \quad \text{with} \quad \frac{1}{K_{\mathrm{int}}} = \frac{d_p^2}{60\varphi D_r}$$

$$\text{gives} \quad \mathrm{HTU} = \frac{2U\varepsilon_e}{K_{\mathrm{ext}}} + \frac{2d_p^2 U\varepsilon_e}{60\varphi D_r} \tag{14}$$

In this case there is a small difference between the porosity functions between Rosen and the statistical moment as well. Comparison of eq. (14) and (12) shows that the internal diffusional contribution is identical in the two equations. For the contribution of the external diffusion in both cases effective coefficients are given. In the stochastic approach there is no rigorous treatment of the effective diffusion coefficient in the case of continuous dynamic adsorption (Frontal elution). There are some fundamental approximations for the case of zone elution but these are not applicable here.

The effective external mass transfer coefficient as given in equation (14) has been discussed by several authors (6, 7). From the relations given it can be derived that the $\mathrm{HTU}_{\mathrm{ext}}$ depends on particle size and linear velocity according to:

$$\mathrm{HTU}_{\mathrm{ext}} = \text{const. } U^{\frac{1}{2}} d_p^{\frac{3}{2}} \tag{15}$$

Experimental

The apparatus used for the adsorption of benzene onto active charcoal is shown schematically in Fig. 1. A measured flow of air is dried by silicagel, thermostated at 25 °C. Because the surface area of the benzene liquid remains practically constant and because of the constant temperature this provides a flow of air with a constant benzene concentration. The desired concentration is obtained by mixing the flow of benzene loaded air with a measured flow of clean dried air. The mixed flow is passed through a fixed bed of charcoal thermostated in a waterbath at 25°C. Finally, the benzene concentration in the column effluent is determined with the aid of a calibrated thermal conductivity cell. Before the start of each experiment the flow and concentration are adjusted to the values desired. During the adjustment the flow is passed directly to the exit via a bypass.

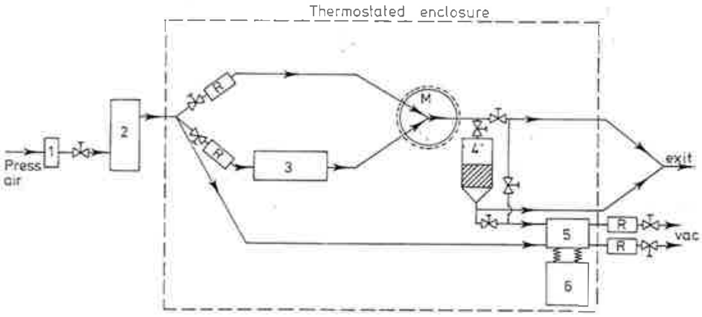

Fig. 1. Diagram of experimental set-up for the recording of breakthrough curves of benzene on charcoal; 1. oil filter; 2. drying towers; 3. benzene saturator; 4. charcoal bed; 5. thermal conductivity cells; 6. recorder, *M* mixing vessel, *R* rotameter.

The charcoal used throughout the experiments was "Norit Riek Standaard" obtained from N.V. Norit Amsterdam, The Netherlands. The Norit charchoal is an extruded charcoal with a diameter of 1 mm of the cylindrical particles. Other particle sizes were obtained by crushing the charcoal and sieving. Great care was taken to obtain a good packing of the charcoal by vibrating the beds with a cylindrical weight on top. In most experiments the charcoal was dried before use. In some cases, in particular the experiments with different particle sizes, the charcoal was not dried and might contain some 2 or 3% (*w*/*w*) of water.

The diameter of the charcoal bed was maintained at 30 mm but bedheights were varied from 15 to 150 mm. Several concentrations of benzene, in the range of 2–45 mg/l were used but the majority of tests were carried out at 4, 17 or 33 mg/l. Air flows ranged from 200–2000 l/h, but most experiments were carried out at 600 l/h.

Application of theory to experiments

From experiments in which only the bedheight was varied the geometric mean of the breakthrough curve (t_m) was plotted as a function of bedheight in order to test the validity of eq. (9). According to both the statistical and Rosen's model the relationship should be a straight line (Fig. 2).

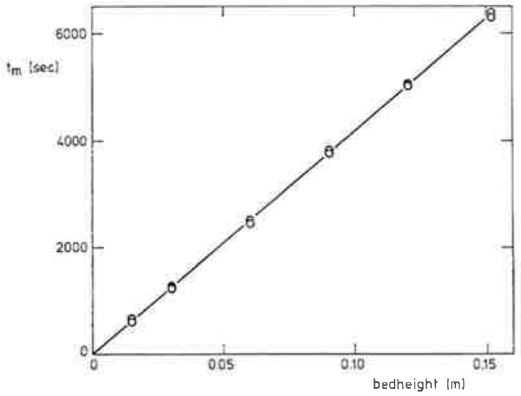

Fig. 2.
t_m as a function of bedheight (L)
$C_0=4$ mg/l;
$U=1.16$ m/sec;
$d_p=1.25$ mm.

The influence of the linear velocity is demonstrated in Fig. 3. A straight line is found for each concentration used. As the other parameters were identical this means (see eq. (9)) that the differences in slope for the different concentrations must be sought in different values of K_n.

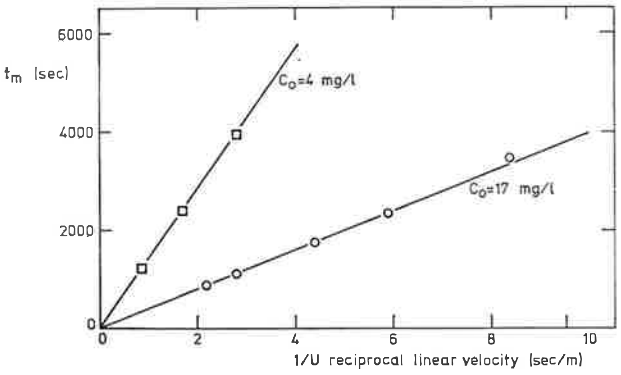

Fig. 3.
t_m as a function of reciprocal linear velocity ($1/U$); $C_0=4$mg/l and 17 mg/l, bedheight $=0.03$ m; $d_p=1.25$ mm.

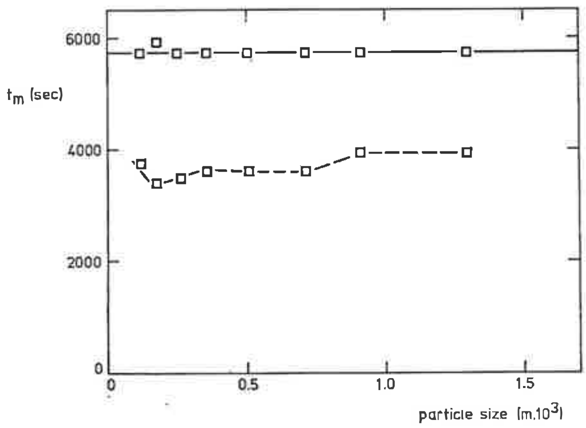

Fig. 4.
t_m as a function of particle size (d_p) before (dotted line) and after correction for porosity differences (full line).
$C_0=4.0$ mg/l;
bedheight 0.03 m;
$U=0.35$ m/sec.

The geometric mean of the breakthrough curve is nearly independent of particle size (dotted line in Fig. 4). If a correction is made for differences in external porosity the t_m value is independent of particle size (full line in Fig. 4), as could be expected from eq. (9). Moreover, it shows that the porosity plays a part in the transport process as predicted by eq. (9).

The total quantity adsorbed at saturation at a given concentration represents a point of the adsorption isotherm. In Fig. 5 the full line is the benzene adsorption isotherm determined statically in the usual way. The dotted line represents the isotherm resulting from the dynamic adsorption experiments. If the adsorption proceeds through equilibrium situations between concentration and quantity adsorbed, following the adsorption isotherm, K_n could not be constant. From the fact that eq. (9) fits the measurements very well it must be concluded that K_n is a constant for each concentration. From the numerical value of K_n in each experiment it appears that these values are identical to those obtained if for each concentration separately the isotherm is considered to be linear (see Fig. 5).

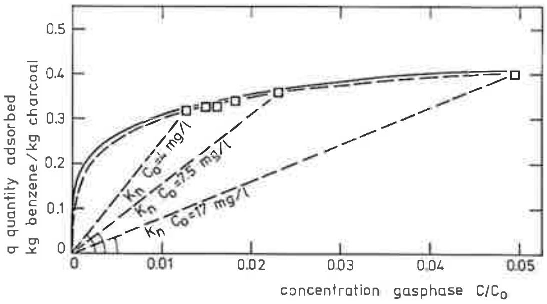

Fig. 5.
Adsorption isotherm of benzene on charcoal, full line according to static procedure, dotted line according to dynamic experiments. The value of K_n is derived as if for each concentration separately the isotherm is considered to be linear.

For each experiment the value of the HTU was obtained according to

$$\mathrm{HTU} = \frac{\tau_{0.95} - \tau_{0.05}}{3.3\tau_{0.5}} \cdot L \tag{16}$$

$\tau_{0.95}$ = time in seconds for which the concentration in the effluent is 95% from the influent concentration
$\tau_{0.05}$ = *ibid.* for 5%
$\tau_{0.5}$ = *ibid.* for 50%
L = bed height

The factor 3.3 arises from the assumption of a Gaussian distribution.

Various plots of HTU *versus* U or d_p^2 (eq. (12)) revealed that in the case of benzene adsorption on charcoal internal diffusional resistance alone cannot be the predominant effect but that the external diffusion also plays a part. A final expression for the HTU is obtained by substituting eq. (15) into (14).

$$\mathrm{HTU} = a\sqrt{d_p U} + b\, d_p^2 U \quad (a \text{ and } b \text{ constants}) \tag{17}$$

The first term represents the contribution of external diffusion, the second term describes the diffusion into the pores.

In Fig. 6 a plot of HTU/U *versus* $1/\sqrt{U}$ and in Fig. 7 a plot of HTU/$\sqrt{d_p}$ *versus* $d_p\sqrt{d_p}$ are given. The velocity dependence is as predicted by eq. (17). However, concentration influences to some extent the slope of HTU/U *versus* $1/\sqrt{U}$, indicating that the constant b is dependent on concentration. The results in Fig. 7 show a much larger variance, this is due to the pretreatment of the charcoal which was not dried in these experiments.

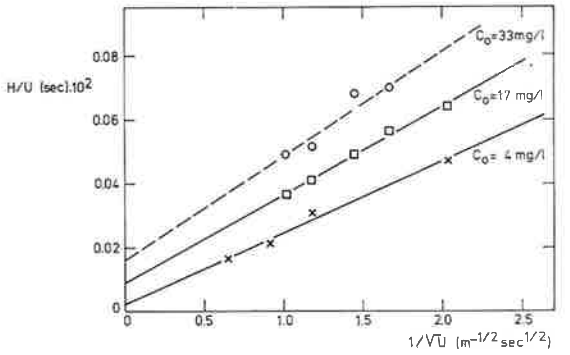

Fig. 6.
Correlation between Height equivalent to a transfer unit and velocity. $(H/U$ *vs.* $1/\sqrt{U})$ at concentrations of 33 mg/l (○), 17 mg/l (□), and 4 mg/l (×). $d_p = 1.25$ mm. Because of the relative large standard deviation the plot at a concentration of 33 mg/l is represented by a dotted line.

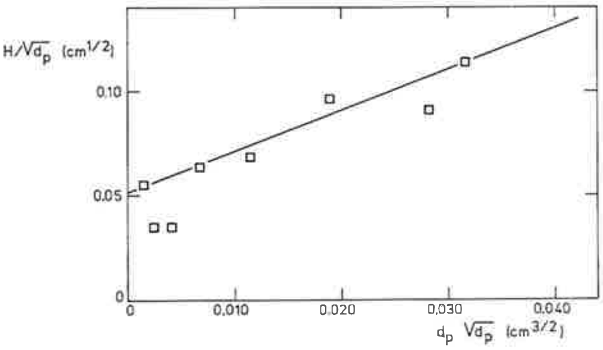

Fig. 7.
Correlation between Height equivalent to a transfer unit and particle size $(H/\sqrt{d_p}$ *vs.* $d_p\sqrt{d_p})$, at $C_0 = 4$ mg/l, bedheight 0.03 m. $U = 0.35$ m/sec. Relative large deviations are present due to small variations in the water content of the charcoal.

Discussion

The complete expression for t_m following from the statistical model without any simplifying assumption is:

$$t_m = \left(\frac{L}{U} + \frac{2D}{U^2}\right)\left[1 + \frac{\varepsilon_i}{\varepsilon_e}\cdot K_c(1+K_n)\right] \qquad (17)$$

From Fig. 2 and 3 it follows that indeed the term $2D/U^2$ may be neglected as was done in the derivation of eq. (9). Both t_m as a function of $1/U$ and t_m as a function of L pass through the origin which implies that the external diffusion (longitudinal and eddy diffusion) have little, if any, influence on the value of t_m. After correction for the porosity t_m is independent of d_p which again proves the validity of eq. (9). That Rosen's expression for t_m is identical to eq. (9) is explained by the fact that longitudinal and eddy diffusion apparently have no influence on t_m and neglecting these in Rosen's model was justified at least as regards the conditions of our experiments. In Rosen's model the adsorption was assumed to proceed through equilibrium situations according to a linear isotherm. In the stochastic approach the adsorption is represented by eq. (4) which in fact gives the rate of desorption. If equilibrium is assumed, the rate of adsorption equals the rate of desorption and in the transformation to Laplace coordinates and the derivation of the first statistical moment K_n is assumed to be independent of concentration. So in a slightly different way adsorption in both models proceeds through equilibrium according to a linear isotherm. Obviously the isotherm is not linear (Fig. 5) but the results presented in Fig. 3 and 5 show that K_n may be considered to be constant for each concentration and that K_n may be derived directly from the adsorption isotherm. This remarkable result might be explained by the assumption that the adsorption does not follow the isotherm but through a first order rate process independent of the shape of the isotherm. The total quantity adsorbed at the end is of course, in this case too, related to the gasphase concentration by K_n. In order to elucidate this first order rate process we have to look more closely at the adsorption phenomena in the system benzene-charcoal. The charcoal has an average pore radius of 10 Å and the shape of the isotherm is such that already at low concentrations a monolayer or more benzene is adsorbed on the charcoal. As a result the pore openings become 30–40% smaller upon adsorption of benzene. Adsorption onto the very large surface inside the pores can now proceed in three different ways:

- by diffusion from the interparticle volume through the reduced pore openings into the pores
- by desorption of the molecules adsorbed in the pore mouth and diffusion of these desorbed molecules into the pores
- by diffusion of the molecules adsorbed in the pore mouth along the surface.

Equation (4) describes the adsorption according to the first case, but in this as well as in the second case the molecules have to diffuse through the gasphase into the pores, colliding with the pore walls and resting for a certain time at these walls. De Boer (8) already pointed out that this type of diffusion is very slow especially in the case of small pores and that the diffusion along the surface is predominant. When this also holds in our case the driving force for adsorption is no longer the difference in actual quantity adsorbed (q) and equilibrium quantity adsorbed (K_nC_i) as given in eq. (4), but the difference in covered and non-covered surface area.

Equation (4) then changes into:

$$Q_n = H_n'(1-\theta_i) \tag{18}$$

Q_n = rate of adsorption
H_n' = rate constant
θ_i = fraction of surface covered $= q/K_n C_0$

Equation (18) can be rearranged into:

$$Q_n = \frac{H_n'}{K_n C_0}(K_n C_0 - q) \tag{19}$$

q = actual quantity adsorbed
K_n = adsorption equilibrium constant
C_0 = concentration in fluid phase at saturation

an equation which is nearly identical to eq. (4). In this equation, however, K_n is a real constant and the shape of the isotherm no longer influence the rate of adsorption.

In Tabel I the values of t_m calculated with eq. (9) for a number of experiments not used in the Fig. 2–4 are compared with the experimentally determined values. The value for K_n is derived directly from the adsorption isotherm of benzene on charcoal following the procedure indicated in Fig. 5.

Table I. Comparison of calculated and experimental values of t_m

No. exp.	L (m)	W 1/h	C_0 mg/1	calcul. t_m (sec)	expt. t_m (sec)	% deviation
40	0.030	300	42.7	1070	1070	0.0
59	0.015	2000	3.85	640	640	0.0
61	0.015	2000	2.85	830	800	−3.8
76	0.060	600	5.15	6800	6700	−1.7
89	0.060	1000	4.05	4800	4700	−2.1
108	0.030	1000	4.22	2350	2430	−3.7
111	0.060	600	4.05	6800	6740	−0.9
112	0.015	600	4.05	1700	1720	+1.2
115	0.030	600	4.05	3400	3420	+0.6

The constants a and b in the equation:

$$H = a\sqrt{Ud_p} + b\,d_p^2 \cdot U \tag{17}$$

can both be derived from Fig. 6 and 7. The constant a following from the plot of H/U *versus* $1/\sqrt{U}$ at a concentration of 4 mg/l gives a value of $a = 6{\cdot}9 \cdot 10^{-3}$ sec$^{\frac{1}{2}}$. From the results presented in Fig. 7, also at a concentration of 4 mg/l, a value of $5{\cdot}9 \cdot 10^{-3}$ sec$^{\frac{1}{2}}$ is found. So there is a satisfactory agreement between the two figures with respect to the constant a. However, from Fig. 6 it appeared that the constant a is also to some extent dependent on concentration. This is caused by the fact that the constant a is also dependent on viscosity which changes when the concentration of benzene in the fluid phase is increased. Anyhow, the contribution of the external diffusion to the broadening of the concentration time profile is as predicted by the adsorption model and is not dependent on the state of the charcoal (dry or relatively wet). This last conclusion is derived from the fact that a dried charcoal (H/U *versus* $1/\sqrt{U}$) or a relatively wet charcoal ($H/\sqrt{d_p}$ *versus* $d_p\sqrt{d_p}$) leads to the same approximation of the constant a.

The contribution of the internal diffusion term bUd_p^2 to the broadening of the breakthrough curve is apparently dependent on concentration as follows from Fig. 6 and entirely different for a dry and a relatively wet charcoal as follows from the comparison of the constant b in Fig. 6 and 7 at the same concentration (resp. $2{\cdot}7{\cdot}10^{-3}$ sec/cm^2 and $2{\cdot}8{\cdot}10^{-2}$ sec/cm^2). The constant b may be written as $(2/60\varphi)\cdot(1/D_r)$ (eq. (12)). The porosity function φ is approximately 1. If D_r is estimated from the relation $D_r = \frac{2}{3}\bar{r}\bar{v}$, in which $\bar{r}$ is the average pore radius and $\bar{v}$ the velocity of the molecules then b can be calculated. The average pore radius (10 Å) was calculated with the aid of the relation $\bar{r} = 2V/S$ in which V is the pore volume and S the specific surface area. Substitution of these values in eq. (12) gives a constant b equal to 17, in comparison with the experimentally determined value in the case of dried charcoal a factor 10^4 too high. However, as was pointed out before, the diffusion rate in very small pores is strongly hampered by the colliding of the molecules against the pore walls and the resting time at these points of collision. Both when this effect predominates the diffusion and in the case of surface migration, the diffusional constant D_r is related to K_n. Without going into details about the exact relation between D_r and K_n in these two cases, we can describe $D_{r_{\text{eff}}}$ as $D_{r_{\text{eff}}} = K_n D_r$. This outcome is in agreement with the statement made by Grubner (5) "that it is normally assumed that $D_{r_{\text{eff}}} = D_r(1+K_n)$" which reduces in our case to $D_{\text{eff}} = D_r K_n$. However, in our adsorption model this is not an assumption but it follows directly from the way in which the adsorption inside the pores take place. On the basis of the above derivation it is now possible to compare the theoretical values of b with the experimental ones for three concentrations. This comparison is made in Table II.

Table II. The values of the constant b from theory and experiment

concentration mg/l	b (Fig. 6) sec/cm^2	K_n	b calculated $b = \frac{2}{60\varphi D_r K_n}\cdot\frac{d_\eta^2\text{eff}}{d_p^2}$
33	$1.6\cdot10^{-2}$	$9.6\cdot10^{3}$	$1.6\cdot10^{-2}$
17	$0.9\cdot10^{-2}$	$2.9\cdot10^{2}$	$0.9\cdot10^{-2}$
4	$0.27\cdot10^{-2}$	$1.6\cdot10^{3}$	$0.26\cdot10^{-2}$

In this comparison φ was taken unity, D_r was derived from $D_r = \frac{2}{3}\bar{r}\bar{v}$, K_n was taken from the adsorption isotherm in Fig. 5. The factor $d_p/d_{p_{eff}}$ arises from the fact that we are dealing with cylindrical particles for which the effective particle diameter $d_{p_{eff}} = d_p \cdot \sqrt{1.5}$ as given by Hougen and Watson (9). The comparison between theory and experiment as shown in Table II seems better than it is because the experimentally determined value of b from Fig. 6 shows a relative large standard deviation especially for the high concentration of 33 mg/l. The theoretical derivation of the constant b immediately shows why in the case of relatively wet charcoal b is so much higher. In this case the water molecules have to be driven out by the benzene molecules which causes a strongly reduced diffusion and therefore a much higher value of b.

Concluding remarks

In the case of dynamic adsorption of benzene on charcoal it appeared that the breakthrough curves can be described by a model given by Rosen (1) as well as by the stochastic approach from Giddings (2). By introducing a change into the proposed adsorption mechanism it was possible to explain the apparently linear isotherm. From this point it was possible to calculate the effect of internal diffusion on the shape of the breakthrough curve, and it appeared that this calculation bears out the experimentally determined values. The contribution of the external diffusion to the broadening of the breakthrough curve could be described by an empirical relation as given in the literature.

The stochastic approach also offers the possibility to describe the asymmetry or skewness of the distribution curve (third moment), whereas the fourth moment indicates whether the breakthrough curve is higher or lower than the Gaussian distribution. It would be very interesting to apply these moments to the experiments but one must note that 0.5% deviation in μ_1 appears as 5% deviation in μ_2 and as 25% in μ_3. Although the error in μ_1 can be reduced it would be necessary to conduct the experiments with even greater accuracy than can be realized at this moment.

References

1. J. B. Rosen, J. Chem. Phys. **20,** 387 (1952).
2. J. C. Giddings, *Dynamics of Chromatography*, Part I, Principles and Theory, Marcel Dekker, Inc., New York (1965).
3. D. A. McQuarrie, J. Chem. Phys. **38,** 437 (1963).
4. O. Grubner and E. Kucera, in *Gas Chromatografie*, (H. G. Struppe, ed.), Akademie Verlag, Berlin (1965), p. 157.
5. O. Grubner, in *Advances in Chromatography*, Vol. 6 (J. C. Giddings and R. A. Keller, eds.), Marcel Dekker, Inc., New York (1968), p. 173.
6. C. R. Wilke and O. A. Hougen, Trans. Am. Inst. Chem. Eng. **41,** 445 (1945).
7. D. Thoenes, Thesis, Delft (1962).
8. J. H. de Boer, *The Dynamical Character of Adsorption*, Oxford University Press (1953).
9. O. A. Hougen and K. M. Watson, *Chemical Process Principles*, Part III, Kinetics and Catalysis, John Wiley & Sons, Inc., New York (1966).

List of symbols

a	constant
b	constant
C	concentration
C_e	concentration in interparticle space
C_i	concentration in intraparticle space
C_0	concentration of solute in influent
d_p	particle size
$d_{p_{eff}}$	effective particle diameter
D	effective fluid phase diffusion coefficient
D_r	pore diffusion coefficient
$D_{r_{eff}}$	effective pore diffusion coefficient
F	cross section of column
HTU	Height of a Transfer Unit $= (\mu_2/\mu_1^2) \cdot L$
$H_{c,n}$	rate constants
$K_{c,n}$	adsorption equilibrium constants
K, K_{int}, K_{ext}	mass transfer coefficients
L	length of column
q	quantity adsorbed
$Q_{c,n}$	flow of mass
r	length coordinate of pore
$\bar{r}$	average pore radius
S	specific surface area
t	time
t_m	geometric mean of breakthrough curve
U	linear velocity
v	velocity of the molecules
V	pore volume
W	volume flow
Z	length coordinate of column
ε_e	interparticle porosity
ε_i	intraparticle porosity
$\mu_1, \mu_2, \ldots$	statistical moments of the 1st, 2nd, ... order
ν	shape factor
σ	standard deviation
φ	porosity function
θ	surface coverage
$\tau_{0.95}, \tau_{0.5}, \tau_{0.05}$	time at concentration ratio $C/C_0 = 0.95$, 0.5 and 0.05

design of a simple gas-mask

M. VAN ZELM

The design of a simple gas-mask is described. Special attention is paid to the development of a non-misting eyepiece material. Other features are a low resistance to breathing, an outlet valve with low leakage and low pressure drop, and a simplified filter design using a special type of charcoal filter.

Introduction

The design of a gas-mask is usually a balance between the required degree of protection on the one hand and the comfort of wear on the other hand. The protection provided by the mask is determined largely by the sealing of the facepiece to the face, the leakage through the outlet valve, and the efficiency and the size of the filter element. Problems associated with the comfort of wear are the provision of a large field of vision, not diminished by misting of the eyepiece, a good speech transmission, and a low resistance to breathing.

For most of these problems existing technical knowledge can provide a satisfactory solution. Using various sealing edges of the facepiece and a suitable attachment of the headharness that keeps the mask in place, a satisfactory sealing can be obtained. Existing outlet valves have low leakage values and the availability of very efficient aerosol filters and adsorbents have made the construction of excellent filters possible.

In modern military and industrial gas-masks the problem of speech transmission is solved by the inclusion of a special speech diaphragm. The problem of misting of the eyepiece is solved either by using special anti-misting materials to be put on the inside of the mask in front of the eyepieces or by using the so-called Tissot principle and/or an inner mask. In the case of the Tissot principle the inhaled air, being relatively dry after passage through the filter, is passed over the surface of the eyepiece to remove condensed water. The inner mask or nose cup prevents the moist exhaled air to reach the eyepiece by passing it directly to the outside of the mask via the outlet valve. Using plastic materials for the eyepiece large fields of vision can be obtained. Incorporating all these provisions in a gas-mask, however, increases its complexity and consequently its costs!

Some time ago we decided to investigate the feasibility of a simple means of respiratory protection which can be used in time of war or during a calamity by the general public. In this case the acceptability of the means of protection by the wearer is at least as important as the required degree of protection. The provisional specifications set up in the first stage of the development reflected this opinion by requiring a very low resistance to breathing and a large field of vision not impaired by the phenomenon of misting. Our subsequent development work led to a simple type of gas-mask which has some features we consider worth while.

General description *

The gas-mask (Fig. 1) consists of a rubber facepiece, two filters (one on each side of the facepiece), and an outlet valve. Outlet valve housing and canisters are made of hard PVC. The filters are connected to a tube that has an oval slit, positioned in such a way that the purified air, being relatively dry, passes over the surface of the eyepiece and assists in keeping it free from fogging (Fig. 2). The filter is of a simple design and

---

* The description refers to a laboratory model.

contains two elements, a glass fibre filter and a charcoal filter to remove toxic substances in aerosol or vapour form, respectively.

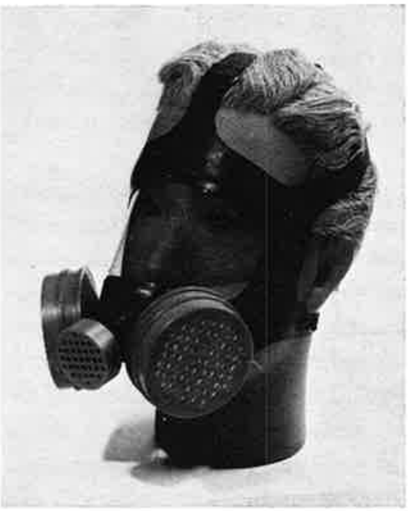

Fig. 1.
Laboratory model of the mask.

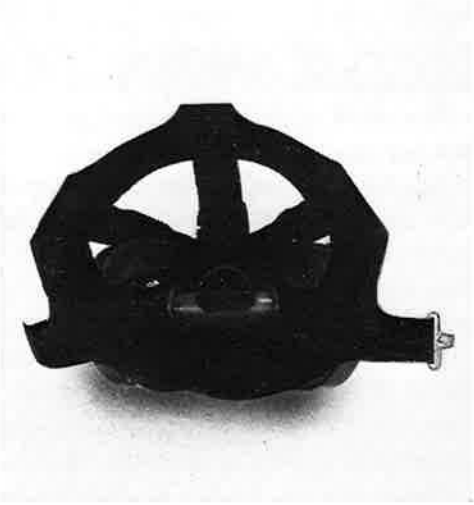

Fig. 2.
View of the interior of the mask.

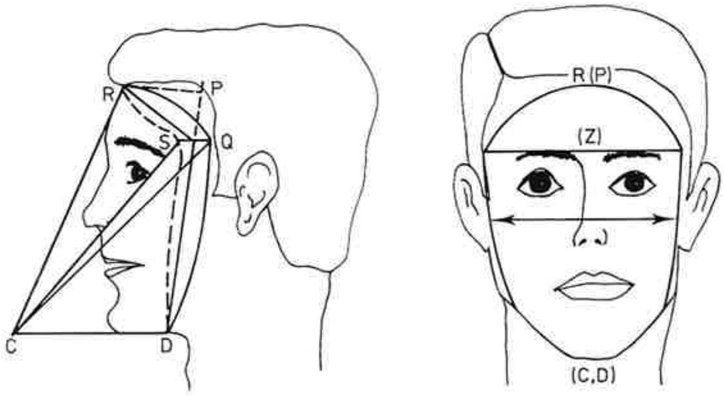

Fig. 3. Shape of the facepiece.

Facepiece

The facepiece can be made from a flat sheet of rubber. For design purposes the facepiece is considered to be composed of two cones as indicated in Fig. 3.

Our computerised calculation method uses five parameters. The most important of these are face length and face width which are defined in the usual way. If sufficient anthropometric data should be available it is possible to calculate the dimensions of the facepiece that would fit the maximum number of people. The result of the calculations will be a draft as given in Fig. 4, which is based on the facial dimensions of a few people working in our laboratory.

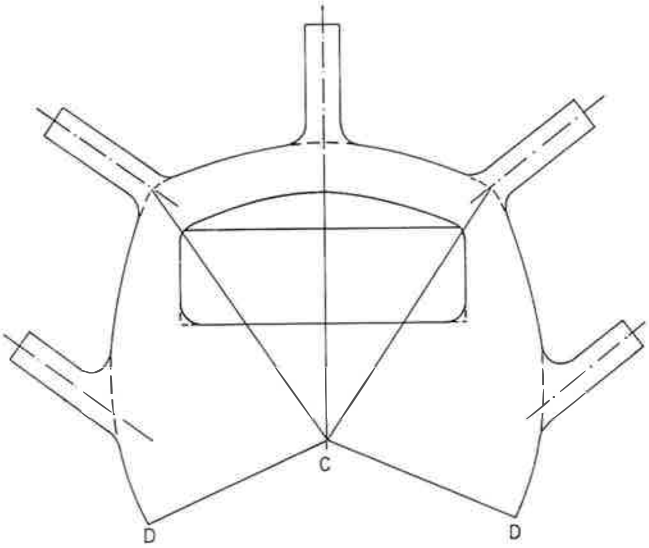

Fig. 4.
Draft of a facepiece as resulting from a computer calculation. The conical shape is obtained by joining the two lines CD.

Eyepiece

Special attention has been paid to the development of an eyepiece that offers a large field of vision and does not mist because of condensing water vapour. Earlier in this paper we listed a number of methods that can be used to prevent fogging of the eyepiece. A nose cup was rejected because this would increase the complexity of the mask considerably. A simple form of the Tissot principle is the oval slit in the tube connecting the two filters (Fig. 2), but this renders the mask rigid and is rather complicated to construct. As we developed a special type of non-misting material to be used for the eyepiece, this connecting tube will not be incorporated in an eventual industrial prototype of this mask.

A simple way to prevent fogging is the use of detergents. When applied carefully before donning of the mask the detergent will make the condensed water spread in a smooth film and vision will be slightly impaired only. The detergent dissolves in the condensed water and is removed from the surface with the water running down the eyepiece. After some time the water vapour will condense in small drops again, particularly on the plastic eyepiece material, and vision will again be seriously impaired. If new detergent could be added to the surface continuously, to compensate for the loss, a long-lasting anti-fogging effect would be obtained.

We developed a transparant material into which a certain amount of detergent is incorporated. This detergent diffuses slowly to the surface and a sufficiently high concentration of the surface active agent is maintained to prevent fogging over long periods. Three plastic base materials and eight different types of detergents were investigated. Because of technical difficulties in the manufacture of the sheets or because of insufficient anti-fogging properties most of the combinations had to be rejected. Finally, two combinations, code numbers B4 and B7, showed excellent properties. Both contain 80% Tenite 036 M (cellulose triacetate, Eastman Kodak Cy., Rochester, U.S.A.) and 15% dimethyl phthalate as a plasticiser. In addition B4 contains 5% Tergitol NPX (detergent, Union Carbide Corp., New York, U.S.A.) and B7 contains 5% Triton X-100 (detergent, Röhm and Haas, Philadelphia U.S.A.). The anti-fogging properties were investigated by inserting a disc of the material into the wall of a rectangular box and passing air saturated with water vapour at 37°C over the inner surface of the disc. The outer side is in contact with the atmosphere (about 20°C and 50% relative humidity). Eight hours' tests were run in the daytime with regular visual inspection of transparency.

In these tests clear vision lasted for 15 hours with B4 and 36 hours with B7 material. After storage at 50°C for 170 hours the B7 material gave a clear vision for 25 hours and showed the least shrinkage. This material was therefore selected. It is remarked that the more often the material is dried after a certain period of use the longer it takes for the complete formation of a water film (up to 10 minutes). During this period vision is slightly impaired. This is not a great disadvantage because the mask is destined for people who only have to find their way; complicated visual tasks will not be carried out.

Outlet valve

The requirement that resistance to breathing should be low implies that the outlet valve has a low resistance too. An investigation of existing outlet valves revealed that either the resistance to breathing is too high or the so-called dynamic leakage is unacceptably large for our purposes. The dynamic leakage, the leak when the valve is functioning, depends on a number of factors, such as the smoothness of the sealing surfaces, the shape and the elasticity of the rubber part and the volume of the valve cover. Dynamic leakage is measured when the valve is operated by a breathing machine simulating human breathing with a given breathing volume and frequency. By placing the valve in an atmosphere containing a few percent of a tracer gas the leakage is easily determined.

Instead of designing a new valve we chose for modification of the outlet valve of the Netherlands military K-respirator. This valve has a resistance which is about 2.5 times too high but the dynamic leakage is far below the maximum allowable value for our mask. The resistance can be decreased by decreasing the valve tension and this is possible in two ways:

- a change in the shape of the mushroom type rubber flap
- choosing a rubber composition with a lower elasticity modulus

Fig. 5 shows a modified rubber flap after removal of a little rubber material by abrasion. The favourable effect of the removal of a little rubber material on the place indicated in Fig. 5 on the resistance of the valve is illustrated in Table I and Fig. 6.

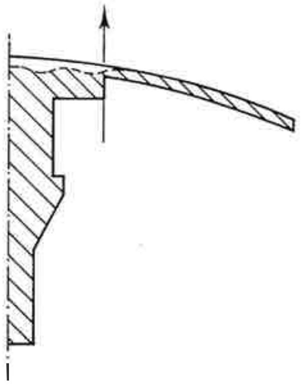

Fig. 5.
The mushroom type rubber flap of the Netherlands military outlet valve after removal of a little rubber material by abrasion.

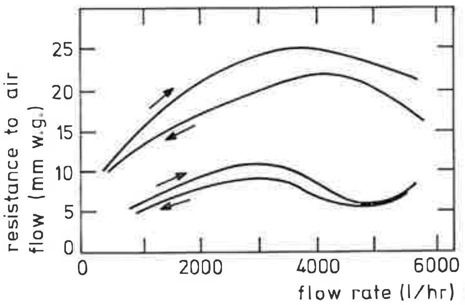

Fig. 6.
Effect of removal of rubber material from the outlet valve of the Netherlands military respirator as indicated in Fig. 5. Upper curves: before removal. Lower curves: after removal.

Table I. Resistance in mm w.g. and dynamic leakage in ml leaked air per respiration of the Netherlands military outlet valve before and after removal of a little rubber material by abrasion.

	before		after	
valve	resistance at 85 l/min (mm w.g.)	dynamic leakage (ml/resp.)	resistance at 85 l/min (mm w.g.)	dynamic leakage (ml/resp.)
1	21.8	4.8×10^{-4}	7.0	3.7×10^{-3}
2	22.3	10.6×10^{-4}	8.9	4.9×10^{-3}
3	19.6	5.0×10^{-4}	6.8	6.2×10^{-3}

The breathing resistance of the modified valve is very much reduced and is well below the value which we considered desirable for our mask. The dynamic leakage, although increased by a factor of ten because of the reduced valve tension, is still well below the maximum allowable leakage. A modification as described above would necessitate the manufacture of new rubber moulds. The use of a different rubber mix can yield an outlet valve with equally low resistance and dynamic leakage. A number of twenty outlet valves manufactured with the moulds of the military outlet valve from different rubber mix showed satisfactory low resistances and low dynamic leakages, also after accelerated aging tests. Fig. 7 shows the resistance curves of one of these valves before and after accelerated aging.

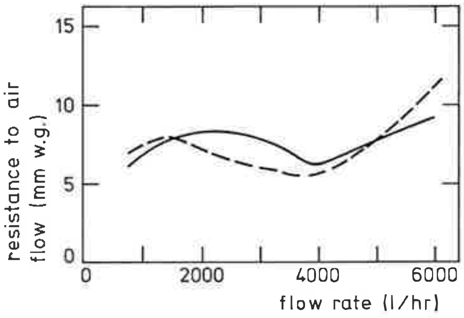

Fig. 7.
Resistance curve before (full line) and after (dotted line) accelerated aging of the outlet valve.

Filters

The filters contain an aerosol filter and a charcoal filter for the removal of toxic substances in aerosol and vapour form, respectively. The required degree of protection in connection with the desirable low resistance to breathing necessitates a large filter area. This area can be attained by using two filters, one at each side of the facepiece. To reduce the drag on the facepiece the filters should have minimum height and the pleated glass fibre filter to be used for aerosol filtration should have a pleat height of about 10 mm. Commercially available glass fibre filters usually have a pleat height of 18 or 20 mm. A French firm (Sofiltra S.A. Paris, France) succeeded in manufacturing a 12 mm high glass fibre filter that proved to be satisfactory in tests with a homodisperse liquid dioctyl phthalate aerosol and a heterodisperse solid sodium chloride aerosol.

The charcoal used is a peat-based, steam-activated, extruded charcoal of Norit with a diameter of the cylindrical particles of 0.8 mm. A charcoal bed with a diameter of 80 mm and a height of 10 mm was found to provide sufficient adsorption capacity.

To simplify the construction of the filter canisters the charcoal was used in the form of a "charcoal briquet", a solid mass of charcoal particles and polymer particles, manufactured in such a way that the charcoal retains its original activity (Norithene, Norit Verkoop Maatschappij, The Netherlands).

The use of Norithene briquets has the advantage that the charcoal filter can be fixed into the filter canister in the same simple way as the glass fibre filter by a lute and there is no need for supporting wire gauzes to keep the charcoal in place. In the laboratory Silcoset lute (ICI) proved to be satisfactory but other types of lute can be used that do not poison the charcoal at the periphery of the relatively thin layer. Fig. 8 shows various components of a laboratory-made filter. Fig. 9 shows a typical breakthrough curve obtained with chloropicrin (CCl_3NO_2) as a test agent.

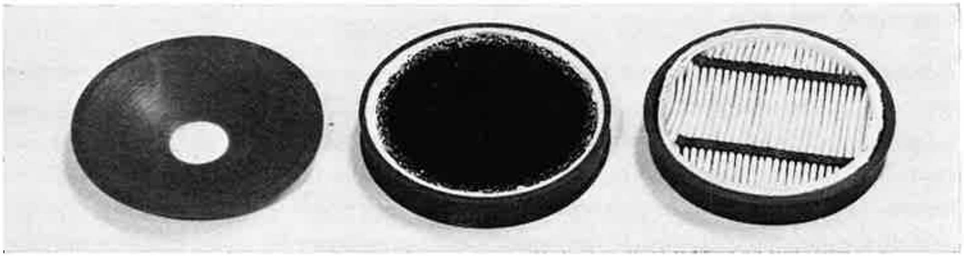

Fig. 8. Components of the filter. From right to left: aerosol filter, charcoal filter and lower cover.

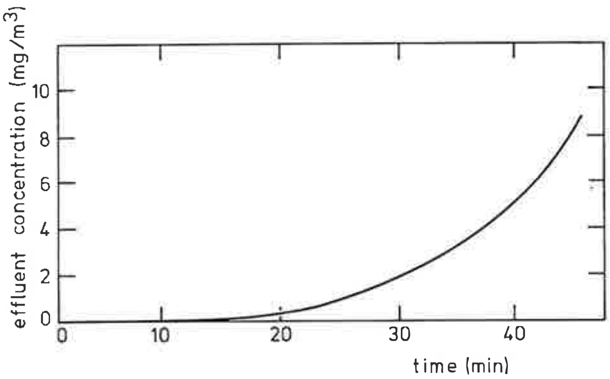

Fig. 9.
Example of a breakthrough curve for chloropicrin. Conditions of test: flow rate 15 l/min, concentration chloropicrin 1 mg/ml, temperature 20°C and relative humidity 50%.

The plastic components of the filter of Fig. 8 are heat-sealed together but it may be more convenient to fix the charcoal filter and aerosol filter into an aluminium canister as shown in Fig. 10.

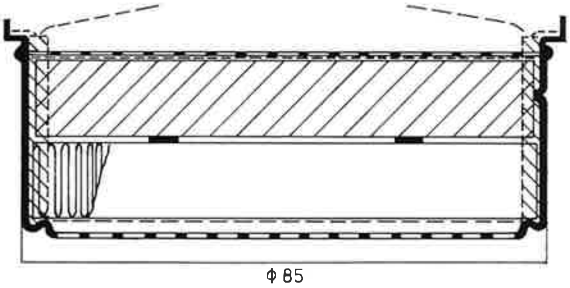

Fig. 10.
Aerosol filter and charcoal filter luted into an aluminium canister.

A limited number of canisters of this type have been manufactured for testing. The resistance to air flow of the filter amounted to 14.5 mm w.g. at 30 l/min with a standard deviation of 0.8 mm w.g. The penetration of 0.3 micron diameter liquid dioctyl phthalate aerosol at a flow rate of 44 l/min was about 0.003% on the average with a highest value of 0.02% found in a single case. Under conditions of test similar to those of Fig. 9 breakthrough times for chloropicrin (breakthrough criterion 1 μg/l) were found to be about 30 minutes.

Concluding remarks

A simple type of gas-mask has been designed. Features of the mask are a non-misting eyepiece, a low resistance to breathing and a simple filter design. The anti-fogging property of the eyepiece material is based upon compensation of the loss of detergent on the surface by diffusion from the interior of the material. The low resistance to breathing is obtained mainly by increasing the filter area using two filters, one on each side of the facepiece. Using a more elastic rubber compound in an existing military outlet valve the corresponding low exhalation resistance has been obtained. The dynamic leakage of this valve is well below the maximum allowable value. A simple design of the filter is possible using so-called charcoal briquets, a solid mass of charcoal particles and polymer particles. Charcoal filter and glass fibre aerosol filter are luted in one operation into the canister.

The mask is a laboratory model that may serve as a basis for further development into an industrial prototype.

emergency water supply

A. VAN VLIET

A procedure for obtaining drinking water from surface water contaminated with chemical warfare agents has been developed. The procedure consists of chlorination with chlorinated lime, dechlorination with activated carbon (Norit SA-1), coagulation with ferric chloride and the coagulant aid Wisprofloc P, filtration, and post-chlorination with calciumhypochlorite granules.

The procedure is reliable, independent of the type of surface water and the nature of the contaminant, and can be carried out in the Paterson installation, the mobile water purification unit of the Royal Netherlands Army.

The procedure offers a possibility for the development of a simple individual purification procedure for surface water to be carried out in a canteen.

F
O
P
C
O
C

Introduction

In time of war or after calamities the civil water supply may fall away. The Royal Netherlands Army has at her disposal a mobile water purification unit, the so-called Paterson installation, to produce drinking water by purification of ordinary surface water.* The installation operates on the principles of coagulation, sedimentation, filtration, and post-chlorination. However, when the surface water is contaminated with persistent chemical warfare (CW) agents (mustard gas, nerve agents) or by insecticides, the above-mentioned procedure fails, because it does not remove or destroy these toxic compounds.

Therefore, a series of experiments has been set up to develop an improved water purification procedure, being independent of the type of water or type of contaminant, which can be applied in the Paterson installation.

Experimental

Chlorination

For the purification of water contaminated with dissolved toxic agents the first step must be the decomposition and/or the adsorption of these harmful compounds. Previous investigations (1, 2) have shown that the most suitable way of destroying persistent CW-agents is decomposition by means of active chlorine. For the purification of distilled water contaminated with CW-agents (concentration about 10 mg/l) 100 mg/l of active chlorine has to be applied. This concentration is obtained by the addition of 300 mg/l of chlorinated lime (30% (*w/w*) available chlorine) or of 150 mg/l of calciumhypochlorite (65–70% (*w/w*) available chlorine).

Field trials at several places in the Netherlands have shown that the surface water itself may have a considerable active chlorine consumption (in some cases more than 100 mg/l).

Consequently, the active chlorine concentration for the decomposition of CW-agents in surface water has to be increased with a quantity necessary to compensate for the consumption by the surface water itself. To keep the procedure simple and because determination of the active chlorine consumption under field conditions is very difficult, the active chlorine concentration was fixed at 100 mg/l for ordinary surface water and at 200 mg/l for surface water contaminated with CW-agents.

Dechlorination

After chlorination the excess of active chlorine is removed by adsorption on activated carbon. Initially, a highly purified powdered activated carbon, Norit SX-1, was used in a concentration of 600 or 1500 mg/l (depending on the initial active chlorine concentration). However, adsorption studies of a chlorine resistant compound (lindane) to several types of powdered activated carbon have shown Norit SA-1 to be a better adsorbent for lindane from water than Norit SX-1. Laboratory experiments, in which the purification of surface water contaminated with CW-agents was checked, have shown that chlorination with 200 mg/l of active chlorine and dechlorination with 1000 mg/l of Norit SA-1 is reliable to obtain drinking water which meets the requirements (for non-contaminated surface water dechlorination is carried out with 400 mg/l of Norit SA-1). A rather high concentration of activated carbon is necessary, in order to adsorb not only the excess of chlorine, but also undecomposed agents and decomposition products.

---

* The Paterson installation has been used in Florence (Italy) after the disastrous flood that devastated this city in 1966.

Coagulation

After chlorination (45 minutes) and dechlorination (15 minutes) a filtration procedure has to be carried out. To prevent a rapid clogging of the filter by the very fine particles of the activated carbon, filtration must be preceded by a coagulation process.

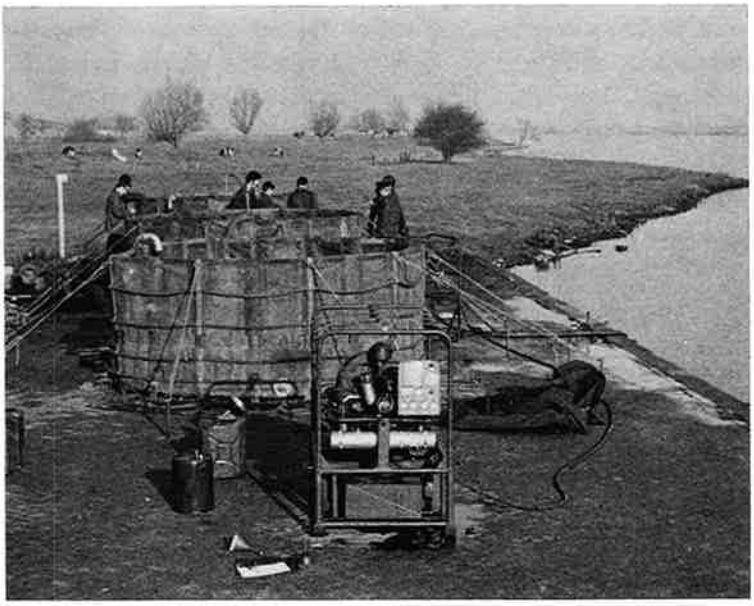

Fig. 1.
The Paterson installation.

The coagulation can be carried out by the addition of limestone and ferric chloride. Because the coagulation process is strongly dependent on the nature of the water, it is difficult to determine the required minimum amounts of limestone and ferric chloride under field conditions. To be on the safe side these concentrations are fixed at 500 mg/l and 350 mg/l, respectively. However, this coagulation procedure has two distinct disadvantages: First, when mixing is too vigorous the flocs already formed are destroyed, resulting in a longer sedimentation time and a more rapid clogging of the filter; and, secondly, the addition of a large amount of ferric chloride increases the chloride ion concentration which is detrimental to the taste of the purified water.

Therefore, an investigation has been set up in order to improve the coagulation procedure by the application of coagulant aids. A number of coagulant aids were compared in the laboratory and some of them were tested in field trials with a modified Paterson installation, which includes canvas tanks (capacity about 11 m^3), pumps, a mixing unit, and a filter unit (Fig. 1).

a. Laboratory Tests

In the laboratory, the purification procedure was simulated in a 5-liter beaker using 4 liters of tap water. Chlorinated lime and activated carbon (Norit SX-1) were used in concentrations of 300 and 600 mg/l, respectively. Mixing was carried out in the same way as in the Paterson equipment, *viz.* by blowing air to the bottom of the beaker through a system of pipes.

When using a coagulant aid, after chlorination and dechlorination, ferric chloride (20 mg/l) was added. After two minutes of mixing (with a force comparable to 15 m^3 of air per hour in the Paterson installation) a 1% (*w/w*) solution of the coagulant aid in water was added, followed by another 13 minutes of mixing. During the sedimentation process, samples were taken with a pipette 9 cm above the bottom of the beaker. The transparency of the water was determined by measuring the light transmission and comparing it with the transmission of tap water, which was fixed at 100%. By means of this test (using the coagulant aid in a concentration of 5 mg/l) several selections were made from 70 different flocculant aids. The selected flocculant aids were used in further investigations.

To determine the influence of the concentration of the aids on coagulation, the procedure was repeated with concentrations of 0.1, 0.5, 2.0, 5.0, 10.0, and 25.0 mg/l for the synthetic polyelectrolytes and 1.0, 5.0, and 10.0 mg/l for the natural coagulants aids. It appeared that the final transmission (reached within 10–15 minutes) is nearly independent of the concentration in the range from 0.5 to 10.0 mg/l for the synthetic and from 5.0 to 10.0 mg/l for the natural coagulant aids. However, the time to reach maximum transmission depends strongly on the concentration. Typical examples are given in Fig. 2 and 3.

For the synthetic polyelectrolytes it was observed that, although generally the size of the floc increases with increasing coagulant aid concentration, at a concentration of about 25 mg/l smaller flocs were present between the larger ones, causing the final transmission to be somewhat lower than that obtained with concentrations in the range 0.5 to 10 mg/l. A concentration lower than 0.5 mg/l is generally insufficient. For the synthetic aids it was concluded that the concentration should be at least 0.5 mg/l, and for the natural products at least 5 mg/l. Although the manufacturers specify that the coagulant aid should be added as a solution in water the effect of adding aids as a solid was investigated, because the chemicals are not very stable when dissolved in water. Moreover, preparing at 1% (*w*/*w*) solution is not easy to carry out in the field as the coagulant aids are wetted with difficulty and coalesce quickly. It was found that in the laboratory a mixing period of 20 minutes is sufficient to obtain a satisfactory rate of sedimentation.

The stability of the floc is another important factor in the coagulation process. With limestone and ferric chloride but in the absence of coagulant aids, the flow of air for mixing has to be reduced in the course of the coagulation process to prevent the disintegration of the flocs already formed. When using coagulant aids it appeared that the floc is much more stable and it is not necessary to reduce the flow of air. Fig. 4 illustrates the difference between several coagulation processes.

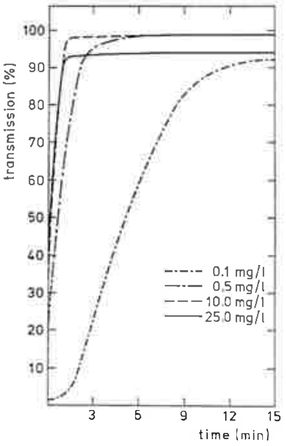

Fig. 2.
Sedimentation curves at different concentrations of Wisprofloc P.

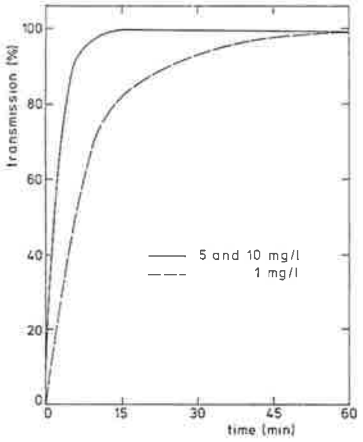

Fig. 3.
Sedimentation curves at different concentrations of Drewfloc 470.

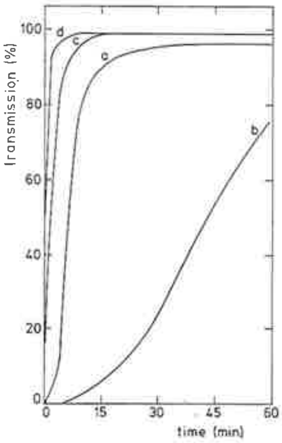

Fig. 4.
Sedimentation curves for different coagulation processes.
a. limestone and ferric chloride; reduced mixing
b. limestone and ferric chloride; thorough mixing
c. ferric chloride and Wisprofloc P; thorough mixing
d. ferric chloride and Drewfloc 470; thorough mixing

b. Field tests

Those coagulant aids which had given favourable results in laboratory tests were now tested in the field with the Paterson installation at six places, using different types of surface water (ranging from rather clean to heavily polluted).

The laboratory experiments were verified by the use of a "normal" polluted surface water from the River IJssel, and from this test the standard conditions for a satisfactory coagulation with flocculant aids were drawn up. To asses the desired universal character of the purification procedure, these conditions were verified with five other types of surface water. The whole purification procedure was followed in each experiment. Only the conditions of the coagulation step were changed with respect to: the type of coagulant aid, the concentration used, the method of addition, the concentration of ferric chloride, the flocculation time, the sedimentation time, the mixing force, and the concentrations of activated carbon and chlorinated lime. The effect of all these variables on the coagulation was studied.

The experiments were evaluated with respect to the time of flocculation, sedimentation and filtration, the number of filterbeds required, the yield of purified water, and the total time needed for the purification. It was concluded that a coagulation with flocculant aids is strongly dependent on the nature of the surface water.

Most of the coagulant aids investigated gave good results with two or three types of surface water, but not with all types. Only one synthetic material, Drewfloc 470 (1 mg/l), and only one natural product, Wisprofloc P (5 mg/l), were found to be satisfactory under all circumstances for all different kinds of water. These materials can be added as a solid. In some cases a concentration of 20 mg/l of ferric chloride is sufficient, but for a general procedure this concentration has to be raised to 50 mg/l. The mixing force during the coagulation is very important and should amount to 15 m^3 of air per hour leading to a flocculation time of 25 minutes.

c. Toxicity of coagulant aids

The coagulant aids investigated are, with a few exceptions, synthetic polymers of low toxicity. However, there is a possibility that these polymers are contaminated with small quantities of the monomer, which may be toxic. Most of the data on physiological effects relate to the irritation of the skin and the eyes. Data concerning the toxicity upon digestion are known for a few coagulants only. In general, those of natural origin are non-toxic. As reported by the manufacturers, the United States Public Health Service has approved several coagulant aids for water treatment as they have no adverse physiological effect when applied in the concentration recommended by the manufacturers. The coagulant aid Wisprofloc P is approved at a maximum concentration of 5.0 mg/l.

Sedimentation and Filtration

The sedimentation time depends on the nature of the surface water and varies between 35–45 minutes. From a practical point of view Wisprofloc P is preferred over Drewfloc 470. In general, a coagulation with 50 mg/l of ferric chloride and 5 mg/l of Wisprofloc P results in a filtration time of about 40 minutes (using two filterbeds) and a yield of almost 9 m^3 of water of good quality.

For comparison, a coagulation with limestone and ferric chloride without addition of a coagulant aid results in a filtration time of about 50 minutes (using two filterbeds) and a yield of about 8 m^3 of water. Apart from the pH, which is somewhat too low (5.9–6.0), the quality of the water is good.

After the filtration (through a multi-element cartridge filter, which consists of 19 perforated tubes wound with stainless steel wire and precoated with a filter aid) the purified water is post-chlorinated to a concentration of about 1 mg/l by means of calcium hypochlorite.

Conclusions

The procedure as described is reliable for the purification of CW-contaminated surface water and can be carried out with the Paterson installation when the equipment is extended with a mixing unit (compressor and system of pipes).

Starting with 10 m^3 of surface water the whole procedure takes 2½–3 hours (depending on the type of water) to obtain 8½–9 m^3 of purified water. A summary of the procedure is given in Table I.

Table I. Purification of surface water contaminated with CW-agents. Starting with 10 m^3 of surface water the yield is 8½–9 m^3 after 2½–3 hours

	concentration of chemicals (mg/l)			
steps in the procedure	ordinary surface water	surface water contaminated with CW-agents	mixing force (m^3 of air/h)	time (min)
chlorination with chlorinated lime (30% (*w*/*w*) available Cl)	300	600	15	45
dechlorination with activated carbon, Norit SA-1	400	1000	15	15
coagulation				
– ferric chloride	50	50	15	2
– coagulant aid Wisprofloc P	5	5	15	23
sedimentation	–	–	–	30–45
filtration	–	–	–	40–50
post-chlorination with calcium hypochlorite (70% (*w*/*w*) available Cl)	1,5	1,5	–	–

According to the experimental results, the coagulation with Wisprofloc P has many advantages compared to the coagulation with limestone and ferric chloride as applied in the original procedure used by the Army. The advantages are the formation of a more stable floc, a higher rate of sedimentation, clearer water after sedimentation so the filtration time can be reduced, reduced quantities of chemicals required, better taste of the purified water because of smaller amount of chloride ions, pH value of the purified water meeting requirements, reduced cost, and a higher yield of water obtained in a shorter time.

The new procedure offers the possibility for the development of a simple individual purification procedure for surface water to be carried out on a smaller scale, *e.g.* in a canteen.

References

1. L. Ginjaar, Thesis, Leiden (1960).
2. L. de Lavieter, Chemisch Weekblad **66**, No. 26, 29 (1970).

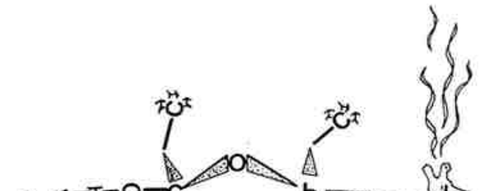

acknowledgements

This collection of papers could be realized only through contributions at the bench or at the desk of the entire staff of the Chemical Laboratory TNO.

We acknowledge the permission of the National Defence Research Organization to publish these papers.

We are indebted to our former director J. van Ormondt and to Dr. C. van Hooidonk for their critical corrections of the manuscripts, and to Mrs. T. Medema for her kind assistance in preparing the type-scripts.

The Editorial Committee,

Henk Boter
Henri Kienhuis
Jan Medema
Marius van Zelm